Reduced observer based friction compensation for a controlled one link robot

Mallon, N.J.

Award date:
2003

Reduced Observer Based Friction Compensation for a Controlled One Link Robot

ing. N.J. Mallon
s000908

Master's thesis
DCT 2003.88

Coaches: Dr. ir. N. van de Wouw
Dr. Ir. R.I. Leine
M.Sc. D. Putra
Supervisor: Prof. Dr. H. Nijmeijer

Eindhoven University of Technology (**TU/e**)
Department of Mechanical Engineering
Dynamics and Control Group

Eindhoven, October 10, 2003

Contents

Summary

Friction, especially dry friction, is an impediment for position accuracy of controlled mechanical systems. To obtain position accuracy without using a high-gain controller, controlled mechanical systems must, therefore, be extended with a *friction beating strategy.* This thesis deals with the application of such a strategy for a one-link robot manipulator (one degree of freedom). For this friction beating strategy, the dry friction will be cancelled approximately by computing the required cancellation force with a mathematical dry friction model. Since friction depends mainly on the relative velocity between the contacting bodies, velocity measurements are needed for the friction compensation. However, the controlled mechanical system under consideration is only equipped with position sensors and not with velocity sensors. The controlled system is, therefore, extended with an observer to obtain velocity estimates from the position measurements. For the purpose of analysis of the resulting nonlinear closed-loop system it is desired that the order of the system is kept as low as possible. Therefore, a reduced-order observer and a linear proportional/derivative (PD) state feedback controller is applied. Consequently, the resulting nonlinear closed-loop system, consisting of the one-link robot with friction, the proportional/derivative (PD) state feedback controller, the reduced-order observer and the dry friction compensation, is only of third order.

The dry friction with Stribeck effect is modelled as a function of the steady-state velocity only. Two cases for the friction modelling are considered. For the first case, denoted as the smooth case, the discontinuous friction (discontinuity at zero velocity) is modelled using a smooth model. For the resulting smooth closed-loop system existence and uniqueness of solutions is guaranteed. However, with the smoothed friction modelling the stiction effect as encountered in real physical situations can not be described correctly. The closed-loop system is, therefore, also considered with a non-smooth friction model. The non-smooth friction model switches between a (asymmetrical) velocity/friction mapping for non-zero velocities and an external-force/friction mapping at zero velocity. Since the non-smooth friction model can return a non-zero friction force for zero velocity, it is capable of describing stiction correctly. For the closed-loop system with the non-smooth friction modelling existence and uniqueness of solutions is proven in this thesis.

For the case where the friction is modelled exactly design specifications are derived, for both the smooth and the non-smooth type of friction modelling, such that the system obeys the desired dynamics (globally asymptotically stable set-point and consequently no other equilibrium points and no limit cycling). The design criteria are based on the stability of the observer error only. Since the error dynamics of the reduced-order observer are not influenced by the controller gains, the controller gains can be chosen independently of the observer gain. The results are derived analytically and are, therefore, applicable for general single-degree-of-freedom mechanical systems for which the friction can described with one of the types of friction modelling considered.

Moreover, the results are illustrated with numerical simulations. These simulation results correspond well to analytical stability results. However, for a moderate observer gain, the observer error does become smaller than the machine accuracy. Consequently, the finite accuracy of the floating point calculations is dominant for the simulation of the closed-loop system. The use of numerical simulation to examine the behaviour of the closed-loop system is, therefore, limited.

To study the effect of small friction modelling inaccuracies, inevitable in practice, the closed-loop system is also examined with a scaled compensation rule. By simply scaling the compensation rule the effect of possible over and under-compensation can be studied. For the closed-loop system with the smooth friction modelling, it is shown analytically that the set-point for the positioning task will always be locally asymptotically stable for the under-compensated case. For the over-compensated case, a stable limit cycle exist. Using the path following technique it has been shown that this limit cycle does not exist for the under-compensated case.

For closed-loop system with the non-smooth friction modelling it is shown by numerical simulations that for the under-compensated case the set-point is stable. However, for this situation the set-point is no longer a unique equilibrium point, but a member of an equilibrium set. A zero steady-state error is, therefore, no longer guaranteed for the under-compensated case. If, however, the friction is only slightly over-compensated a stable limit cycle exists which is fatal for the positioning task. It is, therefore, advisable to under-compensated the actual friction if the friction can not be modelled perfectly. The resulting steady-state error, due to the existence of an equilibrium set instead of a unique equilibrium point, can be decreased by increasing the observer gain and the proportional controller gain or by decreasing the derivative gain. Namely, the equilibrium set becomes smaller by taking these measures.

The reduced-order observer based friction compensation for the one-link robot is also studied experimentally. For the practical implementation, the friction is modelled with the non-smooth friction model. In practice friction modelling errors are inevitable. The experimental results are, therefore, compared with the numerical results for the non-exact case with the non-smooth type of friction modelling. Although, for the practical implementation the error in the friction modelling is far more complicated than accounted for by simply scaling the compensation model, the experimental results agree well with the numerical results.

The disappearance of the limit cycling behaviour and the increase of the maximum steady-state error for a compensation rule with a decreasing scaling parameter is also confirmed experimentally. By assuring that the friction never over-compensated, the application of the reduced-order observer based friction compensation results in an increase of positioning accuracy for this one-link robot, even in the presence of small friction modelling errors.

Samenvatting

Wrijving, en droge wrijving in het bijzonder, vormt een belemmering voor het realiseren van voldoende positie nauwkeurigheid van geregelde mechanische systemen. Voor het verkrijgen van een voldoende positie nauwkeurigheid zonder gebruik te maken van zeer strakke regelaars, kan een wrijvingscompensatie strategie worden toegepast. In deze scriptie is de toepassing van een dergelijke strategie voor een robot met een enkele arm (één graad van vrijheid) behandeld. Voor deze strategie zal de geregelde robot worden geactueerd met een extra wrijvingscompensatie kracht, welke volgt uit een model van de droge wrijving. De wrijving is voornamelijk afhankelijk van de snelheid. De berekening van de compensatiekracht vereist dus kennis ten aanzien van de snelheid van de arm. Echter, de robot is alleen uitgerust met een positiesensor en niet met een snelheidssensor. Het geregelde systeem is daarom uitgebreid met een waarnemer om de snelheid te kunnen schatten uit de positiemetingen.

Voor de analyse van het resulterende niet-lineaire dynamische systeem is het gewenst dat de orde van dit systeem zo laag mogelijk blijft. Daarom is er gekozen voor een reduceerde waarnemer en een lineaire regelaar met alleen een proportionele en differentieërende terugkoppeling. Het resulterende systeem, bestaande uit de robot met wrijving, de proportionele en differentieërende toestandsterugkoppeling, de gereduceerde waarnemer en de droge wrijvingscompensatie, is hierdoor een derde-orde systeem. Er zijn tevens maar drie ontwerpvariabelen, de twee terugkoppelversterkingen voor de regelaar en een waarnemerversterking waarmee de foutdynamica van de gereduceerde waarnemer kan worden beïnvloed.

De droge wrijving met Stribeck effect is gemodelleerd als een statische functie van de snelheid alleen. Er twee modellen van droge wrijving toegepast. Voor het eerste model de discontinu droge wrijving (discontinuïteit bij snelheid nul) is benaderd met een glad wrijvingsmodel. Toepassing van deze gladde beschrijving van de droge wrijving voor de geregelde robot met wrijvingscompensatie levert voor de dynamica van de robot een set gladde differentiaal vergelijking op. Existentie en uniciteit van oplossingen is voor een glad stelsel van differentiaal vergelijking gegarandeerd. Echter met dit gladde model droge wrijvingsmodel kan het blijven plakken van twee onderdelen aan elkaar door de aanwezigheid van de wrijving niet exact worden beschreven. De geregelde robot met wrijvingscompensatie is daarom ook bestudeerd met een niet gladde beschrijving van de wrijving. Dit model schakelt tussen een (asymmetrische) snelheid gerelateerde beschrijving voor snelheden ongelijk aan nul en een externe kracht gerelateerde beschrijving als de snelheid gelijk is aan nul. Existentie en uniciteit van oplossingen voor de resulterende set niet-gladde differentiaal vergelijkingen is aangetoond in deze scriptie.

Voor beide methoden van wrijvingsmodellering zijn ontwerpcriteria afgeleid waarmee de geregelde robot met wrijvingscompensatie de gewenste dynamica bezit: globale asymptotische stabiliteit van het gewenste evenwichtspunt en dus geen andere evenwichtspunten en geen andere periodieke oplossingen. Deze ontwerpcriteria berusten alleen op de stabiliteit van de waarnemerfout. Aangezien de foutdynamica van de waarnemer niet wordt beïnvloed

door de regelaar instellingen, kunnen deze onafhankelijk worden gekozen van de waarnemer instelling. De resultaten zijn analytisch afgeleid en zijn dus toepasbaar voor geregelde systemen onderhevig aan wrijving en met een enkele graad van vrijheid in het algemeen.

De resultaten worden geïllustreerd met numerieke simulaties. De simulatie resultaten komen goed overeen met de analytische resultaten. Echter, al voor lage waarden van de waarnemer versterking komt de waarnemerfout in de buurt van de machine nauwkeurigheid van het gebruikte rekenprogramma. In dit gebied is de eindige nauwkeurigheid van de numerieke rekenwijze dominant. Het gebruik van de numerieke simulaties voor het bestuderen van het dynamisch gedrag van de geregelde en gecompenseerde robot is hierdoor beperkt.

Voor het verkrijgen van inzicht in het effect van kleine onnauwkeurigheden in de wrijvingsmodellering, is de geregelde robot met wrijvingscompensatie ook bestudeerd met een geschaalde wrijvingscompensatiewet. Door deze compensatiewet te schalen kan het effect van onder- en overcompensatie van de wrijving op het positioneringsgedrag van de robot onderzocht worden. Voor het model van de geregelde robot met wrijvingscompensatie met de gladde beschrijving van de wrijving is het analytisch aangetoond dat het gewenste evenwichtspunt altijd lokaal asymptotisch stabiel is voor het ondergecompenseerde geval. Als de wrijving ook maar enigszins wordt overgecompenseerd dan wordt stabiel periodiek gedrag geïnduceerd zodat de arm niet meer tot rust komt in het gewenste evenwichtspunt. Dit gedrag is fataal voor de positioneer taak en dient dus te worden voorkomen. Het is aangetoond middels het numeriek volgen van deze periodiek oplossing voor een teruglopende schalingsconstante dat deze periodieke oplossing niet bestaat voor de ondergecompenseerde toestand.

Voor de geregelde robot met wrijvingscompensatie en niet-gladde beschrijving van de wrijving is het numeriek aangetoond dat het gewenste evenwichtspunt stabiel is voor het ondergecompenseerde geval. Echter voor dit geval ligt het gewenste evenwichtspunt in een evenwichtsset en de positioneringsfout is dus niet meer gegarandeerd gelijk aan nul. Bovendien treedt er ook stabiel periodiek gedrag op als de wrijving wordt overgecompenseerd. Indien de wrijving niet perfect te modelleren is wordt er daarom geadviseerd om te kiezen voor een beperkte ondercompensatie van de wrijving in plaats van een overcompensatie. De resulterende positioneringsfout kan vervolgens worden gereduceerd door het verhogen van de proportionele terugkoppelversterking van de regelaar, het verhogen van de waarnemerversterking of middels het verlagen van de differentiërende terugkoppelversterking van de regelaar. Deze maatregelen leiden namelijk tot een verkleining van de evenwichtsset.

De wrijvingscompensatie gebaseerd op de reduceerde waarnemer is tevens getest op de experimentele opstelling van de robot. Voor de praktische implementatie de wrijving is gemodelleerd middels de niet-gladde beschrijving. In de praktijk zijn foutjes in de wrijvingsmodellering onvermijdelijk. De experimentele resultaten zijn, daarom, vergeleken met de numerieke resultaten voor de geregelde robot met de geschaalde wrijvingscompensatie en niet gladde beschrijving van de wrijving. Hoewel de fout in wrijvingsmodellerings voor de praktische implementatie veel complexer van aard zal zijn dan de geïnduceerde fout door het simpel schalen van de compensatie wet komen de experimentele resultaten kwalitatief goed overeen met de numerieke resultaten.

Het verdwijnen van het ongewenste periodieke gedrag en de toename van de maximale positioneringsfout door de wrijvingswet terug te schalen is tevens experimenteel waargenomen. Zolang de wrijving niet wordt overgecompenseerd kan de wrijvingscompensatie gebaseerd op de gereduceerde waarnemer dus succesvol worden toegepast in de praktijk, zelfs met de onvermijdelijke onnauwkeurigheden in de wrijvingsmodellering.

List of Symbols

b	viscous friction coefficient	[Nm · s/rad]]
e	observer error $e = x_2 - \hat{x}_2$	[rad/s]
$f(v), f(x_2)$	static friction model	[Nm]
$f(u, v), f(u, x_2)$	static non − smooth friction model	[Nm]
$\tilde{f}(u_c, \hat{x}_2)$	non − smooth compensation rule	[Nm]
$\underline{\mathrm{f}}_s$	smooth vector field	
$\underline{\mathrm{f}}_{ns}$	non − smooth vector field	
F_c	coulomb friction force	[Nm]
F_d	dry friction	[Nm]
F_{ex}	external force	[Nm]
F_s	break away force	[Nm]
$g(v)$	Stribeck curve	[Nm]
J	inertia	[kg · m^2/rad]
I	identity matrix	
$l(x, y)$	open line segment $l(x, y) = \{\theta x + (1 - \theta)y, 0 < \theta < 1\}$	
$\max(x^*)$	maximum value of equilbrium set	
n_1	proportional feedback gain	[Nm/rad]
n_2	derivative feedback gain	[Nm · s/rad]
$\underline{\mathrm{n}}_i$	vector normal to switch plane Σ_i	
N	control gain vector $N = [n_1, n_2]$	
L	observer gain	[1/s]
L_c	critical value for observer gain	[1/s]
q, x_1	position	[rad]
$\dot{q}, v, x_2$	velocity	[rad/s]
t	time	[s]
TOL	numerical integration tolerance	
u	total applied torque $u = u_c + u_{fc}$	[Nm]
u_c	control torque	[Nm]
u_{fc}	friction compensation torque	[Nm]
v_s	Stribeck velocity	[rad/s]
x_c	observer state $x_c = x_2 - Lx_1$	[rad/s]
$\underline{\mathrm{x}}$	state vector $[x_1, x_2]^T$	
$\underline{\mathrm{x}}_a$	state vector $[x_1, x_2, x_c]^T$	
$\underline{\mathrm{x}}_b$	state vector $[x_1, x_2, \hat{x}_2]^T$	
$\underline{\mathrm{x}}_c$	state vector $[x_1, x_2, e]^T$	

β	Stribeck shape parameter	[–]
δF	$\delta F = F_s - F_c$	[Nm]
ϵ_{mach}	machine accuracy	[–]
ε	steepness parameter for smooth friction model	[–]
η	tickness parameter for numerical implementation	[rad]
Σ	switch surface	

$[a, b]$	interval $\{x \in \mathbb{R} \vert a \leq x \leq b\}$
$\{a, b\}$	set comprising the elements a and b
$x \in A$	x is an element of the set A
$x \subset A$	x is a subset of A
$A \cup B$	union of set A with set B
$A \cap B$	intersection of set A with set B
$a \rightarrow b$	a tends to b
$a \downarrow b$	a decreases towards b
$a \uparrow$	a increases
$a \downarrow$	a decreases
$p \Rightarrow q$	p implies q
$\|\underline{x}\|$	norm of $\underline{x}$
$\|x\|$	absolute value of x
$\hat{x}$	estimate of x
$\dot{x}$	first time derivative of x
$\ddot{x}$	second time derivative of x
$f'(x)$	first derivative of $f(x)$ with respect to x
$\forall$	for all

$$\operatorname{sgn}(x) = \begin{cases} 1 & \text{if } x > 0 \\ -1 & \text{if } x < 0 \\ 0 & \text{if } x = 0 \end{cases}$$

Chapter 1

Introduction

In many controlled mechanical systems, such as for example optical disk-drives and assembly robots, positioning accuracy is a main contributor to the overal system performance. In all of these mechanical systems friction is present. Friction is an impediment for the position accuracy of controlled mechanical systems. To obtain a sufficiently high position accuracy without the need for a high gain controller, the controlled mechanical system must be extended with a *friction beating strategy.* The succes of such a strategy is, consequently, closely related to the overall performance of the controlled mechanical system. This thesis concerns the analysis of a closed-loop system following from a mechanical system with friction extended with a simple controller and a practically implementable friction beating strategy. The results will provide the necessary insight from both a control and a dynamical point of view such that application this friction beating strategy will give the desired gain in system performance.

In the remainder of this chapter an introduction on friction, the consequences of friction for the performance of controlled mechanical systems and observers is given. Next, the goal of this thesis is formulated and the chapter ends with the outline of the succeeding chapters.

1.1 Friction

Between all contacting bodies which may move relative to each other a contact force in the direction of motion is induced. This force, which in general is highly nonlinear and depends on many conditions such as for example normal load, relative velocity and temperature, is known as dry or Coulomb friction [1]. For understanding the behaviour of dry friction, one has to consider the interaction of contacting surfaces which are very rough on a microscopical scale, as illustrated in figure 1.1. For lubricated contacts there exists a small fluid film between these rough surface contacts. The thickness of this fluid film increases for increasing relative velocity and is of great influence on the frictional behaviour. Four friction regimes, classified by relative velocity, can therefore be distinguished for increasing relative velocity: static friction, boundary lubrication, partial fluid lubrication and full fluid lubrication. In the first regime, the contacting bodies *stick* to each other, a phenomenon also often denoted as *stiction.* The friction in this regime is not dependent on the relative velocity but on the

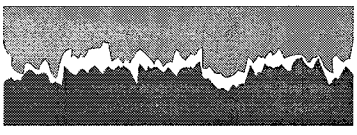

Figure 1.1: Contact between surfaces on a microscopical scale.

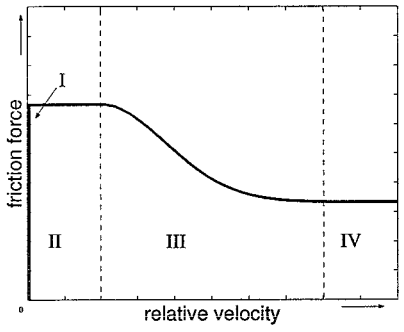

Figure 1.2: Four dry friction regimes : static friction (stiction) (I), boundary lubrication (II), partial fluid lubrication (III) and full fluid lubrication (IV), depicted for positive relative velocity only .

net external force working on the bodies in the direction of sliding. Within the other three regimes the characteristics of the friction depend on the relative velocity. In figure 1.2, a typical shape of the dry friction force within the four regimes is depicted [1].

In addition to dry friction also an other dissipative force proportional to the velocity acts on every moving body known as viscous friction. Since the dry friction characteristics are the dominant factors in performance deterioration of controlled mechanical systems [1], viscous friction characteristics are not considered in more detail.

1.2 Friction in Controlled Mechanical Systems

In controlled mechanical systems concerning positioning tasks, dry friction can give rise to large steady-state errors, large settling times, limit cycling and stick-slip behaviour [1, 2]. From a control point of view, dry friction is therefore an undesired phenomenon and special friction beating strategies must be pursued. Some possible strategies are:

I **High Gain Controllers :** The influence of dry friction can to some extent be reduced by classical high gain controllers. High gain controllers results in fast controller poles. Consequently, an obvious disadvantage of this strategy is the requirement for fast online computation. Another drawback of this strategy is the possibility of for undesired limit cycling [1, 2]. The independency of this strategy with respect to detailed characteristics of the friction is clearly a big advantage.

II **Dither :** By injection of an additional high frequent signal friction effects, such as stick-slip and large steady state-errors, can be reduced to some extent. Moreover, for this strategy no detailed characteristics of the friction have to be known, but it may have undesirable consequences such as the excitation of unmodelled dynamics and fast fatigue of the system actuators [3, 12].

III **Friction Compensation :** If one can predict the actual friction force, then it can be cancelled out by applying an extra force in opposite direction of the friction force. For the prediction of the actual friction with a mathematical model measurements of the states, on which the mathematical friction model depends, are required. In practice often only position measurements are available and since friction depends mainly on velocity, special precautions must be taken. Therefore, the succes of the strategy is

closely related to, firstly, the accuracy of the modelling of the friction phenomenon and, secondly, the availability of the required measurements. Another drawback is possible undesired limit cycling behaviour if the friction is over-compensated [4].

Other strategies follow from the combination of different strategies or extensions like adaptive friction compensation where the parameters for the applied mathematical model automatically adapt to small variations in the actual friction due to for example temperature changes.

1.3 Observers

In practice not all the states, for example the position and velocity, of a controlled mechanical system are measured. The required sensors could simply be too costly, require too much volume or be too heavy. For the estimation of the velocity using position measurements only, numerical differentiation is not desirable since it is very sensitive to measurement noise. Therefore, one has to to rely on a more sophisticated estimator. A regular or full-state observer consist of a full-order model of the system dynamics. By feeding the same input, for example the control force, to the observer as fed to the actual system and starting from the correct initial condition, the states of the observer will be a satisfactory estimator for the actual states. However, it is the lack of information about the actual state values, and consequently also about the initial condition, that requires the application of an estimator.

For successful application of an observer, the observer error, following from a poor estimate for the initial condition, must converge to zero asymptotically. To be able to influence the rate at which the state estimate converges to the true state, the observer is often extended with a feedback loop on the observer error. With an extra feedback loop, a regular observer has as many design variables, in the form of observer feedback gain values, as states to estimate. Extending a controlled system with a full-state observer, therefore, doubles the number of state equations and adds the same number of design variables as the number of states of the actual system.

To reduce the number of extra state equations and design variables a reduced-order observer is a good alternative. A reduced-order observer estimates, in contrast to a regular observer who estimates the full state vector, only those states which are not directly measured. Extending the system with a reduced observer information on each state, in the form of measurements or estimates, is available. A drawback of the reduced observer is the lack of measurement noise suppression. If there is significant noise in the measurements it is better to implement a regular observer since, in addition to estimating unmeasured states, the regular observer also filters the measurements [8].

1.4 Goal of the Thesis

In this thesis, an extension of strategy III, as described in section 1.2, for compensating dry friction in a controlled mechanical system, concerning a positioning task, will be examined. The controlled system is only equipped with a position sensor and not with velocity sensors. As mentioned before, measurements of the states, on which the mathematical friction model depends, are required for this type of friction compensation. Dry friction depends mainly on the relative velocity. The controlled system must, therefore, be extended with an observer to obtain velocity estimates from the position measurements. The following questions now arise on the interaction of the dynamics of the observer and the highly nonlinear friction :

1. How will the controlled system, extended with an observer and friction compensation

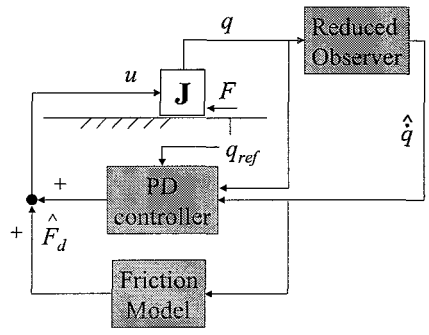

Figure 1.3: Schematic illustration of reduced observer based friction compensation strategie (with F the actual friction consisting of dry and viscous friction ($F = F_d + F_v$), $\hat{F}_d$ the estimated dry friction, q the measured position, q_{ref} the desired position, $\hat{\dot{q}}$ the estimated velocity, J the inertia of the system and u the applied torque).

behave (stable or unstable equilibria, exhibit limit-cycling) depending on settings of the controller and the observer?

2. How can one design a combination of controller, friction compensation and observer such that the desired position is an asymptotically stable equilibrium point of the resulting closed-loop system which consequently does not exhibit limit-cycling?

Analysis of high-order nonlinear dynamical systems depending on multiple design variables is a complex task. To gain in-depth insight in the behaviour of controlled mechanical systems with friction the research will, therefore, often start with the study of a relatively simple system and controller to keep both the order of the total system and the amount of design variables as low as possible. To examine the interaction between an observer and friction, a system with only one degree of freedom will be studied. For the estimation of the velocity a reduced-order observer will be applied such that the combination of the system and observer dynamics will have a minimum number of design variables and is described by a minimum number of state equations. The controller will be of the form of a linear proportional derivative (PD) feedback and the complete system will, therefore, have only three design variables (two controller gains and a single observer gain). The strategy is illustrated schematically in figure 1.3. The goal of this thesis can be formulated as

How can one design a combination of a linear PD controller, friction compensation and a reduced observer such that the practical implementation will be successful and the performance of the controlled mechanical system will be improved.

1.5 Outline of the Thesis

In chapter 2, first the experimental setup will be described, the state equations for the complete system (mechanics, controller and observer) are derived and the values of the physical parameters are identified. In chapter 3, the complete system is analyzed for a smoothed friction description and, in chapter 4, the same analysis is performed for a non-smooth description of the friction. In chapter 5, the consequences of under- or over-compensation due to inaccuracies of the friction model will be examined. In chapter 6, the theoretical results and numerical simulation results will be compared with experimental results and, in the last chapter, conclusions will be drawn and recommendations for further research will be given.

Chapter 2

Closed-Loop System and Some First Properties

In this chapter first the modelling of the dry friction phenomenon will be addressed. Subsequently, the experimental setup, used as a carrier for this project, will be introduced and the model parameters will be identified. Moreover, the design of the controller, the reduced-order observer and the friction compensation is discussed and the resulting closed-loop system is presented. In the second part of this chapter some general characteristics of the closed-loop system are discussed.

2.1 Dry Friction Modelling

In this section, more details on the modelling of dry friction will be given. The plotted curve in figure 1.2 which describes the continuous transition from the stick regime to the slip regime is denoted as the Stribeck curve. For static friction modelling, and consequently neglecting dynamical effects, the Stribeck curve is often modelled as an exponential function of relative velocity only. A typical static friction model will then be of the form

$$f(v) = g(v)\mathrm{sgn}\,(v)\,, \tag{2.1}$$

with the Stribeck curve

$$g(v) = F_c + \delta F e^{-\left(\frac{|v|}{v_s}\right)^{\beta}}, \tag{2.2}$$

where F_c is the Coulomb friction force, δF the difference between the static and Coulomb friction force ($\delta F = F_s - F_c$), v_s the Stribeck velocity and β the Stribeck shape parameter. From a physical point of view the friction model (2.1) is not exact. Since with $\mathrm{sgn}\,(0) = 0$ there will be no friction for zero velocity and the stiction phenomenon as encountered in real physical situations can, therefore, not be described with this friction model. From a mathematical point of view, (2.1) is not directly applicable since due to the discontinuous sign function existence of solutions for differential equations with a discontinuous right-hand side is not guaranteed. In this thesis two variations on (2.1) for describing the by nature discontinuous friction will, therefore, be followed. In the first approach, the discontinuous sign function will be smoothed. The resulting friction model will be smooth but is unable to describe the stiction phenomenon correctly. For the second approach, different descriptions of the friction for the stick and slip phase are applied resulting in a non-smooth friction model. The non-smooth friction model is able to describe stiction correctly.

In the literature [1], values for the Stribeck shape parameter are found between $0.5 \leq \beta \leq 2$. With $\beta < 1$ the first derivative of (2.2) with respect to v becomes unbounded making the

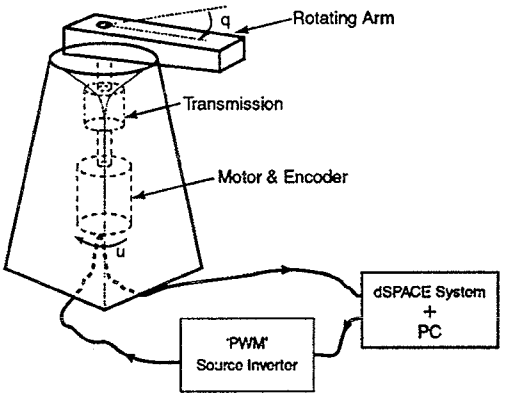

Figure 2.1: Controlled one-link robot setup.

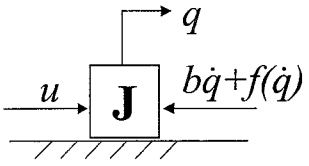

Figure 2.2: Schematic representation of the one-link robot (with q the position of the link, $\dot{q}$ the velocity of the link, J the inertia of the total driveline, b the viscous friction coefficient, $f(\dot{q})$ the dry friction and u the applied torque).

exponential description of the Stribeck curve undesirable for differential equations. Namely, with unbounded derivatives existence and uniqueness of solutions of the differential equations is not guaranteed. Therefore, only values for the shape parameter $\beta \geq 1$ will be considered.

2.2 Modelling of the one-link Robot

The system under consideration is a controlled one-link robot as depicted in figure 2.1. The setup is equipped with only a position sensor and from previous research [2] it is known that the positioning behaviour of this setup suffers largely from friction phenomena. This one-link robot is, therefore, a good carrier for the research of the combination of the PD controller, friction compensation and a reduced-order observer.

If the total driveline of the robot is considered backlash free and infinitely stiff the one-link robot can be schematically represented as in figure 2.2. The dynamics of the simplified one-link robot as depicted in figure 2.2 can be described by the following state equations

$$\begin{aligned} \dot{\underline{x}} &= A\underline{x} + B\underline{u} = \begin{bmatrix} 0 & 1 \\ 0 & -\frac{b}{J} \end{bmatrix} \underline{x} + \begin{bmatrix} 0 \\ \frac{1}{J} \end{bmatrix} (u - f(x_2)) \\ y &= C\underline{x} = \begin{bmatrix} 1 & 0 \end{bmatrix} \underline{x}, \end{aligned} \tag{2.3}$$

with $\underline{x} = \begin{bmatrix} q & \dot{q} \end{bmatrix}^T = \begin{bmatrix} x_1 & x_2 \end{bmatrix}^T$, J the total moment of inertia of the driveline plus arm, b the viscous friction coefficient, u the applied input torque and $f(x_2)$ the dry friction torque.

2.3 Closed-Loop System Design

System (2.3) is only equipped with an angular positioning sensor. For friction compensation, velocity measurements are required and, therefore, the system is extended with a reduced-order observer to estimate the velocity. A reduced-order linear observer has, in comparison with a full-state linear observer, less design variables and is of lower order. The resulting closed-loop system will, therefore, be of minimum order and has only three design variables.

To derive a reduced-order observer for a linear second-order single-input single-output system, the system is defined such that the output equals the first state. The system matrices can now be partitioned as

$$\begin{bmatrix} \dot{x}_a \\ \dot{x}_b \end{bmatrix} = \begin{bmatrix} A_{aa} & A_{ab} \\ A_{ba} & A_{bb} \end{bmatrix} \begin{bmatrix} x_a \\ x_b \end{bmatrix} + \begin{bmatrix} B_a \\ B_b \end{bmatrix} u \tag{2.4}$$

$$y = x_a. \tag{2.5}$$

By introducing the observer state $x_c = x_b - Ly$ with L a proportional observer gain, the reduced-order observer obeys

$$\begin{aligned} \dot{\hat{x}}_c &= \dot{\hat{x}}_b - L\dot{x}_a = A_{bb}\hat{x}_b + A_{ba}x_a + B_b u - L\left(A_{aa}x_a + A_{ab}\hat{x}_b + B_a u\right) \\ &= \left(A_{bb} - LA_{ab}\right)\hat{x}_c + \left(\left(A_{ba} - LA_{aa}\right) + \left(A_{bb} - LA_{ab}\right)L\right)y + \left(B_b - LB_a\right)u. \end{aligned} \tag{2.6}$$

With this observer, the observer error $e_c = x_c - \hat{x}_c$ obeys the following linear dynamics

$$\dot{e}_c = \left(A_{bb} - LA_{ab}\right)e_c. \tag{2.7}$$

If the system is assumed to be observable [8], then $A_{ab} \neq 0$ must hold. The error-dynamics for the reduced-order linear observer can, therefore, be fully influenced with the observer gain L if the system is observable.

Application of the reduced-order linear observer (2.6) to the nonlinear system (2.3) yields

$$\dot{\hat{x}}_c = \left(-\frac{b}{J} - L\right)\hat{x}_c + \left(-\frac{b}{J} - L\right)Lx_1 + \frac{1}{J}(u - \hat{f}(\hat{x}_c + Lx_1)), \tag{2.8}$$

with $\hat{f}(\hat{x}_c + Lx_1)$ an estimate of the current dry friction following from a friction model and the estimated velocity, defined by

$$\hat{x}_2 = \hat{x}_c + Lx_1. \tag{2.9}$$

To be able to control system (2.3) and compensate the dry friction, the input u will consist of a controller force (u_c) plus a friction compensation force (u_{fc}):

$$u = u_c + u_{fc}. \tag{2.10}$$

For compensation of the actual dry friction the compensation force is taken as $u_{fc} = \hat{f}(\hat{x}_c + Lx_1)$ and, consequently, from (2.10) it follows that $u - \hat{f}(\hat{x}_c + Lx_1) = u_c$.

In order to control the one-link robot a proportional derivative (PD) controller will be used:

$$u_c = N \begin{bmatrix} x_{1,ref} - x_1 \\ x_{2,ref} - x_2 \end{bmatrix}, \tag{2.11}$$

with the control feedback gain $N = \begin{bmatrix} n_1 & n_2 \end{bmatrix}$. Without loss of generality, the origin ($\begin{bmatrix} x_{1,ref} & x_{2,ref} \end{bmatrix}^T = \underline{0}$) is assumed to be the desired reference position. Moreover, since

no velocity measurements are available, the estimated velocity is used for the derivative feedback action. The resulting control action reads as

$$u_c = -N \begin{bmatrix} x_1 & \hat{x}_2 \end{bmatrix}^T = -(n_1 + n_2 L)\, x_1 - n_2 \hat{x}_c. \tag{2.12}$$

Extending the system equations (2.3) with the reduced observer (2.8), the friction compensation and substitution of the control law (2.12) results in a set of state equations of third-order, describing the controlled one-link robot with friction compensation in terms of the states $\underline{x}_a = \begin{bmatrix} x_1 & x_2 & \hat{x}_c \end{bmatrix}^T$

$$\dot{\underline{x}}_a = A_a \underline{x}_a + \zeta(\underline{x}_a) = \begin{bmatrix} 0 & 1 & 0 \\ -a_1 & -a_2 & -a_3 \\ -a_4 & 0 & -a_5 \end{bmatrix} \underline{x}_a + \frac{1}{J} \begin{bmatrix} 0 \\ \hat{f}(\hat{x}_c + L x_1) - f(x_2) \\ 0 \end{bmatrix}, \tag{2.13}$$

with

$$\begin{aligned} a_1 &= \frac{n_1 + n_2 L}{J},\ a_2 = \frac{b}{J},\ a_3 = \frac{n_2}{J} \\ a_4 &= \frac{Lb + n_1 + n_2 L + L^2 J}{J} \text{ and } a_5 = \frac{LJ + b + n_2}{J}. \end{aligned} \tag{2.14}$$

2.4 System Identification

Using a frequency-domain identification technique, the total inertia of the system is identified in [2] to be $J = 0.026$ kgm^2/rad. For the identification of the friction parameters, first, the static break away force (F_s) is estimated for positive and negative velocity separately. The break-away forces are estimated by slowly ramping up the input torque until the arm starts rotating. For both positive and negative velocity the input torque is increased with a rate of 0.005 [Nm/s] and 16 different initial positions distributed over the entire revolution are used to cancel possible position-dependency and measurement noise. The resulting estimates for F_s are shown in table 2.1.

For the estimation of the other four friction parameters, input torques computed by a PID control for several constant velocity references are measured. For each constant velocity reference the computed input torque is averaged over a full rotation to cancel possible position-dependency and measurement noise. With a nonlinear least-squares technique the Stribeck curve (2.2) with a viscous friction term is fitted to the measured data for both positive and negative velocity separately. The shape parameter β is manually varied because no lower bound could be implemented in the least squares approach. The results of the least squares fit for the shape parameter value which gave the most satisfactory results are shown in table 2.1 and are depicted in figure 2.4 and 2.3. It can be noted that the friction values for positive and negative velocity differ significantly. For the analysis both a symmetrical friction model, based on the average of the identified values for positive and negative velocity, and an asymmetrical friction model will be used.

Now the closed-loop system equations are derived and the system parameters are identified the modelling part of the closed-loop system is finished. In the second part of this chapter two general properties of the closed-loop system will be derived which hold irrespectively of how the friction is modelled.

parameter	positive velocity	negative velocity	average
β [-]	1	1	1
F_s [Nm]	0.5735 ($\sigma = 10\%$)	0.5123 ($\sigma = 8\%$)	0.5429
F_c [Nm]	0.3990	0.3887	0.3939
v_s [rad/s]	0.0688	0.0817	0.0753
b [Nms/rad]	0.0828	0.0790	0.0809

Table 2.1: Results of friction identification.

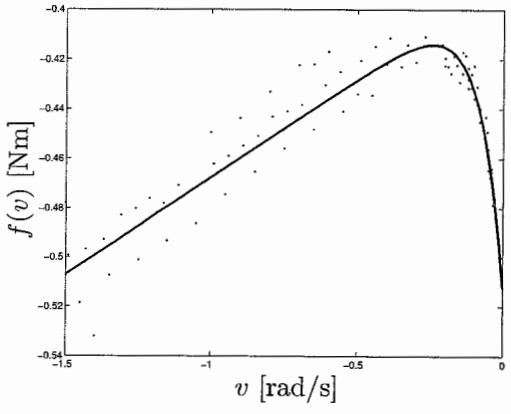

Figure 2.3: Friction measurements (dots) and fit (solid line) for negative velocity.

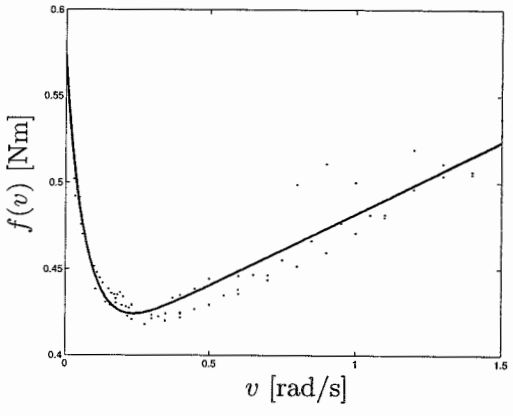

Figure 2.4: Friction measurements (dots) and fit (solid line) for positive velocity.

2.5 Linear Part of the Closed-Loop System

If the closed-loop system (2.13) is considered without dry friction and friction compensation the resulting system equations become linear. For a stability analysis of the linear part of (2.13) the system equations are presented in the states $\underline{x}_c = \begin{bmatrix} x_1 & x_2 & e \end{bmatrix}^T$

$$\dot{\underline{x}}_c = \begin{bmatrix} 0 & 1 & 0 \\ -c_1 & -c_2 & c_3 \\ 0 & 0 & -c_4 \end{bmatrix} \underline{x}_c = \begin{bmatrix} A+BN & K \\ 0 \quad 0 & -c_4 \end{bmatrix} \underline{x}_c, \tag{2.15}$$

with A and B from (2.3), $N = \begin{bmatrix} n_1 & n_2 \end{bmatrix}$, $K = \begin{bmatrix} 0 & c_3 \end{bmatrix}^T$, $c_1 = n_1/J$, $c_2 = (b+n_2)/J$, $c_3 = n_2/J$ and $c_4 = (b+LJ)/J$. The characteristic equation for (2.15) is equal to

$$\det\left(\lambda I - [A+BN]\right)(\lambda - c_4) = 0. \tag{2.16}$$

The set of poles of the closed-loop system consist of the union of the controller poles following from the characteristic equation $\det\left(\lambda I - [A+BN]\right) = 0$ and the observer pole c_4. Consequently, the controller and observer design can be carried out independently and when they are combined the poles remain unchanged. This principle of individual design of controller and observer for linear systems is known as the separation principle [8].

From (2.15), it follows that the observer error dynamics for (2.13) without dry friction and friction compensation obeys the following linear dynamics

$$\dot{e} = \dot{x}_2 - \dot{\hat{x}}_2 = -c_4 e. \tag{2.17}$$

For the linear part of (2.13) the observer error will be asymptotically stable if $c_4 > 0$ and therefore if $L > -b/J$. The controller poles follow from the closed-loop system matrix $A+BN$ with characteristic equation

$$\lambda^2 + \frac{b+n_2}{J}\lambda + \frac{n_1}{J} = 0. \tag{2.18}$$

From *Routh's Stability Criterion* [8] necessary and sufficient conditions for the controller gains n_1 and n_2 are obtained such that the closed-loop system will be asymptotically stable. The resulting conditions are $n_2 > -b$ and $n_1 > 0$. Since in this thesis the controller and observer gains are only considered to be positive, the origin is always an asymptotically stable equilibrium point of the linear part of (2.13).

2.6 Proof for Boundedness of Solutions

Since in (2.13) the linear part ($\dot{\underline{x}}_a = A_a \underline{x}_a$) is asymptotically stable and the non-linearity is bounded (note that $\|\zeta(\underline{x}_a)\| = \|f(\hat{x}_2) - f(x_2)\|/J \leq 2F_s/J$), boundedness of solutions for (2.13) can be proven. The proof starts with the *Lyapunov equation* [7]

$$A_a^T P + P A_a = -Q. \tag{2.19}$$

Since A_a is Hurwitz, the unique symmetric solution of (2.19), for given symmetric $Q > 0$, satisfies $P > 0$. Now, consider the Lyapunov candidate function

$$V(\underline{x}_a) = \underline{x}_a^T P \underline{x}_a, \tag{2.20}$$

with P the symmetric positive definite matrix following for a symmetric positive definite matrix Q from (2.19). The time-derivative of (2.20) is equal to

$$\dot{V}(\underline{x}) = -\underline{x}_a^T Q \underline{x}_a + 2\underline{x}_a^T P \zeta(\underline{x}_a). \tag{2.21}$$

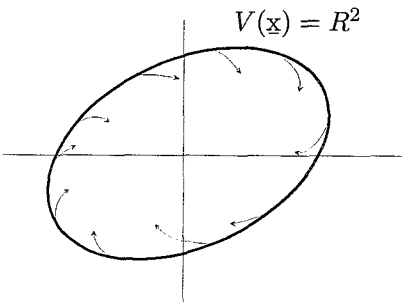

Figure 2.5: Illustration of boundedness of solutions. Since for $\{\underline{x} \in \mathbb{R}^n | V(\underline{x}) = R^2\}$ it holds that $\dot{V}(\underline{x}) \leq 0$ solutions can not leave the ellipsoid $V(\underline{x}) = R^2$.

By defining $\lambda^P_{\min}$ and $\lambda^P_{\max}$ as the smallest and largest eigenvalue of the matrix P, respectively, it follows that $\lambda^P_{\min} I \leq P \leq \lambda^P_{\max} I$. For the matrix Q follows similar $\lambda^Q_{\min} I \leq Q \leq \lambda^Q_{\max} I$ and with $\lambda^P_i, \lambda^Q_i > 0$, $i = 1, 2, 3$, it holds that

$$Q \geq \alpha P, \tag{2.22}$$

with $\alpha = \lambda^Q_{\min}/\lambda^P_{\max}$. Substitution of (2.22) in (2.21) yields

$$\dot{V}(\underline{x}_a) \leq -\alpha \underline{x}_a^T P \underline{x}_a + 2\underline{x}_a^T P \zeta(\underline{x}_a). \tag{2.23}$$

With the decomposition $P = S^T S$, with S a non-singular (n,n)-matrix, it follows that

$$|\underline{x}_a^T P \zeta(\underline{x}_a)| = |\tilde{\underline{x}}_a^T \tilde{\zeta}(\underline{x}_a)| \leq \|\tilde{\underline{x}}_a\| \|\tilde{\zeta}(\underline{x}_a)\|, \tag{2.24}$$

where $\tilde{\underline{x}}_a = S\underline{x}_a$, $\tilde{\zeta}(\underline{x}_a) = S\zeta(\underline{x}_a)$, $\|\tilde{\underline{x}}_a\| = \sqrt{\tilde{\underline{x}}_a^T \tilde{\underline{x}}_a} = \sqrt{\underline{x}_a^T P \underline{x}_a} = \|\underline{x}_a\|_P$ and similarly for $\|\tilde{\zeta}(\underline{x}_a)\| = \|\zeta(\underline{x}_a)\|_P$. Substitution of (2.24) in (2.23) yields

$$\dot{V}(\underline{x}_a) \leq -\alpha \underline{x}_a^T P \underline{x}_a + 2\|\underline{x}_a\|_P \|\zeta(\underline{x})\|_P = \|\underline{x}_a\|_P^2 \left(-\alpha + 2\frac{\|\zeta(\underline{x}_a)\|_P}{\|\underline{x}_a\|_P}\right). \tag{2.25}$$

From (2.25), it can be concluded that the interior of any ellipsoid defined by $\{\underline{x}_a \in \mathbb{R}^3 | V(\underline{x}_a) = \underline{x}_a^T P \underline{x}_a = R^2\}$ with

$$\sup_{\|\underline{x}_a\|_P = R} \frac{\|\zeta(\underline{x}_a)\|_P}{R} \leq \frac{\alpha}{2}, \tag{2.26}$$

is an invariant set as illustrated in figure 2.5. Note that since $\|\zeta(\underline{x}_a)\| \leq 2F_s/J$ also $\|\zeta(\underline{x}_a)\|_P$ is bounded and, therefore, a bounded value for R for which (2.26) holds exist. Consequently, boundedness of solutions for (2.13) is guaranteed.

Chapter 3

Closed-Loop System Analysis : Smooth Case

In this chapter, the properties of the closed-loop system with a smoothed friction model for both the actual friction and the friction compensation will be examined. A standard smoothening of the by nature discontinuous dry friction is the arctangent approximation. The resulting friction model reads as

$$f(v) = \frac{2g(v)}{\pi}\text{atan}\,(\varepsilon v)\,, \tag{3.1}$$

with $g(v)$ the Stribeck friction curve (2.2) and $\varepsilon \gg 1$. The resulting shape of the smooth friction model is depicted in figure 3.1 where the approximation improves, especially for velocities close to zero, for an increasing steepness parameter ε. The small region where the discontinuous velocity/friction mapping is smoothed is indicated by $\left|\frac{2}{\pi}\text{atan}\,(\varepsilon v)\right| \ll 1$.

With the smooth friction model the closed-loop system is described by a smooth set of ordinary differential equations for which existence and uniqueness of solutions is guaranteed. Since with the smooth friction model the friction is zero for zero velocity ($f(0) = 0$) the smooth friction model is unable to describe stiction properly. Another drawback of the smooth friction model is the stiffness of the resulting set of ordinary differential equations for increasing values of ε.

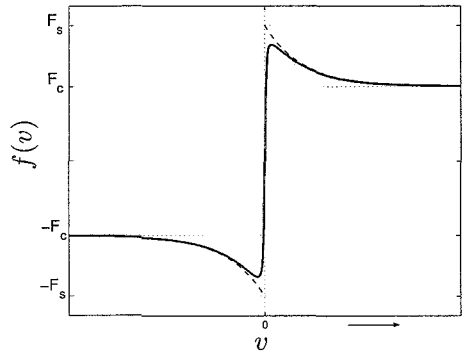

Figure 3.1: Exact friction curve $g(v)\text{sgn}\,(v)$ (dashed) and smooth friction model (solid).

For purpose of analysis, it is more convenient that the friction model depends on a single state. Therefore, the system equations of (2.13) are rewritten in terms of the states $\underline{x}_b = \begin{bmatrix} x_1 & x_2 & \hat{x}_2 \end{bmatrix}^T$

$$\dot{\underline{x}}_b = \underline{f}_s(\underline{x}_b) = \begin{bmatrix} 0 & 1 & 0 \\ -b_1 & -b_2 & -b_3 \\ -b_1 & L & -b_4 \end{bmatrix} \underline{x}_b + \frac{1}{J} \begin{bmatrix} 0 \\ f(\hat{x}_2) - f(x_2) \\ 0 \end{bmatrix}, \tag{3.2}$$

where

$$b_1 = \frac{n_1}{J}, b_2 = \frac{b}{J}, b_3 = \frac{n_2}{J} \text{ and } b_4 = \frac{LJ + b + n_2}{J}.$$

In the this chapter, first, aspects concerning the observer error will be addressed. Next equilibrium and stability issues for the closed-loop system will be examined. Subsequently the analytical results are illustrated with numerical results. The chapter ends with a short discussion.

3.1 The Zero Observer Error Set

Within the three-dimensional state-space of (3.2), a two-dimensional set is formed by the zero observer error set. This plane is defined by $e = x_2 - \hat{x}_2 = 0$. On this plane, the actual friction and friction compensation equal each other exactly ($f(\hat{x}_2) - f(x_2) = 0$). Consequently, it follows that the projection of the vector field on the normal to this plane is equal to

$$\underline{n}^T \underline{f}_s(\underline{x}_b)\big|_{x_2 = \hat{x}_2} = 0, \tag{3.3}$$

with the normal vector $\underline{n} = [0, 1, -1]^T$. The vector field (3.2) is locally parallel to the plane $x_2 = \hat{x}_2$. Consequently, solutions can neither cross nor leave this plane. The plane $x_2 = \hat{x}_2$, therefore, divides the state space of (3.2) in two parts (the sign of e can not change) and is an invariant set. Within this invariant set, the actual friction is always cancelled by the friction compensation. The closed-loop system dynamics within the zero observer error set follow, therefore, from only:

$$\dot{x}_1 = x_2 \tag{3.4}$$

$$\dot{x}_2 = -\frac{n_1}{J} x_1 - \frac{b + n_2}{J} x_2, \tag{3.5}$$

for which the origin is an asymptotically stable equilibrium point.

3.2 Observer Error Dynamics

For the implementation of the reduced-order observer it is desired that the observer error converges to zero and subsequently stays equal to zero. Therefore, global asymptotically stability of $e = 0$ is desired. In section 2.5, it is already shown that for $L > -b/J$ the observer error, and consequently the zero observer error set, will always be asymptotically stable if the system without the dry friction and compensation is considered. For (3.2) the difference between the friction compensation and the actual friction is, therefore, the only possible repelling force from the invariant set $e = 0$. From (3.2) it follows that the observer error $e = x_2 - \hat{x}_2$ obeys the following dynamics

$$\dot{e} = \dot{x}_2 - \dot{\hat{x}}_2 = -\frac{b + LJ}{J} e + \frac{f(\hat{x}_2) - f(x_2)}{J}. \tag{3.6}$$

x_2	$\hat{x}_2$	$e = x_2 - \hat{x}_2$	$f(\hat{x}_2) - f(x_2)$
0	0	0	0
>0	<0	>0	<0
<0	>0	<0	>0
0	>0	<0	>0
0	<0	>0	<0
<0	0	<0	>0
>0	0	>0	<0
>0	>0	$[-\infty, \infty]$	$(1-\alpha)[-F_s, F_s]^*$
<0	<0	$[-\infty, \infty]$	$(1-\alpha)[-F_s, F_s]^*$

*with $\alpha \downarrow 0$ for $\varepsilon \rightarrow \infty$

Table 3.1: Bounds for the difference between the friction compensation ($f(\hat{x}_2)$) and the actual friction ($f(x_2)$).

The error dynamics for $e \neq 0$ can clearly be influenced by the observer gain L and are independent of the control gains n_1 and n_2. For purpose of the stability analysis of the invariant zero observer error set ($e = 0$) *Lyapunov*'s direct method [7] will be followed. Consider the Lyapunov candidate function

$$V(x_2, \hat{x}_2) = \frac{1}{2}e^2, \tag{3.7}$$

with $e = x_2 - \hat{x}_2$. The time-derivative of (3.7) is

$$\dot{V}(x_2, \hat{x}_2) = e\dot{e} = e\left[-\frac{b + LJ}{J}e + \frac{f(\hat{x}_2) - f(x_2)}{J}\right]. \tag{3.8}$$

In table 3.1, bounds for the difference between the compensation and actual friction are shown for all possible situations. From this table, it can be noted that for all situations $e \neq 0$ other than $\text{sgn}(x_2) = \text{sgn}(\hat{x}_2)$ the difference $f(\hat{x}_2) - f(x_2)$ is always of opposite sign as the observer error. From (3.8) it follows that with $\text{sgn}(f(\hat{x}_2) - f(x_2)) \neq \text{sgn}(e)$ the time derivative of (3.7) is strictly negative and only the case $e \neq 0$ with $\text{sgn}(x_2) = \text{sgn}(\hat{x}_2)$ needs extra consideration.

The smoothed friction model is continuously differentiable and the difference between the compensation and actual friction ($f(\hat{x}_2) - f(x_2)$) can therefore be approximated with a Taylor expansion

$$f(\hat{x}_2) - f(x_2) = f(x_2 - e) - f(x_2) = -f'(x_2)e + \text{h.o.t.} \tag{3.9}$$

and, for $e \ll 1$, the higher-order terms can be neglected. Substitution of the approximation (3.9) in (3.8) yields

$$\dot{V}(x_2, \hat{x}_2)\Big|_{e \ll 1} = -\frac{b + LJ + f'(x_2)}{J}e^2. \tag{3.10}$$

The derivative of the smooth friction model with respect to x_2 is

$$f'(x_2) = \underbrace{\frac{2g'(x_2)\text{atan}(\varepsilon x_2)}{\pi}}_{<0} + \underbrace{\frac{2\varepsilon g(x_2)}{\pi(1 + \varepsilon^2 x_2^2)}}_{>0} \geq g'(x_2)\text{sgn}(x_2). \tag{3.11}$$

The lower bound for (3.11) follows from the fact that the first part of (3.11) is strictly negative and the second part strictly positive and $|\frac{2}{\pi}\text{atan}(\varepsilon x_2)| \leq |\text{sgn}(x_2)|$, $\forall x_2$. The derivative of

the Stribeck curve times the sign of the velocity is bounded from below for all non-zero velocities (see appendix A). Note that for the case $e \neq 0$ with $\text{sgn}(x_2) = \text{sgn}(\hat{x}_2)$ it follows $x_2 \neq 0$. With $(g'(x_2)\text{sgn}(x_2))_{\min} = g'(x_2)_{\min}$, therefore, a critical value for the observer gain can be derived such that

$$b + LJ + g'(x_2)\text{sgn}(x_2) > 0 \ \forall x_2 \neq 0 \text{ if } L > \frac{-g'(x_2)_{\min} - b}{J}. \tag{3.12}$$

The critical value for the observer gain is equal to

$$L > \frac{1}{J}\left(\eta\frac{\delta F}{v_s} - b\right) = L_c \text{ with } \eta = \begin{cases} 1 & \text{if } \beta = 1 \\ \frac{(\beta-1)e^{-\frac{\beta-1}{\beta}}}{\sqrt[\beta]{\frac{\beta-1}{\beta}}} & \text{if } \beta > 1 \end{cases}. \tag{3.13}$$

From the lower bound of the derivative of the smooth friction model (3.11) a sufficient condition ($L > L_c$) for locally asymptotically stability of $e = 0$ follows from (3.10). With the Mean Value, Theorem[1] it can be proven that, for $L > L_c$, the stability result not only holds for small observer errors but for arbitrary observer errors. Using the Mean Value Theorem, the difference between the compensation and actual friction can be written as

$$f(\hat{x}_2) - f(x_2) = f'(z)(\hat{x}_2 - x_2) = -f'(z)e, \tag{3.14}$$

with z some point on the line segment $l(x_2, \hat{x}_2)$. Substitution of (3.14) in (3.8) yields

$$\dot{V}(x_2, \hat{x}_2) = -\frac{b + LJ + f'(z)}{J}e^2. \tag{3.15}$$

From (3.11) it follows that $f'(z) \geq g'(\hat{x}_2)_{\min}$. Since (3.12) is based on $g'(\hat{x}_2)_{\min}$, it can be concluded that (3.15) is negative definite for $L > L_c$. The critical value (3.13) for the observer gain is, therefore, a sufficient condition for global asymptotically stability of the zero observer error set.

Also another property of the observer error dynamics can be revealed from (3.10). If x_2 is in the small region where $\left|\frac{2}{\pi}\text{atan}(\varepsilon x_2)\right| \ll 1$ it follows that (3.11) and, therefore, (3.10) are positive definite. The observer error is, therefore, in this region local asymptotically stable. For a good approximation a large value for the steepness parameter must be applied. The derivative of the smooth friction model will, therefore, be extremely steep. The rate of decay for (3.7), and consequently for e, will be locally extremely large in the region $\left|\frac{2}{\pi}\text{atan}(\varepsilon x_2)\right| \ll 1$.

For the smooth friction model only symmetrical friction can be modelled (for an asymmetrical friction curve the model must switch between separate curves for positive and negative velocity, the model would then still be continuous but not smooth). With the average values from table 2.1, the critical value for the observer gain (3.13) is equal to $L_c = 73$. In figure 3.2, the sufficient nature of the determined critical value for the observer gain for $\varepsilon = 1 \cdot 10^6$ is illustrated. From this figure, it can be noted that the area of the regions where the time-derivative of (3.7) is positive is decreasing for increasing values of L. From graphical examination it follows that the zero observer error set will be asymptotically stable for approximately $L > 68.9$ which is lower than, but close to the determined critical value.

[1] **Mean Value Theorem**: Assume that $f : \mathbb{R}^n \to \mathbb{R}$ is continuously differentiable at each point x of an open set $S \subset \mathbb{R}^n$. Let x and y be two points of S such that the line segment $l(x, y) \subset S$. Then there exist a point z on $l(x, y)$ such that $f(y) - f(x) = \frac{\partial f}{\partial x}\big|_{x=z}(y - x)$ [5].

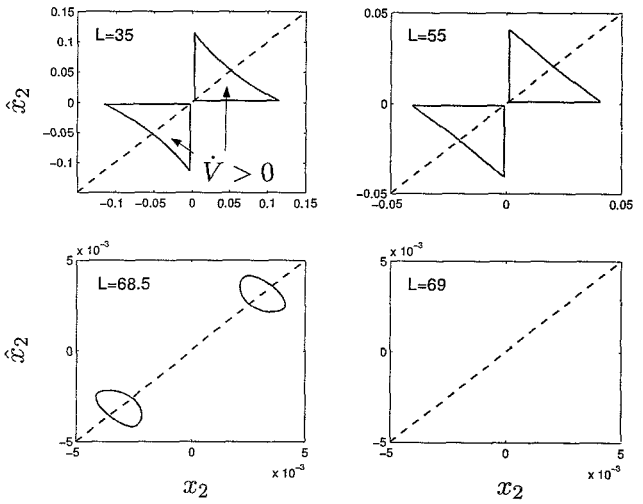

Figure 3.2: Contour plot of the regions (solid) where $\dot{V} > 0$ for increasing values of L and the zero observer error set (dashed).

3.3 Equilibrium Points

Equilibrium points for a set of ordinary differential equations follow from the algebraic set of equations $\dot{\underline{x}} = \underline{0}$. Equilibria of (3.2) trivially satisfy $x_2 = 0$ and consequently

$$-n_1 x_1 - n_2 \hat{x}_2 + f(\hat{x}_2) = 0 \tag{3.16}$$

$$-n_1 x_1 - (b + LJ + n_2)\hat{x}_2 = 0 \Rightarrow x_1 = -\frac{b + LJ + n_2}{n_1}\hat{x}_2. \tag{3.17}$$

Substitution of (3.17) into (3.16) yields

$$(b + LJ)\hat{x}_2 + f(\hat{x}_2) = 0. \tag{3.18}$$

Since $\text{sgn}\,((b + LJ)\hat{x}_2) = \text{sgn}\,(f(\hat{x}_2))$ only $\hat{x}_2 = 0$ is a solution of (3.18). Consequently, it follows from (3.17) that the origin $\underline{x}_b^* = \underline{0}$ is the unique equilibrium point of (3.2).

3.4 Local Stability of the Origin

By means of linearization of the system equations (3.2), local stability of the origin ($\underline{x}_b^* = \underline{0}$) will be examined. The Jacobian matrix of the linearization about the origin equals

$$\frac{\partial \underline{f}_s(\underline{x}_b)}{\partial \underline{x}_b} = \begin{bmatrix} 0 & 1 & 0 \\ -b_1 & -b_2 - f'(0)/J & -b_3 + f'(0)/J \\ -b_1 & L & -b_4 \end{bmatrix}, \tag{3.19}$$

with $f'(0) = 2\varepsilon F_s/\pi$ the derivative of the smooth friction model for zero velocity. The coefficients of the characteristic polynomial $\lambda^3 + a\lambda^2 + b\lambda + c = 0$ for (3.19) are equal to

$$a = f'(0)/J + b_4 + b_2 \tag{3.20}$$

$$b = b_1 + f'(0)(b_4 - L)/J + b_3 L + b_2 b_4 \tag{3.21}$$

$$c = b_1 b_4 - b_1 b_3 + b_1 f'(0)/J. \tag{3.22}$$

With Routh's Stability Criterion [8] it can be concluded that the origin will be locally asymptotical stable if and only if $a, c > 0$ and $ab > c$. Since n_1, n_2 and L are only considered

positive, it holds that $b_i > 0$, $i = 1,2,3,4$. With $f'(0)$ strictly positive, $b_4 > L$ and $b_4 > b_3$ local asymptotical stability of the origin for the closed-loop system (3.2) can be concluded. Note that this result holds for any arbitrary combination of $n_1, n_2, L > 0$.

3.5 Global Stability of the Origin for $L > L_c$

With the observer gain larger than the critical value ($L > L_c$) the zero observer error set is asymptotically stable (see section 3.2). Within this invariant set, the compensation and actual friction cancel each other exactly and the dynamics within this set follow from the asymptotically stable linear part of (3.2) only. Since solutions for (3.2) are bounded (see section 2.6) and for $L > L_c$ always tend to the zero observer error set, the origin can be considered globally attractive[2] for this case. To strengthen this result global *asymptotical stability*[3] of the origin of (3.2) for $L > L_c$ will be proven using *Lyapunov*'s direct method. Consider the Lyapunov candidate function

$$V(\underline{x}_b) = J\left[(b_1 x_1^2 + x_2^2 + \alpha e^2)/2 + \gamma|e|\right], \tag{3.23}$$

with $e = x_2 - \hat{x}_2$, $\alpha = n_2/2(b + LJ)$ and $\gamma > 0$. The time-derivative of (3.23) is equal to

$$\begin{aligned} \dot{V}(\underline{x}_b) &= J\left[b_1 x_1 \dot{x}_1 + x_2 \dot{x}_2 + (\alpha e + \gamma \mathrm{sgn}\,(e))\dot{e}\right] \\ &= -b x_2^2 - (b + LJ)(\alpha e^2 + \gamma|e|) - n_2 x_2 \hat{x}_2 + \\ &\quad (x_2 + \gamma \mathrm{sgn}\,(e) + \alpha e)(f(\hat{x}_2) - f(x_2)), \end{aligned} \tag{3.24}$$

where $d|e|/dt$ is considered to be single-valued for $e = 0$, namely $\dot{e}(e = 0) = 0$. The analysis of (3.24) will be split up in two cases. First, the case where the estimated velocity and the actual velocity are not of equal sign will be addressed. Subsequently, the case where the estimated and actual velocity are of equal sign will be addressed. Since (3.24) only depends on x_2 and $\hat{x}_2$ only stability of the origin can be proven with this Lyapunov function. However, with La Salle Invariance Principle this result will be extended to global *asymptotically* stability of the origin.

I Actual and estimated velocity not of equal sign
In section 3.2, it is shown that for $\mathrm{sgn}\,(x_2) \neq \mathrm{sgn}\,(\hat{x}_2)$ the difference between the compensation and actual friction is always of opposite sign compared to the sign of the observer error. The product $(\gamma \mathrm{sgn}\,(e) + \alpha e)(f(\hat{x}_2) - f(x_2))$ is therefore negative definite in this case. From the passivity property of the friction model ($vf(v) \geq 0$) it follows $-x_2 f(x_2) \leq 0$ and for $\mathrm{sgn}\,(x_2) \neq \mathrm{sgn}\,(\hat{x}_2)$ also $x_2 f(\hat{x}_2) \leq 0$ holds. Since $e^2 = x_2^2 - 2x_2\hat{x}_2 + \hat{x}_2^2$, the product $-n_2 x_2 \hat{x}_2$ is cancelled due to the specific choice for the constant α. As a consequence is $\dot{V}(\underline{x}_b) \leq 0$ for $\mathrm{sgn}\,(x_2) \neq \mathrm{sgn}\,(\hat{x}_2)$.

II Actual and estimated velocity of equal sign
For the case $\mathrm{sgn}\,(x_2) = \mathrm{sgn}\,(\hat{x}_2)$ the difference between the compensation and actual friction is rewritten using the Mean Value Theorem as

$$f(\hat{x}_2) - f(x_2) = f'(\hat{x}_2)\big|_{\hat{x}_2 = z}(\hat{x}_2 - x_2) = -f'(z)e, \tag{3.25}$$

with z some point on the line segment $l(x_2, \hat{x}_2)$. Substitution of (3.25) in (3.24) yields

$$\begin{aligned} \dot{V}(\underline{x}_b) &= -b x_2^2 - (b + LJ + f'(z))(\alpha e^2 + \gamma|e|) - n_2 x_2 \hat{x}_2 \\ &\quad -f'(z) x_2 e. \end{aligned} \tag{3.26}$$

[2]The equilibrium point $\underline{x} = 0$ is called globally attractive if $\lim_{t\to\infty} |\underline{x}(t)| = 0$ for all $\underline{x}(0) \in \mathbb{R}^n$[7].

[3]The equilibrium point $\underline{x} = 0$ is called globally asymptotically stable if $\underline{x} = 0$ is both stable, that is for all $t_0 \geq 0$ there exist $\delta(t_0, \epsilon)$ such that $|\underline{x}(0)| < \delta(t_0, \epsilon) \Rightarrow |\underline{x}(t)| < \epsilon \; \forall \; t \geq t_0$, as well as globally attractive [7].

From the stability analysis of the observer error (see section 3.2) it follows that $b + LJ + f'(z) > 0$ if $L > L_c$. With $\text{sgn}(x_2) = \text{sgn}(\hat{x}_2)$ it holds that $-n_2 x_2 \hat{x}_2 \leq 0$ and the only part in (3.26) which could give a positive contribution is the product $-f'(z)x_2 e = x_2(f(\hat{x}_2) - f(x_2))$. With $\text{sgn}(x_2) = \text{sgn}(\hat{x}_2)$ it holds that $|f(\hat{x}_2) - f(x_2)| \leq F_s$, from which it follows that $bx_2^2 > |x_2(f(\hat{x}_2) - f(x_2))|$ if $|x_2| > F_s/b$. For $|x_2| \leq F_s/b$, (3.26) is clearly semi-negative definite if

$$(b + LJ + f'(z))\gamma|e| \geq \left| f'(z)\frac{F_s}{b}e \right| \quad \forall e, z \tag{3.27}$$

and, therefore, if

$$\gamma \geq \sup_{\hat{x}_2 \in \mathbb{R}} \frac{|f'(\hat{x}_2)|}{(b + LJ + f'(\hat{x}_2))}\frac{F_s}{b}. \tag{3.28}$$

The supremum (3.28) exist since $f'(\hat{x}_2)$ is bounded and $b + LJ + f'(\hat{x}_2) > 0$ for $L > L_c$.

It can be concluded that the time derivative of (3.23) is semi-negative definite for the choice for γ according to (3.28), the specific choice for α and $L > L_c$. From La Salle's Invariance Principle [7], it follows that solutions always tend to the largest invariant set in $S = \{\underline{x}_b \in \mathbb{R}^3 | \dot{V}(\underline{x}_b) = 0\} = \{\underline{x}_b \in \mathbb{R}^3 | x_2 = 0 \wedge e = 0\} = \{\underline{x}_b \in \mathbb{R}^3 | x_2 = 0 \wedge \hat{x}_2 = 0\}$. Substitution of $x_2, \hat{x}_2 = 0$ in (3.2) yields $\dot{x}_1 = 0$, $\dot{x}_2 = -b_1 x_1$ and $\dot{\hat{x}}_2 = -b_1 x_1$. Consequently, the only invariant set within S is the origin. The origin of the closed-loop system (3.2) is, therefore, asymptotically stable for $L > L_c$ or in other words when the observer error is globally asymptotically stable.

3.6 Numerical results

In this section, the gained knowledge on the closed-loop system of (3.2) will be illustrated with some numerical results. For the friction, the average values from table 2.1 will be applied ($L_c = 73$). The numerical integration of the stiff set of ODEs is done with the *ODE15s* routine of MATLAB with an integration tolerance[4] of TOL $= 1 \cdot 10^{-12}$. In figure 3.3 a numerical solution of (3.2) is shown for $n_1 = 0.4$, $n_2 = 0.02$, $L = 5$ and $\varepsilon = 1 \cdot 10^3$. The corresponding friction $f(x_2)$, friction compensation $f(\hat{x}_2)$ and the time history of e on a logarithmic scale are depicted in figure 3.4. The time history of the observer error (e) reveals all properties as found in the analysis of the observer error dynamics (see section 3.2).

At $t = t_1$ both the actual friction and the friction compensation are increasing due to the Stribeck effect. In this Stribeck region the friction model has a negative slope. In section 3.2 it is shown that the time derivative (3.10) of the Lyapunov function, used for the stability analysis of $e = 0$, can be become positive if $f'(x_2) < 0$ and $L < L_c$. This is no proof for instability, however, the numerical solution shows that the observer error is indeed unstable. For $t_1 < t < t_2$ the actual friction is over-compensated due to the non-zero observer error and as a consequence the link diverges from the origin. From the stability analysis of $e = 0$ it is also known that e will decrease if the actual velocity and the estimated velocity are not of equal sign. For the numerical solution the estimated velocity changes of sign at $t = t_2$ (see also figure 3.5 (left)). The observer error reacts, as expected, to this event by a fast decrease until the estimated and actual velocity are of equal sign again.

[4]The integration tolerance is defined such that at each step, the integration error $\underline{e}_i$ in component i of the solution $\underline{y}$ satisfies $|\underline{e}_i(i)| \leq \max(TOL \cdot |\underline{y}(i)|, TOL)$ [11]

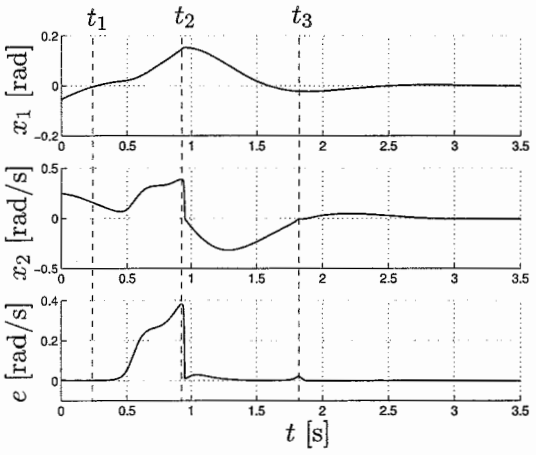

Figure 3.3: Numerical solution of (3.2) with $\underline{x}_b(0) = [-0.055, 0.25, 0.2465]^T$ for $n_1 = 0.4$, $n_2 = 0.02$, $L = 5$ and $\varepsilon = 1 \cdot 10^3$. (From top to bottom states x_1, x_2 and e against time t).

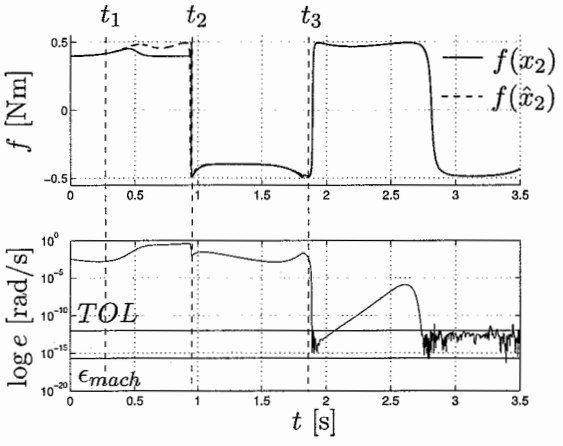

Figure 3.4: Friction $f(x_2)$, friction compensation $f(\hat{x}_2)$ and $\log e$ corresponding to the numerical solution as depicted in figure 3.3.

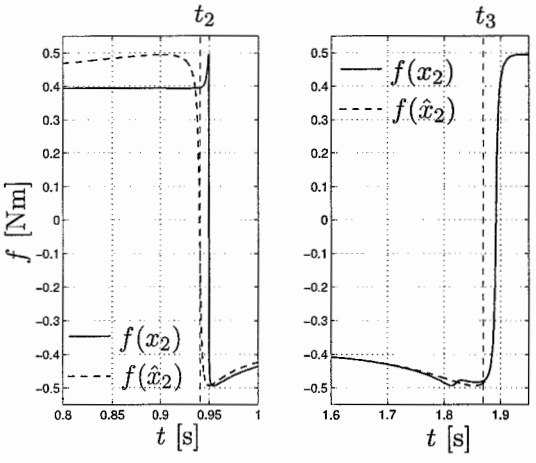

Figure 3.5: Details of friction $f(x_2)$ (solid) and friction compensation $f(\hat{x}_2)$ (dashed) at $t = t_2$ and $t = t_3$.

At $t = t_3$ both the actual friction and the friction compensation are in the region where $\left|\frac{2}{\pi}\text{atan}(\varepsilon v)\right| \ll 1$ (see also figure 3.5 (right)). From equation (3.10) it is known that the rate of decay for e is locally extremely large in this region; the observer error in the numerical solution confirms this property. However, the observer error decays very fast to a level lower than the integration tolerance and even close to the machine accuracy[5]. Consequently, the accuracy of the numerical approximation of the very small observer error due to this fast decay is doubtful. For the actual solution the observer error could even decay to a much smaller level. Unfortunately, this can not be simulated with MATLAB due to finite machine accuracy. After this event the observer error again shows instability but after another fast decay due to the positive slope of the friction model the solution ends at the set-point within the integration tolerance. The fact that the set $e = 0$ exhibits both attracting and repulsing regions for $L < L_c$ is confirmed with this simulation.

Next, the observer gain and the steepness parameter are increased to $L = 35$ and $\varepsilon = 1 \cdot 10^6$. The corresponding numerical result is shown in figure 3.6. From the time history of the observer error (bottom plot) two facts can clearly be distinguished. First, $e = 0$ is still not stable for the applied observer gain and secondly the solution crosses the zero observer error set (the sign of e changes) which is theoretical impossible since this set is invariant.

A numerical integration routine suffers from two distinct sources of error [10], the rounding error which is due to the finite precision of floating-point computation and the discretization error, which is due to the integration method used. The latter could be avoided by taking smaller integration steps, but solutions which come close to the machine accuracy can not be integrated accurately. It will be shown that both sources contribute to the cause for the crossing of the zero observer error set.

In figure 3.7, the actual friction, the friction compensation and the observer error (now zoomed in close to $e = 0$) are depicted. From this figure, it can be noted that for the first crossing of the zero observer error set the observer error becomes very close to the machine accuracy and as a result the solution crosses the invariant set $e = 0$ due to rounding errors. The other crossings occur when both the friction and the compensation are in the smoothing region $\left|\frac{2}{\pi}\text{atan}(\varepsilon v)\right| \ll 1$. The rate of decay for e is locally extremely large in this region. In this region, the numerical solution, therefore, crosses the invariant plane due to discretization errors.

With event detection of $e = 0$ the integration routine can be stopped at the moment when the solution crosses the zero observer error set. By restarting the integration routine from the last point of the solution (one step back) before it arrived at $e = 0$ the crossings of the solution due to discretization errors can be avoided. Note that at the restart of the integration routine an appropriate step size for the desired integration tolerance is determined by starting with a very small step size. The discretization errors are, therefore, minimal at this point. The result of this approach is depicted in figure 3.8, for similar parameter settings and initial condition as in figure 3.6.

It should be noted that at the time instance where earlier the solution did cross the zero observer error set for the first time it now remains equal to zero and does not shown any instabilities any more. From the time history of the actual friction and the compensation it can be noted that the Stribeck region (the region where the observer error set is not attractive) still can be distinguished after this event.

[5]The machine accuracy of MATLAB is $\epsilon_{mach} = 2.22 \cdot 10^{-16}$.

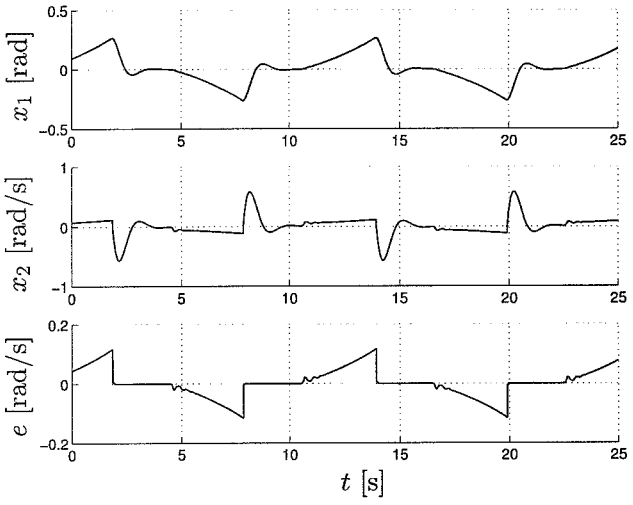

Figure 3.6: Numerical solution of (3.2) with $\underline{x}_b(0) = [0.092, 0.073, 0.030]^T$ for $n_1 = 0.4$, $n_2 = 0.02$, $L = 35$ and $\varepsilon = 1 \cdot 10^6$ (from top to bottom states x_1, x_2 and e against time t).

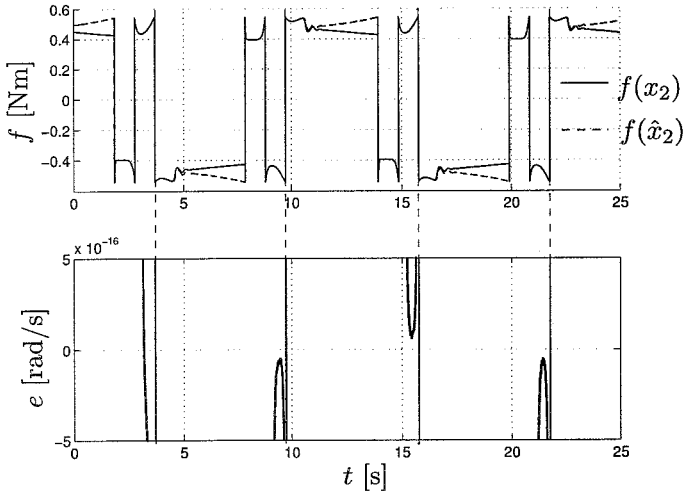

Figure 3.7: Friction $f(x_2)$, friction compensation $f(\hat{x}_2)$ and e (zoomed in close to $e = 0$) corresponding to the numerical solution as depicted in figure 3.6

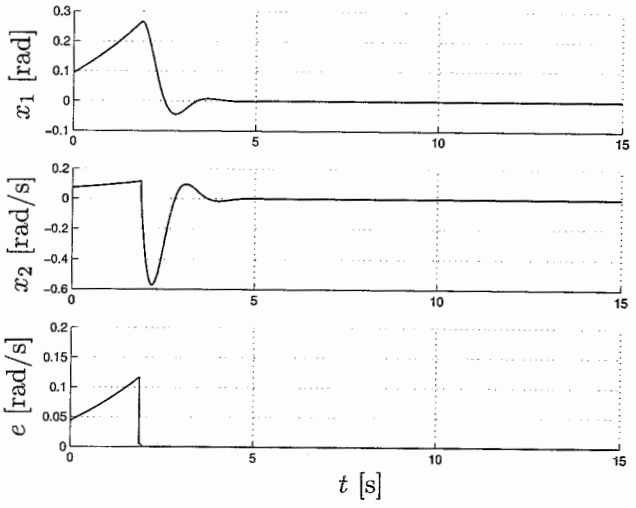

Figure 3.8: Numerical solution of (3.2) (solved with event detection of $e = 0$) with $\underline{x}_b(0) = [0.092, 0.073, 0.030]^T$ for $n_1 = 0.4$, $n_2 = 0.02$, $L = 35$ and $\varepsilon = 1 \cdot 10^6$ (from top to bottom states x_1, x_2 and e against time t).

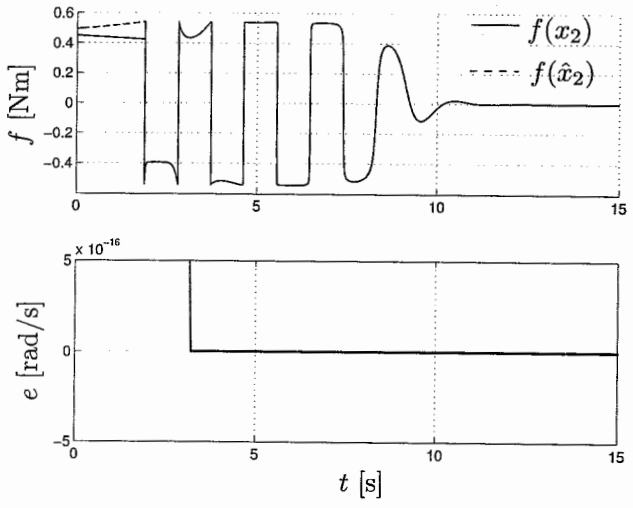

Figure 3.9: Friction $f(x_2)$, friction compensation $f(\hat{x}_2)$ and e (zoomed in close to $e = 0$) corresponding to the numerical solution as depicted in figure 3.8.

The fact that the observer error does not show any instability in this region is most likely due to rounding errors. After all, for $e < \epsilon_{mach}$ the numerical routine will compute $f(\hat{x}_2) - f(x_2) = f(x_2 - e) - f(x_2) = 0$. For $e < \epsilon_{mach}$ the numerical solution, therefore, behaves as if $e = 0$ but theoretically $e = 0$ can not be reached in finite time. Whether this solution is a good approximation of the exact solution is, therefore, also doubtful.

It can be concluded that solutions for (3.2) can not be computed accurately close to $e = 0$ with MATLAB due to both discretization errors in the region $\left|\frac{2}{\pi}\text{atan}\left(\varepsilon v\right)\right| \ll 1$, where (3.2) is very stiff, and rounding errors due to the finite precision of floating-point computation. Whether or not (stable) limit cycles exist can, therefore, not be concluded from numerical simulations. The only conclusion which can be drawn is the fact that for $L = 35$ the observer error is not globally asymptotically stable as desired.

However, if $e = 0$ is asymptotically stable the solution will no longer be repelled from it. The numerical solution will in the worst case oscillate closely around $e = 0$ due to small integration errors, but will still be a good approximation of the exact solution. In figure 3.10 the solution is depicted for a super-critical observer gain ($L = 73.5$ and other parameters and the initial condition are chosen identical to those in figure 3.8). The observer error now decays to zero but the integration routine still has difficulties in the smoothing region $\left|\frac{2}{\pi}\text{atan}\left(\varepsilon v\right)\right| \ll 1$. But since the observer error set is now asymptotically stable the solution is not repelled from it but starts to oscillate close around $e = 0$. The solution now tends to the set-point without any undesired instability.

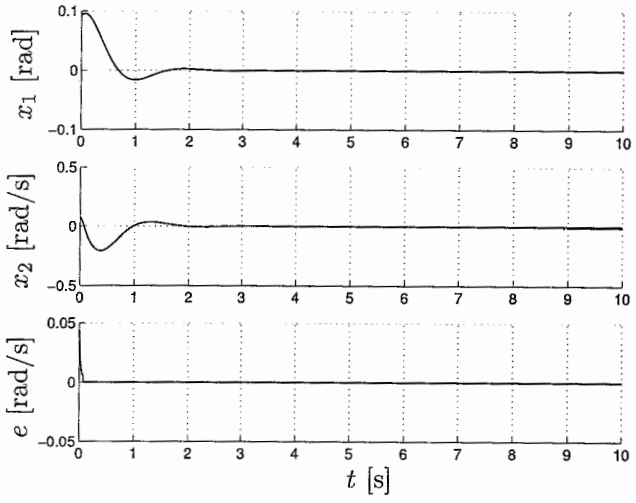

Figure 3.10: Numerical solution of (3.2) with $\underline{x}_b(0) = [0.092, 0.073, 0.030]^T$ for $n_1 = 0.4$, $n_2 = 0.02$, $L = 73.5$ and $\varepsilon = 1 \cdot 10^6$ (left top to bottom states x_1, x_2 and e against time t).

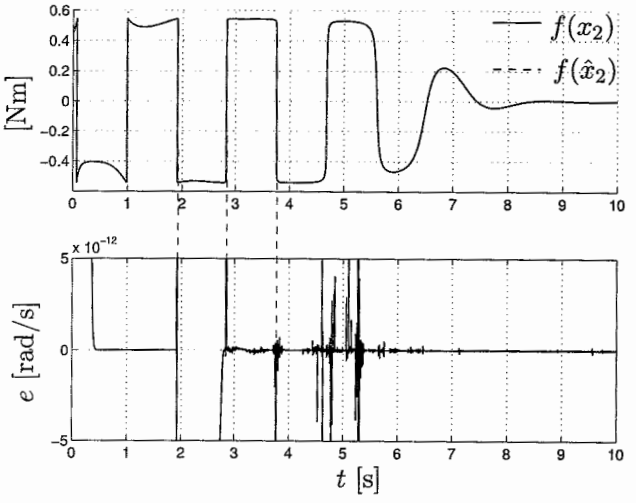

Figure 3.11: Friction $f(x_2)$, friction compensation $f(\hat{x}_2)$ and e (zoomed in close to $e = 0$) corresponding to the numerical solution as depicted in figure 3.10.

3.7 Discussion

Design specifications for the closed-loop system (3.2) are derived such that the closed-loop system exhibits the desired dynamics (globally asymptotically stable set-point and consequently no other equilibrium points and no limit cycling). The design criteria are based on the stability of the observer error. Since the error dynamics of the reduced-order observer are not influenced by the controller gains, the controller gains can be chosen independently of the observer gain. A similar separation principle, as known for linear systems [8], also holds for the nonlinear closed-loop system with friction (3.2).

With design criteria such that global asymptotically stability of the set-point is guaranteed, the strategy of reduced-order observer based friction compensation can, therefore, be successfully applied for the closed-loop system with smooth friction modelling. Unfortunately, the friction in a practical environment does behave more complicated than accounted for in the smooth friction model. In the next chapter, therefore, the closed-loop system will be analyzed with a non-smooth friction model. The non-smooth friction model can describe a richer set of friction phenomena, as encountered in real physical situations, than the smooth friction model.

Chapter 4

Closed-Loop System Analysis : Non-Smooth Case

In this chapter, properties of the system with a non-smooth description for the dry friction will be examined. Within the non-smooth description, the friction for the slip phase and the stick phase are described separately. In the slip phase ($v \neq 0$) the friction depends only on velocity and follows from the Stribeck curve (2.2). For the friction force in the stick phase ($v = 0$), it is assumed that the contacts between the asperities are infinitely stiff and that the resulting friction force is in static equilibrium with the applied external force as long as the external force does not exceed the static break away force (F_s). For zero velocity the friction is, therefore, modelled as a saturation function of the external force (F_{ex}) only. The non-smooth friction model reads as

$$f(F_{ex}, v) = \begin{cases} \min(|F_{ex}|, F_s)\mathrm{sgn}\,(F_{ex}) & \text{if } v = 0 \\ g(v)\mathrm{sgn}\,(v) & \text{if } v \neq 0 \end{cases}, \tag{4.1}$$

with $g(v)$ the Stribeck curve (2.2), F_s the static break away force and F_{ex} the external force. The non-smooth friction model is illustrated in figure 4.1. In contrast with the smooth friction model the model of (4.1) can return a non-zero friction force for zero velocity. The non-smooth friction is, therefore, capable of describing the stiction phenomenon as encountered in real physical situations correctly. For the actual friction, the external force is equal to the controller force plus the compensation ($F_{ex} = u_c + u_{fc} = u$). However, the friction compensation is designed such that the external force in the friction compensation rule is chosen to be $F_{ex} = u_c$. Otherwise, the compensation rule would be defined in an implicit way.

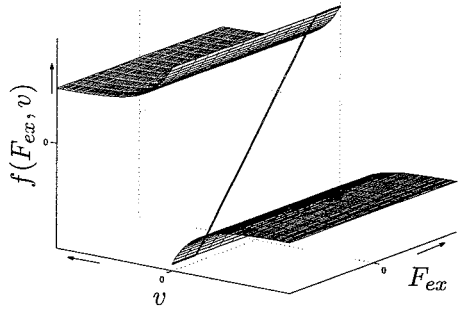

Figure 4.1: Non-smooth friction model.

Moreover, in the next section it is shown that (4.1) is not directly a favourable compensation rule and is, therefore, adapted to be used as compensation rule.

In this chapter, first the need for the adapted friction compensation rule will be explained, on the basis of aspects concerning the zero observer error set. Next, stability aspects concerning the observer error will be addressed. Subsequently, equilibria and stability issues for the closed-loop system will be examined. The chapter ends with numerical results to illustrate the analytical results and a short discussion.

4.1 The Zero Observer Error Set

With the smooth friction model of (3.1), the compensation and actual friction will always cancel each other if the observer error is equal to zero. For the non-smooth friction model, the friction for zero velocity depends on the external force. Since the external force for the compensation rule and for the actual friction differ, the friction compensation and the actual friction will not always cancel each other anymore on the plane $x_2 = \hat{x}_2$ (zero error observer set). From the analysis of the zero observer error set for the smooth case (3.2) it is known that for invariance of this set the actual friction and the compensation must always cancel each other if the observer error is equal to zero. Since this invariance of the zero observer error set is a favourable characteristic, the question arises how to compensate friction for zero velocity such that the net sum of the compensation and actual friction is always equal to zero if the observer error is equal to zero. The answer follows from reversing the causality.

For $\hat{x}_2 \neq 0$, the compensation force indirectly follows from the estimate of the actual friction. In stick, the actual friction returns a force equal to the external force though in opposite direction. However, the maximum static friction level is bounded such that $|f(F_{ex}, 0)| \leq F_s$. Consequently, the actual friction depends, for zero velocity, on the applied compensation force. To cancel the actual friction exactly for zero velocity the saturation principle of the actual friction must be exploited. This is realized by taking the compensation equal to the maximum static friction force in the direction of the controller force u_c. Consequently, the compensation rule reads as

$$\tilde{f}(u_c, v) = \begin{cases} F_s \text{sgn}(u_c) & \text{if } v = 0 \\ g(v)\text{sgn}(v) & \text{if } v \neq 0 \end{cases}, \tag{4.2}$$

with $g(v)$ the Stribeck curve (2.2) and F_s the static break away force. With the compensation rule (4.2) and the friction model (4.1) it follows

$$(\tilde{f}(u_c, \hat{x}_2) - f(u_c + \tilde{f}(u_c, \hat{x}_2), x_2))\Big|_{x_2=\hat{x}_2} = 0, \tag{4.3}$$

as required for invariance of the zero observer set (see section 3.1). The dynamics of the non-smooth closed-loop system in terms of the states $\underline{x}_b = \begin{bmatrix} x_1 & x_2 & \hat{x}_2 \end{bmatrix}^T$ are formulated by

$$\dot{\underline{x}}_b = \underline{f}_{ns}(\underline{x}_b) = \begin{bmatrix} 0 & 1 & 0 \\ -b_1 & -b_2 & -b_3 \\ -b_1 & L & -b_4 \end{bmatrix} \underline{x}_b + \frac{1}{J} \begin{bmatrix} 0 \\ \tilde{f}(u_c, \hat{x}_2) - f(u, x_2) \\ 0 \end{bmatrix}, \tag{4.4}$$

where

$$b_1 = \frac{n_1}{J}, b_2 = \frac{b}{J}, b_3 = \frac{n_2}{J} \text{ and } b_4 = \frac{LJ + b + n_2}{J}.$$

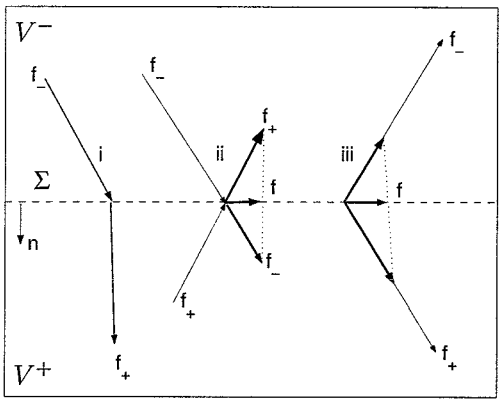

Figure 4.2: Three basic ways in which the discontinuous vector $\underline{f}$ can behave around the switching boundary Σ between two regions of continuity: transversal intersection (i), attracting sliding mode (ii) and repulsive sliding mode (iii).

4.2 Existence and Uniqueness of Solutions

Both the friction model (4.1) and the compensation rule (4.2) switch between a velocity/friction mapping and an external-force/friction mapping after evaluation of the relevant velocity. The transition between the two mappings is non-smooth and can even be discontinuous. With such models incorporated in the state equations of the closed-loop system, the existence and uniqueness of solutions is not automatically guaranteed. In this section, these properties are therefore further investigated for the closed-loop system (4.4).

For continuous ordinary differential equations, global existence and uniqueness of solutions of a set of ordinary differential equations follows if a *Lipschitz* constant C [7] may be found such that $||\underline{f}(\underline{x}_1, t) - \underline{f}(\underline{x}_2, t)|| \leq C||\underline{x}_1 - \underline{x}_2||$, $\forall\, t$ for any two vectors $\underline{x}_1$ and $\underline{x}_2$. Obviously, for a discontinuous system, this condition will be violated if $\underline{x}_1$ and $\underline{x}_2$ are on different sides of a switch surface and $||\underline{x}_1 - \underline{x}_2|| \to 0$. Outside the switch plane both the friction model as the compensation rule are continuously differentiable the Lipschitz constant for this situations follows from the bounded first partial derivatives of (4.4). For existence and uniqueness of solutions of (4.4) the vector field around the switch planes must be examined in more detail.

For the purpose of the evaluation of a set of state equations with a single discontinuity, the state space is divided into two regions V^- and V^+ separated by a switch surface Σ such that $\mathbb{R}^n = V^- \cup \Sigma \cup V^+$. The switch surface Σ is defined by a scalar indicator function $h(\underline{x})$ such that the state $\underline{x}$ is in Σ if $h(\underline{x}) = 0$. The signs of the regions V^- and V^+ correspond to the sign of $h(\underline{x})$. For the vector field there are three basic ways to behave around a switch surface as depicted in figure 4.2. For the first way (i), the vector field points towards Σ on one side and away from Σ on the other side. In this case solutions will intersect Σ transversally. A necessary condition for a transversal intersection of Σ is

$$\left(\underline{n}^T \underline{f}^-(\underline{x}(t))\right)\left(\underline{n}^T \underline{f}^+(\underline{x}(t))\right) > 0, \tag{4.5}$$

where $\underline{n}^T \underline{f}^-(\underline{x}(t))$ and $\underline{n}^T \underline{f}^+(\underline{x}(t))$ are the projections of $\underline{f}^-(\underline{x}(t))$ and $\underline{f}^+(\underline{x}(t))$ on the vector $\underline{n}$ normal to Σ evaluated infinitely close to Σ. For transversal intersections, solutions stay only for one discrete time instance on the switch surface. Consequently, the value of the vector field on the discontinuity gives no contribution to a transversal intersecting solution as long as the

vector field is bounded. Consequently, a solution which transversal intersect a switch plane is similar to the union of the two pieces of solutions to and from the intersection point at the switch surface. For solutions outside is existence and uniqueness guaranteed and, therefore, also for solutions which transversal intersect a switch plane.

The vector field could also push (ii) or repel (iii) the solution to or away from the switch surface. These type of solutions or modes are called sliding modes. An attraction sliding mode (ii) at Σ occurs if

$$\underline{n}^T\underline{f}^-(\underline{x}(t)) > 0 \text{ and } \underline{n}^T\underline{f}^+(\underline{x}(t)) < 0, \tag{4.6}$$

and a repulsive sliding mode (iii) at Σ if

$$\underline{n}^T\underline{f}^-(\underline{x}(t)) < 0 \text{ and } \underline{n}^T\underline{f}^+(\underline{x}(t)) > 0. \tag{4.7}$$

For sliding modes the solution must be able to stay for some period of time on the discontinuity as illustrated in figure 4.2 (ii) and (iii). The vector field at the discontinuity should therefore be such that these type of solutions are permitted. Existence of solutions for this case will be examined using the solution concept of *Filippov* [6, 7]. An absolute continuous function $\underline{x}(t) : [0, \tau] \to \mathbb{R}^n$ is a solution of $\dot{\underline{x}} = \underline{f}(\underline{x})$ in the sense of Filippov if for almost all[1] $t \in [0, \tau]$ it holds that

$$\dot{\underline{x}}(t) \in \underline{F}(\underline{x}(t)), \tag{4.8}$$

where $\underline{F}(\underline{x}(t))$ is the closed convex hull of all limit points of $\underline{f}(\underline{x}(t))$. Solutions, in the form of sliding modes, exist in the sense of Filippov if

$$\dot{\underline{x}}(t) \in \text{conv}\{\underline{f}^-(\underline{x}(t)), \underline{f}^+(\underline{x}(t))\}, \tag{4.9}$$

with

$$\text{conv}\{\underline{f}^-(x(t)), \underline{f}^+(\underline{x}(t))\} = \{z | z = (1-q)\underline{f}^-(\underline{x}(t)) + q\underline{f}^+(\underline{x}(t)), q \in [0,1]\}, \tag{4.10}$$

the convex hull of the set with the two points $\underline{f}^-(\underline{x}(t))$ and $\underline{f}^+(\underline{x}(t))$ for $\underline{x}(t) \in \Sigma$. For a repulsive sliding mode the solution can either stay on the switch surface or leave the switch surface to either of both sides and is clearly not unique. For uniqueness of solutions, repulsive sliding modes should not be allowed.

The state space of (4.4) contains two of the so-called switch surfaces, one due the discontinuity in the friction model and one due the discontinuity in the friction compensation rule. For the actual friction the scalar indicator function is taken as $h_1(\underline{x}_b) = x_2$ and analogously for the compensation $h_2(\underline{x}_b) = \hat{x}_2$. The regions and switch surfaces for the evaluation of (4.1) and of (4.2) are defined as

$$\begin{array}{rclcrcl} V_1^- & = & \{\underline{x}_b \in \mathbb{R}^3 | x_2 < 0\} & & V_2^- & = & \{\underline{x}_b \in \mathbb{R}^3 | \hat{x}_2 < 0\} \\ V_1^+ & = & \{\underline{x}_b \in \mathbb{R}^3 | x_2 > 0\} & & V_2^+ & = & \{\underline{x}_b \in \mathbb{R}^3 | \hat{x}_2 > 0\} \\ \Sigma_1 & = & \{\underline{x}_b \in \mathbb{R}^3 | x_2 = 0\} & & \Sigma_2 & = & \{\underline{x}_b \in \mathbb{R}^3 | \hat{x}_2 = 0\} \end{array} . \tag{4.11}$$

For the two switch surfaces in the phase space of (4.4) the two corresponding normal vectors are defined as $\underline{n}_1 = \nabla h_1(\underline{x}) = [0,1,0]^T$ and $\underline{n}_2 = \nabla h_2(\underline{x}) = [0,0,1]^T$. The behaviour of the vector field (4.4) around Σ_1 is first examined. The projections of the vector field on the corresponding normal evaluated infinitely close to the switch surface are for both sides

$$\underline{n}_1^T\underline{f}_{ns}^-(\underline{x}(t)) = \frac{1}{J}(u_c + \tilde{f}(u_c, \hat{x}_2) + F_s) \text{ and } \underline{n}_1^T\underline{f}_{ns}^+(\underline{x}(t)) = \frac{1}{J}(u_c + \tilde{f}(u_c, \hat{x}_2) - F_s). \tag{4.12}$$

[1] for almost all t means except for a set t of measure 0.

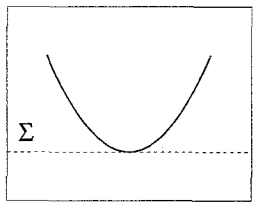

Figure 4.3: Non-transversal intersection of a solution with the switch surface Σ.

Therefore, transversal intersections occur if and only if

$$\frac{1}{J^2}\left((u_c+\tilde{f}(u_c,\hat{x}_2))^2-F_s^2\right)>0 \Rightarrow |u_c+\tilde{f}(u_c,\hat{x}_2)|>F_s, \tag{4.13}$$

attracting sliding modes appear if

$$\frac{1}{J}(u_c+\tilde{f}(u_c,\hat{x}_2)+F_s)>0 \text{ and } \frac{1}{J}(u_c+\tilde{f}(u_c,\hat{x}_2)-F_s)<0 \Rightarrow |u_c+\tilde{f}(u_c,\hat{x}_2)|<F_s, \tag{4.14}$$

and repulsive sliding modes appear if

$$\frac{1}{J}(u_c+\tilde{f}(u_c,\hat{x}_2)+F_s)<0 \text{ and } \frac{1}{J}(u_c+\tilde{f}(u_c,\hat{x}_2)-F_s)>0 \Rightarrow \text{ Not Possible.} \tag{4.15}$$

Next, possible modes at Σ_2 are examined. Due to the fact that only the second equation of the right hand side of (4.4) is discontinuous the projection on $\underline{n}_2$ of the vector field evaluated infinitely close to the switch surface Σ_2 is continuous and equal to

$$\underline{n}_2^T\underline{f}_{ns}^-(\underline{x}_b(t))=\underline{n}_2^T\underline{f}_{ns}^+(\underline{x}_b(t))=Lx_2-b_1x_1. \tag{4.16}$$

Except on the line

$$\left\{\underline{x}_b\in\Sigma_2|x_1=\frac{L}{b_1}x_2\right\}, \tag{4.17}$$

solutions are, therefore, always transversal to the switch plane Σ_2. On the line (4.17) the special situation occurs that $\underline{n}_2^T\underline{f}_{ns}^-(\underline{x}_b(t))=\underline{n}_2^T\underline{f}_{ns}^+(\underline{x}_b(t))=0$ meaning that the vector field is locally parallel to Σ_2. On the line (4.17), the first time derivative of $\hat{x}_2$ is equal to zero but for a possible sliding modes along (4.17) to occur also the second time derivative of $\hat{x}_2$ must be equal to zero. With $x_1=L/b_1x_2$, $u_c|_{\hat{x}_2=0}=-n_1x_1$ and $\tilde{f}(u_c,0)=F_s\text{sgn}(u_c)=-F_s\text{sgn}(x_1)=-F_s\text{sgn}(x_2)$ the second derivative of $\hat{x}_2$ is

$$\begin{aligned}\ddot{\hat{x}}_2\Big|_{\dot{\hat{x}}_2,\hat{x}_2=0} &= -b_1\,\dot{x}_1|_{\dot{\hat{x}}_2,\hat{x}_2=0}+L\,\dot{\hat{x}}_2|_{\dot{\hat{x}}_2,\hat{x}_2=0}\\ &= -(b_1+L^2+Lb_2)x_2-L\left(\frac{F_s\text{sgn}(x_2)+f(u,x_2)}{J}\right)\end{aligned} \tag{4.18}$$

Since $\text{sgn}\left((b_1+L^2+Lb_2)x_2\right)=\text{sgn}\left(L\left(\frac{F_s\text{sgn}(x_2)+f(u,x_2)}{J}\right)\right)$, the second derivative of $\hat{x}_2$ (4.18) is always of opposite sign than x_2 and is only equal to zero at the origin ($\underline{x}_b=\underline{0}$). On the line (4.17), solutions touch the switch plane Σ_2 only at a single time instance without crossing it as illustrated in figure 4.3. This behaviour is denoted as a non-transversal intersection [9].

Next to sliding modes along a single switch plane, solutions could also slide along the intersection of the two switch planes along the line $x_2=\hat{x}_2=0$. Sliding across the line $x_2=\hat{x}_2=0$

would yield a change in position x_1. Consequently, it follows directly from $\dot{x}_1 = x_2$ that sliding across the line is impossible, except if $\underline{x}_b = \underline{0}$ (in the section 4.4 it will be shown that this is an equilibrium point). The last point of consideration is the discontinuity following from the compensation rule for zero velocity ($F_s \text{sgn}(F_{ex})$). With $F_{ex}|_{\hat{x}_2=0} = u_c|_{\hat{x}_2=0} = -n_1 x_1$ the line of discontinuity in Σ_2 is the line $x_1 = 0$ with normal $\underline{n}_3 = [1, 0, 0]^T$. Since the first equation of (4.4) is continuous also the projection of the vector field within Σ_2 on $\underline{n}_3$ is continuous and no sliding modes exist.

From the analysis of the vector field around both switch surfaces it can be concluded that both (non)transversal intersections and attracting sliding modes can occur. For (non)transversal intersections, existence of solutions, follows without any constraints on the value of the vector field returned on the switch surface it self, except that it is bounded. Sliding modes occur only at the switch plane for the actual friction. Since the actual friction force for zero velocity falls within the smallest convex set containing both limits ($\{-F_s, +F_s\}$), (4.4) obeys an differential inclusion of the form (4.9) in each case where sliding modes occurs. Consequently, solutions in sense of Filippov for this case exist. Since no repulsive sliding modes exist these solutions are also unique.

4.3 Observer Error Dynamics

For a successful implementation of the reduced-order observer, stable observer error dynamics are required. From (4.4) follows that the observer error dynamics obey

$$\dot{e} = \dot{x}_2 - \dot{\hat{x}}_2 = -\frac{b + LJ}{J} e + \frac{\tilde{f}(u_c, \hat{x}_2) - f(u, x_2)}{J}. \tag{4.19}$$

For the purpose of stability analysis of the invariant zero observer error set ($e = 0$) *Lyapunov*'s direct method will be followed. Consider the Lyapunov candidate function

$$V(x_2, \hat{x}_2) = \frac{1}{2} e^2, \tag{4.20}$$

with $e = x_2 - \hat{x}_2$. The time-derivative of (4.20) is

$$\dot{V}(x_2, \hat{x}_2) = e\dot{e} = e\left[-\frac{b + LJ}{J} e + \frac{\tilde{f}(u_c, \hat{x}_2) - f(u, x_2)}{J}\right]. \tag{4.21}$$

For the analysis of (4.21) three sets are defined,

$$S^I = \{(x_2, \hat{x}_2) | \text{sgn}(x_2) \neq \text{sgn}(\hat{x}_2) \wedge x_2, \hat{x}_2 \neq 0\} \tag{4.22}$$

$$S^{II} = \{(x_2, \hat{x}_2) | \text{sgn}(x_2) = \text{sgn}(\hat{x}_2) \wedge x_2, \hat{x}_2 \neq 0\} \tag{4.23}$$

$$S^{III} = \{(x_2, \hat{x}_2) | x_2 = 0 \vee \hat{x}_2 = 0 \vee x_2 = \hat{x}_2 = 0\}, \tag{4.24}$$

such that $(x_2, \hat{x}_2) \in \mathbb{R}^2 = S^I \cup S^{II} \cup S^{III}$ as illustrated in figure 4.4. For the stability analysis it will be shown first that if $(x_2, \hat{x}_2) \in S^I$ (4.21) is negative definite for arbitrary $L > -b/J$. Next, a critical value for the observer gain will be derived such that (4.21) will be negative definite if $(x_2, \hat{x}_2) \in S^{II}$. Finally it will be shown that the critical condition for L also holds for the case $(x_2, \hat{x}_2) \in S^{III}$.

I Actual and estimated velocity not of equal sign and not equal to zero
In table 4.1 bounds for $\tilde{f}(u_c, \hat{x}_2) - f(u, x_2)$ are tabulated for all situations for the case $(x_2, \hat{x}_2) \in S^I$. From this table, it can be concluded that the difference between the compensation and actual friction for the case $(x_2, \hat{x}_2) \in S^I$ is always of opposite sign of the observer error. For this case, (4.21) is, therefore, strictly negative.

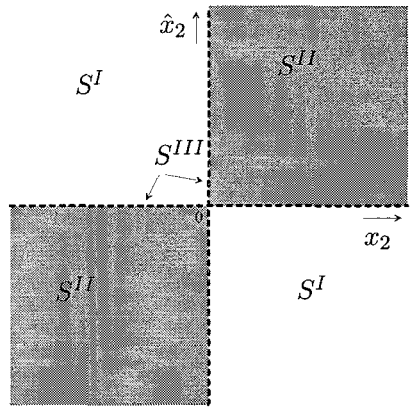

Figure 4.4: Defined sets S^I, S^{II} and S^{III}.

x_2	$\hat{x}_2$	$e = x_2 - \hat{x}_2$	$\tilde{f}(u_c, \hat{x}_2) - f(u, x_2)$
> 0	< 0	> 0	$\leq -2F_c$
< 0	> 0	< 0	$\geq 2F_c$

Table 4.1: Bounds for the difference between the compensated and the actual friction for the case $\operatorname{sgn}(x_2) \neq \operatorname{sgn}(\hat{x}_2)$ and $x_2, \hat{x}_2 \neq 0$ ($(x_2, \hat{x}_2) \in S^I$).

II Actual and estimated velocity of equal sign and not equal to zero

The difference between the actual and the compensated friction can be written for $(x_2, \hat{x}_2) \in S^{II}$ as

$$\tilde{f}(u_c, \hat{x}_2) - f(u, x_2)\Big|_{(x_2,\hat{x}_2)\in S^{II}} = (g(\hat{x}_2) - g(x_2))\operatorname{sgn}(x_2)\,. \tag{4.25}$$

For $(x_2, \hat{x}_2) \in S^{II}$ the Stribeck curve (2.2) is continuously differentiable (since $x_2, \hat{x}_2 \neq 0$) and $g(\hat{x}_2) - g(x_2)$ can therefore be replaced with a Taylor expansion

$$g(\hat{x}_2) - g(x_2) = g(x_2 - e) - g(x_2) = -g'(x_2)e + \text{h.o.t.} \tag{4.26}$$

and for $e \ll 1$ the higher order terms can be neglected. Substitution of the approximation (4.26) in (4.25) and subsequently (4.25) in (4.21) yields

$$\dot{V}(x_2, \hat{x}_2)\Big|_{\substack{(x_2,\hat{x}_2)\in S^{II} \\ e\ll 1}} = -\frac{b + LJ + g'(x_2)\operatorname{sgn}(x_2)}{J}e^2, \tag{4.27}$$

which is strictly negative if $b + LJ + g'(x_2)\operatorname{sgn}(x_2) > 0\ \forall x_2 \neq 0$. The latter condition is equivalent to (3.12) following from the local stability analysis of the observer error for the smooth friction model (see section 3.2). The same critical value for the observer gain (3.13), such that (4.21) is negative definite for the case $(x_2, \hat{x}_2) \in S^{II}$ with $e \ll 1$, also applies. Critical values for design variables such stability can be proven with Lyapunov's direct method are in general not of a necessary nature. However, if the local perturbation of the scalar differential equation (4.19) is inspected:

$$\dot{e}|_{\substack{(x_2,\hat{x}_2)\in S^{II} \\ e\ll 1}} = -\frac{b + LJ + g'(x_2)\operatorname{sgn}(x_2)}{J}e, \tag{4.28}$$

$e = 0$ can only be asymptotically stable if and only if $b+LJ+g'(x_2)\text{sgn}(x_2) > 0 \; \forall x_2 \neq 0$. With the non-smooth friction modelling, the critical observer gain is, therefore, not a sufficient condition but a necessary condition.

For $(x_2, \hat{x}_2) \in S^{II}$ the Stribeck curve (2.2) is continuously differentiable and the difference between the compensation and actual friction (4.25) can be expressed for arbitrary observer errors with the Mean Value Theorem

$$(g(\hat{x}_2) - g(x_2))\,\text{sgn}(x_2) = \left(g'(z)(\hat{x}_2 - x_2)\right)\text{sgn}(\hat{x}_2) = -g'(z)\text{sgn}(\hat{x}_2)\,e, \tag{4.29}$$

with z some point on the line segment $l(x_2, \hat{x}_2)$. Substitution of (4.29) in (4.21) yields

$$\dot{V}(x_2, \hat{x}_2)\Big|_{(x_2,\hat{x}_2)\in S^{II}} = -\frac{b + LJ + g'(z)\text{sgn}(\hat{x}_2)}{J} e^2. \tag{4.30}$$

Since $g'(z)\text{sgn}(\hat{x}_2) \geq g'(\hat{x}_2)_{\min}$ (4.21) will be strictly negative for arbitrary $(x_2, \hat{x}_2) \in S^{II}$ if $L > L_c$.

III Actual or estimated velocity equal to zero

If both velocities are equal to zero then $e = 0$ and consequently (4.21) is equal to zero. With the actual velocity equal to zero, the actual friction will only depend on the external force and is bounded such that $-F_s \leq f(u, 0) \leq F_s$. For $x_2 = 0$, the observer error is always of opposite sign of the estimated velocity ($e = -\hat{x}_2$) and the worst case situation for (4.21) is therefore

$$\dot{V}(\underline{x}_b)\Big|_{x_2=0} \leq -\hat{x}_2 \left[\frac{b + LJ}{J}\hat{x}_2 + \frac{(g(\hat{x}_2) - F_s)\text{sgn}(\hat{x}_2)}{J}\right], \tag{4.31}$$

since $g(\hat{x}_2) - F_s \leq 0$. For $\hat{x}_2 \neq 0$, the Stribeck curve is a smooth function and with $g(\hat{x}_2) - F_s = g(\hat{x}_2) - g(0)$ and application of the Mean Value Theorem as in (4.29), (4.31) can be written as

$$\dot{V}(x_2, \hat{x}_2)\Big|_{x_2=0} \leq -\frac{b + LJ + g'(z)\text{sgn}(\hat{x}_2)}{J}\hat{x}_2^2, \tag{4.32}$$

with z some point on the line segment $l(0, \hat{x}_2)$[2]. For $L > L_c$ (4.32) is clearly strictly negative.

If the estimated velocity is equal to zero the compensation can take one of the three values of the set $\tilde{f}(u_c, 0) = \{-F_s, 0, F_s\}$. For $\hat{x}_2 = 0$, the observer error is always of equal sign of the actual velocity and the worst case for (4.21) is therefore

$$\dot{V}(x_2, \hat{x}_2)\Big|_{x_2=0} \leq x_2 \left[-\frac{b + LJ}{J}x_2 + \frac{(F_s - g(x_2))\text{sgn}(x_2)}{J}\right], \tag{4.33}$$

which is equivalent to the worst case for $x_2 = 0$ and, therefore, a corresponding condition for the observer gain follows.

[2]Note that $g(z)$ is not differentiable for $z = 0$, however, since $l(x, y) = \{\theta x + (1-\theta)y, 0 < \theta < 1\}$ it holds that $z \neq 0$ in this case.

Summarizing for (4.20) it holds that

$$\dot{V}(\underline{x}_b) = e\dot{e} < \begin{cases} 0 & \text{for case I} \\ e\left(-\frac{b+LJ+g'(\hat{x}_2)_{\min}}{J}e\right) & \text{for case II and III} \end{cases}, \tag{4.34}$$

and with the observer gain taken larger than the critical value (3.13) $e = 0$ can be considered globally asymptotically stable.

Similar to the smooth case the regions where the time-derivative of (4.20) is positive for various values of the observer gain L are depicted in figure 4.5 (top) for the average values of table 2.1. Note that for the situations $x_2, \hat{x}_2 = 0$ both the friction and the friction compensation depend on the external force u respectively u_c and, therefore, on x_1. To be able to illustrated the regions where (4.20) is positive in a two-dimensional contour-plot the worst case values for the value $f(u,0)$ and $\tilde{f}(u_c,0)$, as described for case III in section 4.3, are chosen. From graphical examination it follows that for $L > 73$ the observer error will be asymptotically stable which confirms the necessary nature of the critical value ($L_c = 73$) of the observer gain for the non-smooth case. In figure 4.5 (bottom) it is shown that the critical value for the observer gain also holds for asymmetrical friction models by taking $L_c = \max(L_c^+, L_c^-)$. The critical values for the observer gain for positive and negative velocity for the asymmetrical friction parameters of table 2.1 are equal to $L_c^+ = 94.4$ and $L_c^- = 55.07$.

4.4 Equilibrium Points

Equilibrium points for a set of ordinary differential equations follow from the algebraic set of equations $\dot{\underline{x}} = \underline{0}$. Equilibrium of (4.4) satisfy $x_2 = 0$ and consequently

$$-n_1x_1 - n_2\hat{x}_2 + \tilde{f}(u_c,\hat{x}_2) - f(u,0) = 0 \tag{4.35}$$

$$-n_1x_1 - (b+LJ+n_2)\hat{x}_2 = 0 \rightarrow x_1 = -\frac{b+LJ+n_2}{n_1}\hat{x}_2. \tag{4.36}$$

The controller force in equilibrium follows from (4.36) to be equal to $u_c^* = -n_1x_1 - n_2\hat{x}_2 = (LJ+b)\hat{x}_2$. From substitution of $u_c = u_c^*$ and (4.36) into (4.35) and $f(u,0) \leq F_s\text{sgn}(u)$ it follows

$$u_c^* + \tilde{f}(u_c^*,\hat{x}_2) - f(u,0) = 0 \rightarrow |u_c^* + \tilde{f}(u_c^*,\hat{x}_2)| \leq F_s. \tag{4.37}$$

Since for $\hat{x}_2 = 0$ both the control force (u_c^*) as well as the compensation ($\tilde{f}(\hat{x}_2, u_c^*)$) are equal to zero (4.37) is satisfied for $\hat{x}_2 = 0$. With (4.36) it follows, therefore, that the origin is an equilibrium point of (4.4). For $\hat{x}_2 \neq 0$, (4.37) can be written as

$$m(\hat{x}_2) = |(b+LJ)\hat{x}_2 + g(\hat{x}_2)\text{sgn}(\hat{x}_2)| - F_s \leq 0, \tag{4.38}$$

which could be an empty or a non-empty set depending on the value of L. For a zero steady-state error it is necessary that this set is empty. With $j(0^+) = j(0^-)^3 = 0$ a sufficient condition for emptiness of the extra equilibrium set is that (4.38) is strictly increasing. The derivative of (4.38) reads as

$$\left.\frac{\partial m(\hat{x}_2)}{\partial \hat{x}_2}\right|_{\hat{x}_2=0} = \text{sgn}(\hat{x}_2)\left(b+LJ+g'(\hat{x}_2)\text{sgn}(\hat{x}_2)\right). \tag{4.39}$$

and (4.38) will be strictly increasing if $\text{sgn}\left(\frac{\partial m(\hat{x}_2)}{\partial \hat{x}_2}\right) = \text{sgn}(\hat{x}_2)$. Consequently, a sufficient condition for emptiness of the extra equilibrium set is $b + LJ + g'(\hat{x}_2)\text{sgn}(\hat{x}_2) > 0$ which is equivalent to the condition following from the stability analyses of the observer error (see section 4.3). For $L > L_c$ the extra equilibrium set will, therefore, be empty as desired.

[3] with $m(0^+) = \lim_{\hat{x}_2 \downarrow 0} m(\hat{x}_2)$ and $m(0^-) = \lim_{\hat{x}_2 \uparrow 0} m(\hat{x}_2)$.

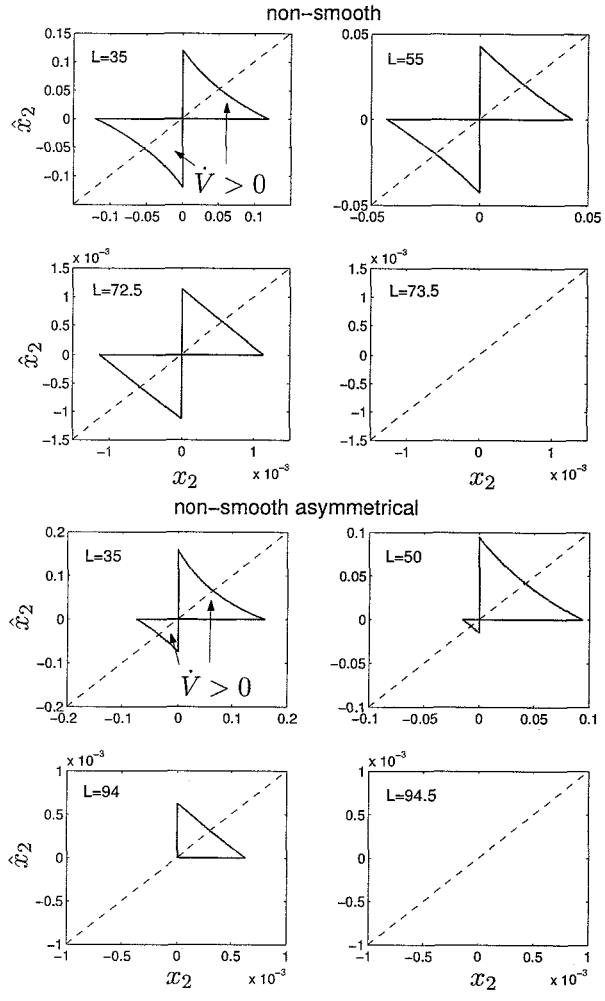

Figure 4.5: Contour plot of the closed regions (solid) where (3.8) is larger then zero for increasing values of L and the zero observer error set (dashed) for the symmetric non-smooth friction model (top) and the asymmetrical non-smooth friction model (bottom)

4.5 Global Stability of the Origin for $L > L_c$

Similar to the smooth case, the observer error is globally asymptotically stable for $L > L_c$ and the origin of (4.4) is the unique equilibrium point. Since solutions for (4.4) are bounded (see section 2.6) and, for $L > L_c$, always tend to the zero observer error set, the origin can be considered globally attractive for this case. To strengthen this result, global *asymptotic stability* of the origin of (4.4) will be proven for $L > L_c$ using *Lyapunov*'s direct method. Consider the Lyapunov candidate function

$$V(\underline{x}_b) = J\left[(b_1 x_1^2 + x_2^2 + \alpha e^2)/2 + \gamma|e|\right], \tag{4.40}$$

with $e = x_2 - \hat{x}_2$, $\alpha = n_2/2(b + LJ)$ and $\gamma > 0$. The time-derivative of (4.40) equals

$$\begin{aligned} \dot{V}(\underline{x}_b) &= J\left[b_1 x_1 \dot{x}_1 + x_2 \dot{x}_2 + (\alpha e + \gamma \mathrm{sgn}\,(e))\dot{e}\right] \\ &= -b x_2^2 - (b + LJ)(\alpha e^2 + \gamma|e|) - n_2 x_2 \hat{x}_2 + \\ &\quad (x_2 + \gamma \mathrm{sgn}\,(e) + \alpha e)(\tilde{f}(u_c, \hat{x}_2) - f(u, x_2)), \end{aligned} \tag{4.41}$$

where $d|e|/dt$ is considered to be single-valued for $e = 0$, namely $\dot{e}(e = 0) = 0$. Since (4.41) depends only on x_2 and $\hat{x}_2$ the analysis of (4.41) can be divided in the equivalent three cases as defined in (4.22), (4.23) and (4.24) for the stability analysis of the observer error (see section 4.3). The analysis starts with the proof for semi-negative definiteness of (4.41) with the specific choice for $\alpha = n_2/2(b + LJ)$ and if $(x_2, \hat{x}_2) \in S^I$. For the case $(x_2, \hat{x}_2) \in S^{II}$ the difference between the actual friction and the friction compensation will be rewritten using the Mean Value Theorem. Next, a lower bound for the constant γ will be derived such that (4.41) will be semi-negative definite for $L > L_c$ if $(x_2, \hat{x}_2) \in S^{II}$. Finally, it will be shown that (4.41) is also semi-negative definite for the case $(x_2, \hat{x}_2) \in S^{III}$ if $L > L_c$ and with the constant γ larger then the derived lower bound. Since (3.24) only depends on x_2 and $\hat{x}_2$ only stability of the origin can be proven with this Lyapunov function. However, with La Salle Invariance Principle this result will be extended to global *asymptotically* stability of the origin.

I Actual and estimated velocity not of equal sign and not equal to zero
In section 4.3, it is shown that for $(x_2, \hat{x}_2) \in S^I$ the difference between the compensation and actual friction is always of opposite sign of the observer error. With $\alpha, \gamma > 0$ the product $(\gamma \text{sgn}\,(e) + \alpha e)(\tilde{f}(u_c, \hat{x}_2) - f(u, x_2))$ is consequently negative definite in this case. From the passivity property of the friction model $(vf(v) \geq 0)$ it follows $-x_2 f(u, x_2) \leq 0$ and for $\text{sgn}\,(x_2) \neq \text{sgn}\,(\hat{x}_2)$ also $x_2 \tilde{f}(u_c, \hat{x}_2) \leq 0$ holds. Since $e^2 = x_2^2 - 2x_2\hat{x}_2 + \hat{x}_2^2$ the product $-n_2 x_2 \hat{x}_2$ is cancelled due to the specific choice for the constant α. Consequently, is $\dot{V}(\underline{x}_b) \leq 0$ for the case $(x_2, \hat{x}_2) \in S^I$.

II Actual and estimated velocity of equal sign and not equal to zero
Using the Mean Value theorem, it is shown in section 4.3, that for $(x_2, \hat{x}_2) \in S^{II}$ the difference between the actual can be written as

$$\tilde{f}(u_c, \hat{x}_2) - f(u, x_2)\Big|_{(x_2, \hat{x}_2) \in S^{II}} = (g(\hat{x}_2) - g(x_2))\,\text{sgn}\,(x_2) = -g'(z)\text{sgn}\,(\hat{x}_2)\, e \tag{4.42}$$

with z some point on the line segment $l(x_2, \hat{x}_2)$. Substitution of (4.42) in (4.41) yields

$$\begin{aligned} \dot{V}(x_2, \hat{x}_2) \;=\; & -bx_2^2 - (b + LJ + g'(z)\text{sgn}\,(\hat{x}_2))(\alpha e^2 + \gamma|e|) - n_2 x_2 \hat{x}_2 - \\ & g'(z)|x_2|e, \end{aligned} \tag{4.43}$$

where $(b + LJ + g'(z)\text{sgn}\,(\hat{x}_2)) > 0$ for $L > L_c$ (see section 4.3). For $(x_2, \hat{x}_2) \in S^I I$ follows $-n_2 x_2 \hat{x}_2 < 0$ and the only part in (4.43) which could give a positive contribution is the product $-g'(z)|x_2|e = x_2(f(u_c, \hat{x}_2) - f(u, x_2))$ (note that $|\tilde{f}(u_c, \hat{x}_2) - f(u, x_2)| \leq \delta F$ for $(x_2, \hat{x}_2) \in S^{II}$). Since for $|x_2| > \delta F/b$ follows $bx_2^2 > |x_2(f(u_c, \hat{x}_2) - f(u, x_2))|$ is (4.43) clearly semi-negative definite for $|x_2| \leq \delta F/b$ if

$$(b + LJ + g'(z)\text{sgn}\,(\hat{x}_2))\gamma|e| \geq \left| g'(z)\frac{\delta F}{b} e \right| \quad \forall e, z, \tag{4.44}$$

and consequently if

$$\gamma \geq \sup_{\hat{x}_2 \in \mathbb{R} - \{0\}} \frac{|g'(\hat{x}_2)|}{b + LJ + g'(\hat{x}_2)\text{sgn}\,(\hat{x}_2)} \frac{\delta F}{b}. \tag{4.45}$$

Since $g'(\hat{x}_2)$ is bounded for $\hat{x}_2 \neq 0$ and $(b + LJ + g'(z)) > 0$ for $L > L_c$ the supremum (4.45) exist.

III Actual or estimated velocity equal to zero.
If both x_2 and $\hat{x}_2$ are equal to zero then $\dot{V}(\underline{x}_b) = 0$. For $x_2 = 0$ (4.41) reduces to

$$\dot{V}(\underline{x}_b)\Big|_{x_2=0} = J(\alpha e + \gamma \mathrm{sgn}\,(e))\dot{e}. \tag{4.46}$$

In section 4.3 it is shown that $e\dot{e} \leq 0$ for $L > L_c$ and with $J, \alpha, \gamma > 0$ this result is also applicable for (4.46). With $\hat{x}_2 = 0$, (4.41) reduces to

$$\begin{aligned} \dot{V}(\underline{x}_b)\Big|_{\hat{x}_2=0} &= -bx_2^2 - (b + LJ)(\alpha e^2 + \gamma|e|) + (x_2 + \gamma \mathrm{sgn}\,(e) + \alpha e)(\tilde{f}(u_c, 0) - f(u, x_2)) \\ &\leq -bx_2^2 - (b + LJ)(\alpha e^2 + \gamma|e|) + \\ &\quad (x_2 + \gamma \mathrm{sgn}\,(e) + \alpha e)(F_s \mathrm{sgn}\,(x_2) - f(u, x_2)). \end{aligned} \tag{4.47}$$

The lower bound in (4.47) follows from $\tilde{f}(u_c, 0) \in \{-F_s, 0, F_s\}$, $e|_{\hat{x}_2=0} = x_2$ and $-x_2 f(u, x_2) \leq 0$. With the Mean Value theorem follows

$$[F_s \mathrm{sgn}\,(x_2) - f(u, x_2)]_{x_2 \neq 0} = (g(0) - g(x_2))\mathrm{sgn}\,(x_2) = -g'(z)\mathrm{sgn}\,(x_2)\, e, \tag{4.48}$$

with z some point on the line segment $l(0, x_2)$. Substitution of (4.48) into (4.47) yields

$$\dot{V}(\underline{x}_b)\Big|_{\hat{x}_2=0} \leq -bx_2^2 - (b + LJ + g'(z)\mathrm{sgn}\,(\hat{x}_2))(\alpha e^2 + \gamma|e|) - g'(z)|x_2|e, \tag{4.49}$$

which is equivalent to (4.43). Moreover, since also $|F_s \mathrm{sgn}\,(x_2) - f(u, x_2)|_{x_2 \neq 0} \leq \delta F$, (4.49) is semi-negative definite with the choice for γ according to (4.45).

With the specific choice for α and $L > L_c$ it can be concluded that the time-derivative of (4.40) is semi-negative definite for γ chosen as in (4.45). With the application of La Salle's Invariance Principle [7] it follows that solutions always tend to the largest invariant set in $S = \{x \in \mathbb{R}^n | \dot{V}(\underline{x}_b, t) = 0\} = \{x \in \mathbb{R}^n | x_2 = 0 \wedge e = 0\} = \{x \in \mathbb{R}^n | x_2 = 0 \wedge \hat{x}_2 = 0\}$. Substitution of $x_2, \hat{x}_2 = 0$ in (4.4) yields $\dot{x}_1 = 0$, $\dot{x}_2 = -b_1 x_1$ and $\dot{\hat{x}}_2 = -b_1 x_1$. Similar to the smooth case the only invariant set within S is the origin and global asymptotical stability of the origin can, therefore, be concluded for $L > L_c$.

4.6 Numerical Implementation

In section 4.2 it is shown that in some regions on the switch surface Σ_1 ($x_2 = 0$) attracting sliding modes occur. In this regions solution slide for some period of time along the plane Σ_1 due to the fact that the discontinuous vector field points towards Σ_1 on both sides. In a numerical environment solutions will never come exact on the sliding surface and the numerical integration routine will therefore have collocation points on both sides of the switch surface. As a result, the numerical solution will start to chatter very fast around the switch surface resulting in an excessive amount of integration steps.

For the purpose of efficient numerical integration in the neighborhood of sliding modes, therefore, a thin space V_Σ is constructed symmetric around the switch surface as illustrated in figure 4.6. The height of the thin space with respect to the switch surface is denoted with the constant η, the total width of the thin space is consequently 2η. In the regions where attracting sliding modes occur the solution is pushed to the center of the small band but now with a continuous vector field. The thickness parameter η should be taken sufficiently small such that the numerical approximation has no qualitative influence on the solution and the

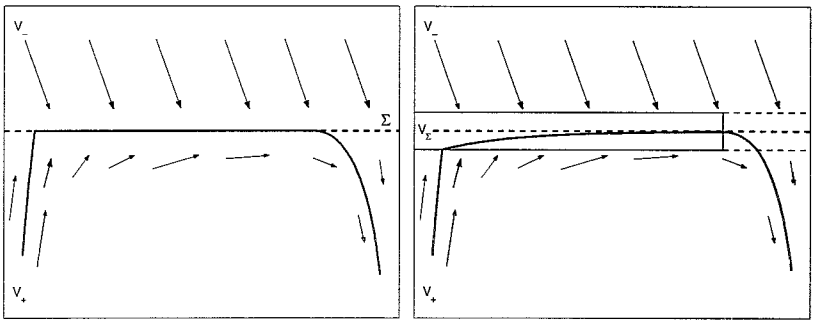

Figure 4.6: Exact sliding mode (left) and numerical approximation (right).

integration tolerance should be taken such that $TOL \ll \eta$ [6].

The resulting switch model for the numerical implementation of the non-smooth actual friction reads as

$$f(u,x_2) = \begin{cases} g(x_2)\mathrm{sgn}\,(x_2) & \text{if } |x_2| > \eta & \text{(slip)} \\ u & \text{if } |x_2| \leq \eta \text{ and } u \leq F_s & \text{(stick)} \\ F_s\mathrm{sgn}\,(u) & \text{otherwise} & \text{(transition)} \end{cases} . \tag{4.50}$$

In the stick phase, solutions must be pushed to the center of V_Σ. This is accomplished since in the stick phase, (4.50) makes equilibrium with the external force

$$(u - f(u,x_2))|_{|u|\leq F_s, |x_2|\leq\eta} = 0. \tag{4.51}$$

Consequently, the required deceleration of the link in the stick phase follows from the viscous friction term $(-bx_2)$.

For the switch surface of the compensation rule no sliding modes exist. Nevertheless the compensation rule is also adapted since it is based on the modelling of the actual friction. Otherwise the actual friction will not always be cancelled by the compensation rule once the observer error is equal zero. The adapted compensation rule for numerical simulation reads as

$$\tilde{f}(u_c,\hat{x}_2) = \begin{cases} g(\hat{x}_2)\mathrm{sgn}\,(\hat{x}_2) & \text{if } |\hat{x}_2| > \eta & \text{(slip)} \\ F_s\mathrm{sgn}\,(u_c) & \text{otherwise} & \text{(transition/stick)} \end{cases} . \tag{4.52}$$

4.7 Numerical Results

In this section the gained knowledge on the regulated and compensated non-smooth system of (4.4) will be illustrated with some numerical results. For the friction, the average values from table 2.1 will be applied ($L_c = 73$). The numerical integration of (4.4) is done with the *ODE45* routine of MATLAB with an integration tolerance of TOL $= 1 \cdot 10^{-12}$. In figure 4.7, two solutions computed for $n_1 = 0.4$, $n_2 = 0.02$, $L = 35$, $\eta = 1 \cdot 10^{-9}$ and two different initial conditions are depicted. In figure 4.8, the actual friction, the friction compensation and the observer error (now zoomed in close to $e = 0$) are depicted. It can be noted that the observer error becomes very close to the machine accuracy but the zero observer error set is not crossed. Both solutions are, therefore, theoretically correct. For an increasing observer gain the observer error will become even smaller and accuracy problems, similar as found for the smooth case (see section 3.6), are likely to occur.

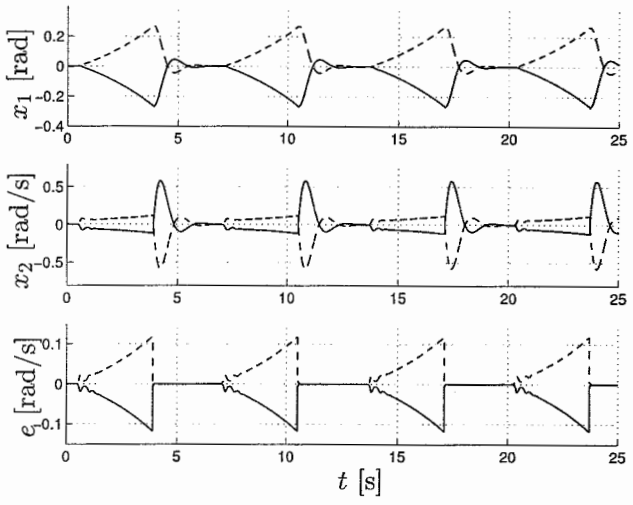

Figure 4.7: Numerical solution of (4.4) with $\underline{x}_b(0) = [0.001, 0.001, 0.002]^T$ (solid) and $\underline{x}_b(0) = -[0.001, 0.001, 0.002]^T$ (dashed) for $n_1 = 0.4$, $n_2 = 0.02$, $L = 35$ and $\varepsilon = 1 \cdot 10^6$ (from top to bottom states x_1, x_2 and e against time t).

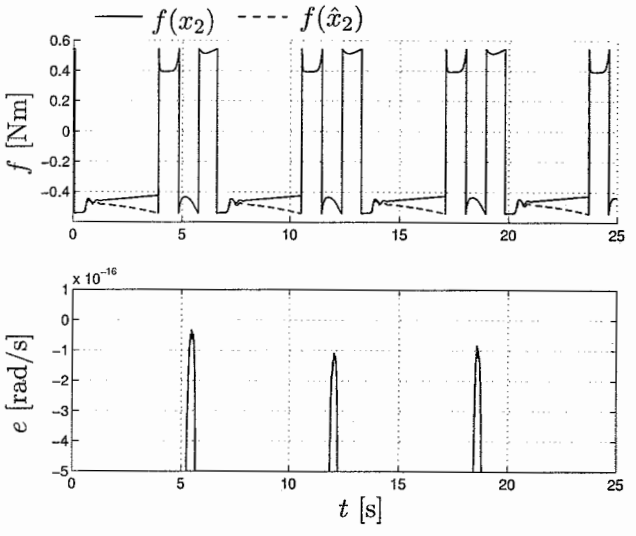

Figure 4.8: Friction $f(x_2)$, friction compensation $f(\hat{x}_2)$ and e (zoomed in close to $e = 0$) corresponding to the numerical solution as depicted in figure 4.7.

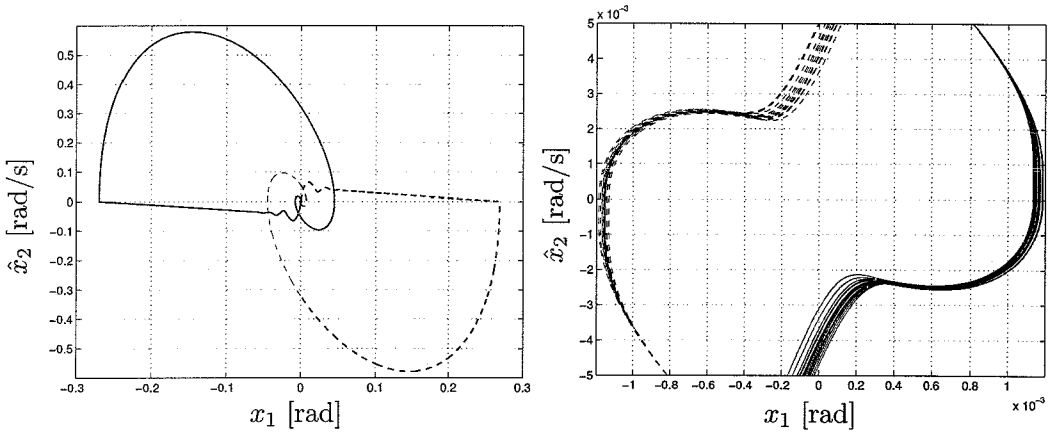

Figure 4.9: Left: Perpendicular projection of two numerical solutions for (4.4) (also depicted in figure 4.7) on the plane $x_2 = 0$. Right: similar but zoomed in close to $(x_1, \hat{x}_2) = (0, 0)$.

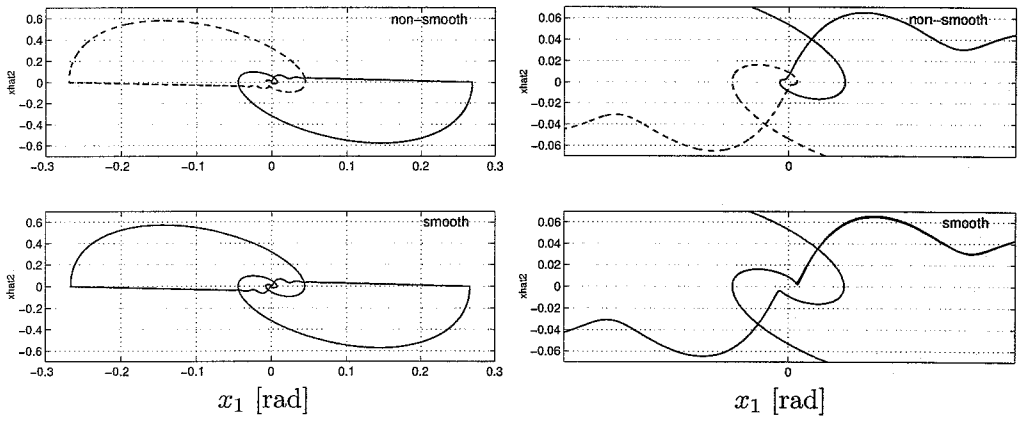

Figure 4.10: Left: from top to bottom perpendicular projection of the two limit cycle found for the non-smooth system (also depicted in figure 4.7) on the plane $x_2 = 0$ and projection of the limit cycle found for the smooth system (also depicted in figure 3.6) on the plane $x_2 = 0$. Right: similar but zoomed in.

Both solutions, as depicted in figure 4.7, seem to be periodic. However, this could not be confirmed by solving the two boundary value problem $\underline{x}_b(t) = \underline{x}_b(t+T)$, with for example the shooting method [14]. In figure 4.9 (left) the result, perpendicular projected on the plane $x_2 = 0$, of solving (4.4) for a longer timescale ($t \in [0, 150]$) for the same initial conditions and settings as in figure 4.7) is depicted. To eliminate possible transient effects, the first 60 seconds of the solution are left out of this figure. The projections seems to be two different closed orbits confirming the periodicity of the solutions. However, by zooming in, the projections reveal to be multiple different encirclements of the origin. Consequently, the numerical solutions are either periodic with a period time in which the origin is encircled multiple times or are not periodic at all. The exact nature of this behaviour is not examined further. However, the lack of periodicity makes analysis of this behaviour with for example path-following techniques [13, 14] impossible.

In figure 4.10, the perpendicular projections on the plane $x_2 = 0$ of the two theoretically correct solutions found for the non-smooth system and the incorrect solution found for the smooth system for the equivalent parameter settings are depicted. By comparing the resulting shape of the junction of the two correct solutions with the shape of the incorrect solution it could be that that the two theoretically correct limit cycles also exist for the smooth system and that the numerical solution jumps from one to the other periodically.

In figure 4.11, the solution is depicted for similar parameters settings as in figure 4.7 but the observer gain increased to $L = 37$. In the left plot the observer error (now zoomed in close to $e = 0$) is depicted. It can be noted that the observer error becomes now even smaller than for $L = 35$. As a result the solution switches between the two correct limit cycles arbitrary. Numerical analysis of te closed-loop system (4.11) with unstable observer error dynamics is, similar to the smooth case, limited due to the finite accuracy of the floating-point computation.

Finally, a solution is depicted for the non-smooth system with a super-critical observer gain ($L = 74$) in figure 4.11 (left). The computed input torque (u) for the solution and the norm of the solution compared to the applied integration tolerance are depicted in figure 4.11 (right). The solution tends to the origin without any instabilities of the observer error as expected as long as the solution can be considered accurate with respect to the applied integration tolerance. Once the integration tolerance becomes significant the computed input force start to chatter due to the combination of the discontinuous compensation rule for zero velocity and the inevitable integration errors.

For the experimental setup the electrical motor is powered with Pulse Width Modulation (PWM). The input torque u may chatter in this case provided that the necessary real-time computations can be handled at a rate which is beyond the frequency range of the unmodelled dynamics [12]. If the identification and modelling of the friction is of such accuracy that the origin is reach within the integration tolerance the occurring chattering is acceptable if the sample rate is beyond resonances of possible flexible modes. No extra precautions are, therefore, taken to prevent the chattering of the input torque within the numerical simulation.

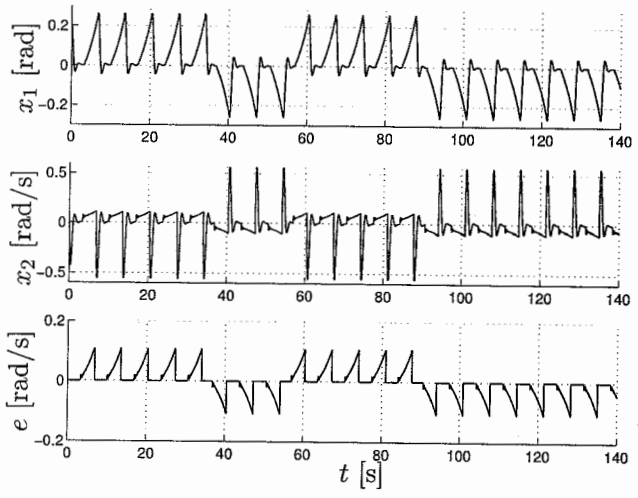

Figure 4.11: Numerical solution of (4.4) and $\underline{x}_b(0) = [0.2, 0, 0]^T$ for $n_1 = 0.4$, $n_2 = 0.02$, $L = 37$ and $\eta = 1 \cdot 10^{-9}$ (from top to bottom states x_1, x_2 and e against time t).

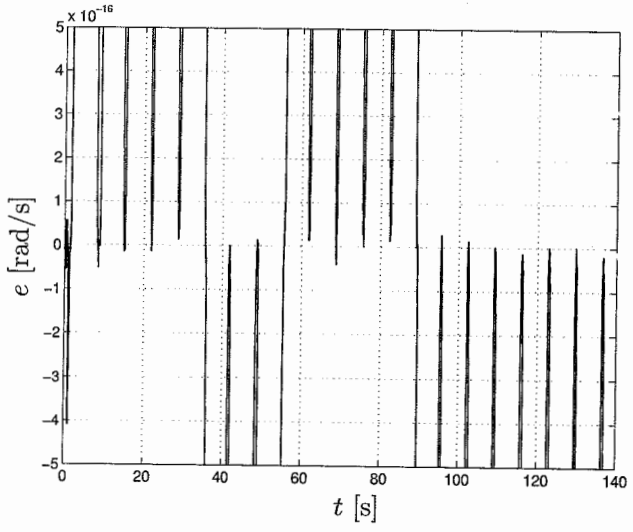

Figure 4.12: Observer error (zoomed in close to $e = 0$) corresponding to the numerical solution as depicted in figure 3.8.

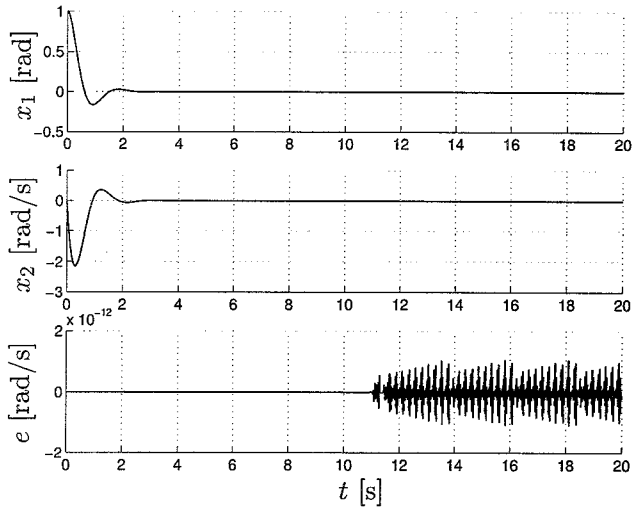

Figure 4.13: Numerical solution of (4.4) and $\underline{x}_b(0) = [1, 0, 0]$ for $n_1 = 0.4$, $n_2 = 0.02$, $L = 74$ and $\eta = 1 \cdot 10^{-9}$ (from top to bottom x_1, x_2 and e against time t).

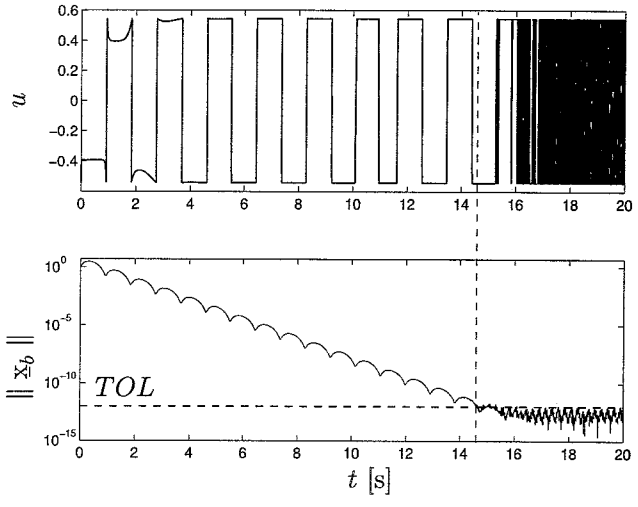

Figure 4.14: Computed input torque u against time t and $||\underline{x}_b||$ against time t corresponding to the numerical solution depicted in figure 4.13.

4.8 Discussion

The design specification for a guaranteed globally asymptotically stable set-point, similar as derived for the smooth case, happens to be also applicable for the closed-loop system with the non-smooth friction and friction compensation. The conclusions drawn for the smooth case are, therefore, also hold for the non-smooth case. There are, however, two main differences with the smooth case. The first difference with the smooth case is the fact that for the non-smooth case the origin is no longer, irrespectively of the observer gain and controller gains, a unique equilibrium point as desired. It is, however, shown that a sufficient condition for the observer gain such that the set-point is a unique equilibrium point is similar to the condition derived for the asymptotic stability of the observer error. The second main difference is the fact that the derived sufficient condition for the observer gain as derived for the smooth case is a necessary condition for the non-smooth case. The critical observer gain is, therefore, even more stringent for the non-smooth case.

The succes of the strategy of reduced-order observer based friction compensation can therefore be extended for the closed-loop system with the non-smooth friction modelling. Although the non-smooth friction model is capable of describing a rich set of friction phenomenon, the modelling is still not perfect. In a practical environment the friction parameters will be contaminated with some small errors or could exhibit small deviations, due to for example temperature changes.

In next chapter, the effect of possible over or under-compensation due to small identification inaccuracies will be examined by simply scaling the compensation rule with a single scaling constant. Both the smooth and the non-smooth type of friction modelling will be addressed.

Chapter 5

Closed-Loop System Analysis : A Non-Exact Case

In an experimental environment the modelling and identification of dry friction will never be exact. The actual dry friction will therefore almost always be over-compensated or under-compensated. To obtain insight in the consequences of over-compensation or under-compensation a simple form of non-exact friction compensation will be examined following in this chapter. For the resulting closed-loop system both the smooth and the non-smooth type of friction modelling will be addressed.

The non-exact friction compensation as examined in this chapter follows from simply scaling the friction compensation rule. By scaling this compensation rule a mismatch of constant rate will be introduced between the actual friction and the friction compensation as illustrated for the smooth friction model in figure 5.1. For the experimental implementation the rate of over-compensation or under-compensation can differ for each point on the velocity/friction mapping. Due to dynamical friction effects, position dependencies and temperature changes the rate of over-compensation or under-compensation can even be varying for constant velocities. For the practical implementation of the friction compensation the error in the friction modelling is, therefore, far more complicated than accounted for by simply scale the compensation model. The simply scaled compensation rule is, however, a good starting point to study the effects of small friction modelling errors for the reduced-order observer based friction compensation.

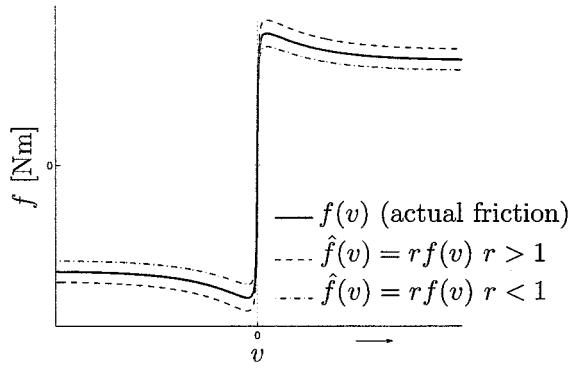

Figure 5.1: Simply non-exact friction compensation ($\hat{f}(v)$) illustrated for the smooth friction model.

L	ε	b_4/L	r_b	$\lambda_{1,2}$	λ_3
7.3500	$1 \cdot 10^4$	1.52780	1.52803	$0 \pm 4.8483i$	$-1.3295 \cdot 10^5$
7.3500	$1 \cdot 10^6$	1.52780	1.52800	$0 \pm 4.8486i$	$-1.3293 \cdot 10^7$
73.500	$1 \cdot 10^4$	1.05279	1.05282	$0 \pm 4.0245i$	$-1.3301 \cdot 10^5$
73.500	$1 \cdot 10^6$	1.05279	1.05279	$0 \pm 4.0245i$	$-1.3293 \cdot 10^7$
735.00	$1 \cdot 10^6$	1.00528	1.00528	$0 \pm 3.9289i$	$-1.3293 \cdot 10^7$
7350.0	$1 \cdot 10^6$	1.00053	1.00053	$0 \pm 3.9233i$	$-1.3301 \cdot 10^7$

Table 5.1: Computed bifurcation value $[r]$ and corresponding eigenvalues of (5.2) for various values of L and ε and with $n_1 = 0.4$, $n_2 = 0.02$ and for the average friction parameters of table 2.1.

5.1 Smooth System with Scaled Compensation Rule

For simple non-exact friction compensation following from a scaled compensation rule the system equations of (3.2) become

$$\dot{\underline{x}}_b = \underline{f}_{sr}(\underline{x}_b) = \begin{bmatrix} 0 & 1 & 0 \\ -b_1 & -b_2 & -b_3 \\ -b_1 & L & -b_4 \end{bmatrix} \underline{x}_b + \frac{1}{J} \begin{bmatrix} 0 \\ rf(\hat{x}_2) - f(x_2) \\ 0 \end{bmatrix}, \tag{5.1}$$

with the scaling parameter $r \approx 1$. With $r > 0$ the equilibrium analysis for (5.1) is similar as in section 3.3 and, consequently, the origin is also the unique equilibrium point of (5.1). For local stability analysis of this unique equilibrium point, (5.1) is linearized about the origin, yielding the Jacobian matrix

$$\frac{\partial \underline{f}_{sr}(\underline{x}_b)}{\partial \underline{x}_b} = \begin{bmatrix} 0 & 1 & 0 \\ -b_1 & -b_2 - f'(0)/J & -b_3 + rf'(0)/J \\ -b_1 & L & -b_4 \end{bmatrix}, \tag{5.2}$$

where $f'(0) = 2\varepsilon F_s/\pi$. The coefficients of characteristic polynomial $\lambda^3 + a\lambda^2 + b\lambda + c = 0$ for (5.2) are equal to

$$a = f'(0)/J + b_4 + b_2 \tag{5.3}$$

$$b = b_1 + b_4 f'(0)/J - Lrf'(0)/J + b_3 L + b_2 b_4 \tag{5.4}$$

$$c = b_1(b_4 - b_3) + b_1 rf'(0)/J. \tag{5.5}$$

With Routh's Stability Criterion [8] it can be concluded that the origin will be locally asymptotical stable if and only if $a, c > 0$ and $ab > c$. Since $b_i, f'(0), r > 0$ and $b_4 > b_3$ it follows that $a, c > 0$ and the origin will, therefore, only become unstable if $b < c/a$. The critical value for r happens to be

$$r > \frac{\frac{b_1 + b_4 f'(0)/J + b_3 L + b_2 b_4}{Lf'(0)/J} - \frac{b_1(b_4 - b_3)}{(Lf'(0)/J)(f'(0)/J + b_4 + b_2)}}{1 + \frac{b_1}{L(f'(0)/J + b_4 + b_2)}} \triangleq r_b. \tag{5.6}$$

With $\lim_{\varepsilon \to \infty} f'(0) = \infty$ it follows from (5.6) $\lim_{\varepsilon \to \infty} r_b = \frac{b_4}{L}$. Since $b_4 > L$ the origin will become unstable only for $r > 1$ or in other words when the actual friction is over-compensated. Since $\lim_{L,\varepsilon \to \infty} r_b = 1$ it follows that the origin only exchanges stability at exactly $r = 1$ if both the approximation of the discontinuity is taken infinitely steep and the observer gain is set infinitely large (when the observer is extremely sensitive).

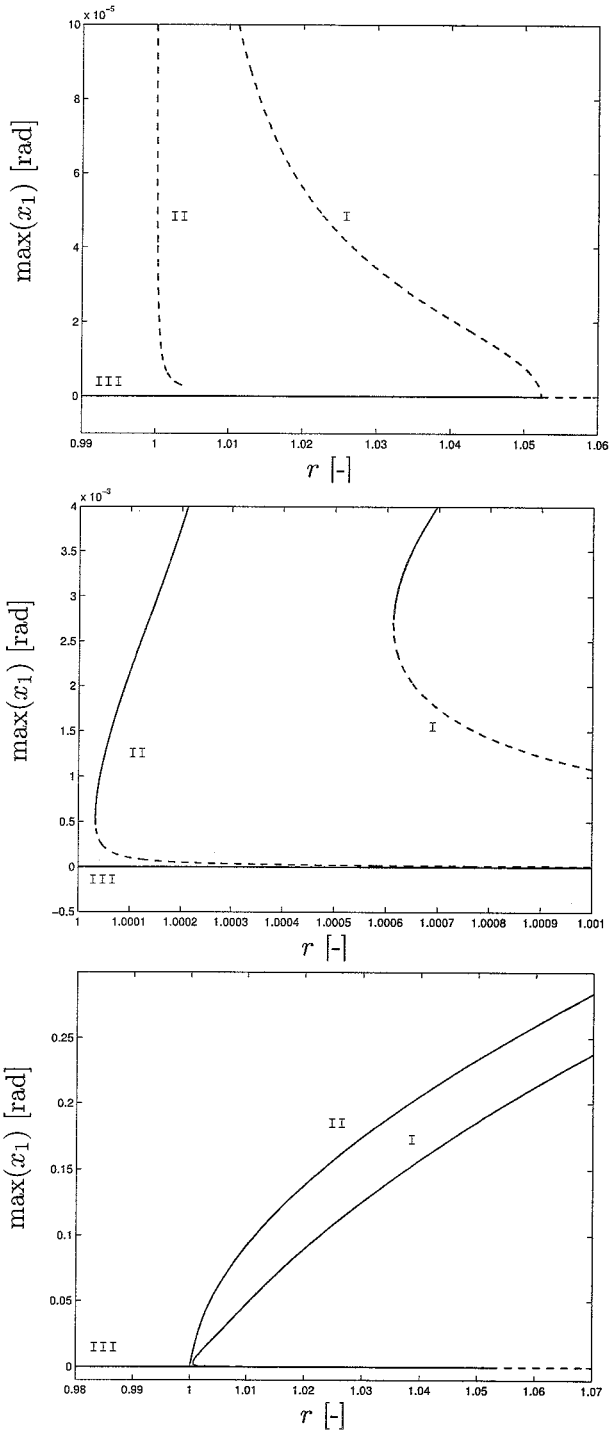

Figure 5.2: Various details of the two computed branches of limit cycles for $n_1 = 0.4$, $n_2 = 0.02$, $L = 73.5$, the friction parameters the average values of table 2.1 ($L_c = 73$) and $\varepsilon = 10^4$ (I) and $\varepsilon = 10^6$ (II) and equilibrium point (III) (unstable solutions dashed and stable solutions solid).

L	n_1	n_2	ε	r_b	r_{Fold}
73.5	0.4	0.02	$1 \cdot 10^4$	1.05282	1.000612
73.5	0.4	0.02	$1 \cdot 10^6$	1.05279	1.000033
73.5	0.4	0.20	$1 \cdot 10^4$	1.14708	1.001637
73.5	0.4	0.20	$1 \cdot 10^6$	1.14699	1.000086

Table 5.2: Computed bifurcation value [r] for various values for n_1, n_2, L, ε and for the friction parameters the average values of table 2.1.

In table 5.1, exact values for r_b with corresponding eigenvalues of (5.2) are shown for $n_1 = 0.4$, $n_2 = 0.02$, the friction parameters the average values of table 2.1 ($L_c = 73$) and various values for L, ε. At the bifurcation point a pair of complex conjugated eigenvalues exist on the imaginary axis. The bifurcation can, therefore, be classified as a *Hopf* bifurcation [7]. Consequently, the stability of the equilibrium point will be lost for $r > r_b$ and a limit cycle will be born at the bifurcation point.

With the *pseudo arclength continuation* [13] technique a branch of limit cycles can be followed while varying a parameter. With this technique, limit cycles for a varying value of r are followed for steepness parameters of $\varepsilon = 10^4$ and $\varepsilon = 10^6$, $n_1 = 0.4$, $n_2 = 0.02$, $L = 73.5$ and the friction parameters the average values of table 2.1 ($L_c = 73$). In figure 5.2 (top) the computed branches are depicted close to the equilibrium point. For the branch of limit cycles for $\varepsilon = 10^4$ (I), the limit cycle at the Hopf bifurcation is unstable and the Hopf bifurcation is, therefore, subcritical. The branch of limit cycles for $\varepsilon = 10^6$ could not be followed until the Hopf bifurcation point due to the excessive instability of the found limit cycle, but a similar scenario as for branch I is most likely.

The branch of unstable limit cycles born from the Hopf bifurcation point folds into a branch of stable limit cycles close to $r = 1$ as shown in figure 5.2 (middle). From the two computed branches it seems that for an increasing steepness parameter (ε) the location of the fold bifurcation tends to $(r, \max(x_1)) = (1, 0)$. In other words, the minimum rate of over-compensation, such that limit cycling occurs, tends to $r = 1$ for $\varepsilon \uparrow$. In table 5.2, the exact computed bifurcation values for these two cases and for a similar case but with a higher derivative gain ($n_2 = 0.2$) are shown. With the higher derivative gain the distance between the Hopf and the fold bifurcation is much larger but the fold bifurcation still occurs close to $r = 1$. After the fold bifurcation no further bifurcations for the branch of stable limit cycles are found as shown in figure 5.2 (bottom). The complete bifurcation diagram for the smooth system with a scaled compensation rule is, therefore, as depicted in figure (5.3).

In figure 5.4 the coexisting stable and unstable limit cycle for $r = 1.01$, $L = 73.5$, $n_1 = 0.4$, $n_2 = 0.02$ are depicted. In the bottom plots also the computed friction ($f(x_2)$) is plotted for the range of the actual velocity (x_2) of the corresponding limit cycle. It can be noted that for the unstable solution the actual friction is only described by the smoothing of the discontinuous velocity/friction mapping (the small region where $\left|\frac{2}{\pi}\text{atan}\left(\varepsilon x_2\right)\right| \ll 1$). Since the observer error is an order of magnitude lower that the actual velocity a similar reasoning holds for the friction compensation. Consequently, both the friction and friction compensation, for the unstable limit cycle, are described by the smoothing region.

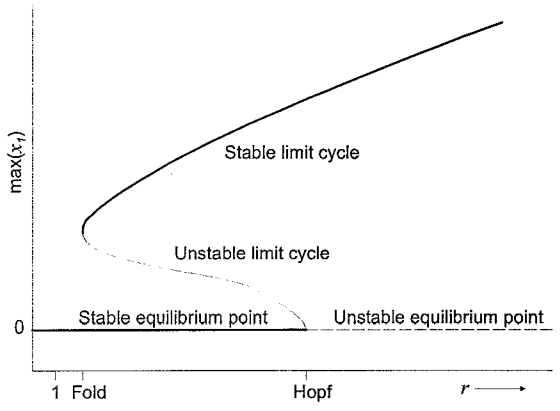

Figure 5.3: Bifurcation diagram for smooth system with scaled compensation rule.

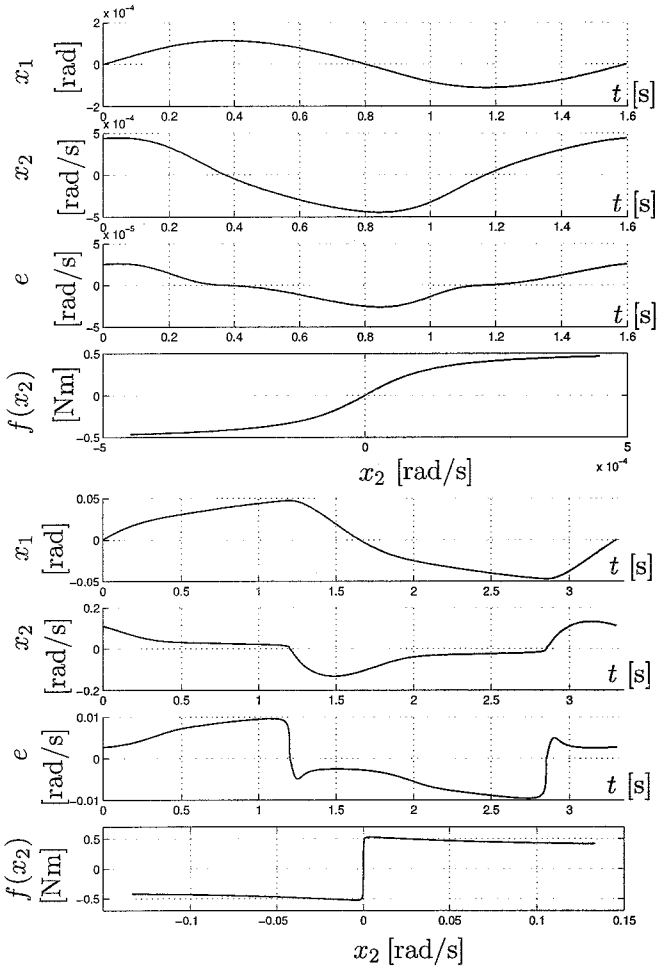

Figure 5.4: Stable (top) and unstable (bottom) limit cycle for $r = 1.01$, $L = 73.5$, $n_1 = 0.4$, $n_2 = 0.02$, $\varepsilon = 10^4$ and for the friction parameters the average values of table 2.1. From top to bottom x_1,x_2 and e against time t and actual friction $f(x_2)$ against actual velocity x_2.

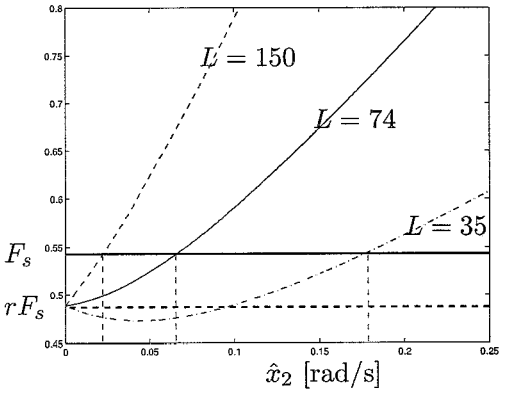

Figure 5.5: Set where (5.10) is satisfied for $\hat{x}_2 > 0$, $r = 0.9$, for various values of L and the average friction parameters of 2.1 ($L_c = 73$).

5.2 Non-Smooth System with Scaled Compensation Rule

For simple non-exact friction compensation following from a scaled compensation rule the system equations of (4.4) become

$$\dot{\underline{x}}_b = \begin{bmatrix} 0 & 1 & 0 \\ -b_1 & -b_2 & -b_3 \\ -b_1 & L & -b_4 \end{bmatrix} \underline{x}_b + \frac{1}{J} \begin{bmatrix} 0 \\ r\tilde{f}(u_c, \hat{x}_2) - f(u, x_2) \\ 0 \end{bmatrix}, \tag{5.7}$$

with the scaling parameter $r \approx 1$. Equilibria of (5.7) satisfy $x_2 = 0$ and consequently

$$|u_c^* + r\tilde{f}(\hat{x}_2, u_c^*)| \leq F_s \text{ where } u_c^* = (b + LJ)\hat{x}_2 \tag{5.8}$$

$$x_1 = -\frac{b + LJ + n_2}{n_1}\hat{x}_2. \tag{5.9}$$

Since for $\hat{x}_2 = 0$ both the control force (u_c^*) and the compensation ($\tilde{f}(\hat{x}_2, u_c^*)$) are equal to zero is the origin an equilibrium point of (5.7) irrespectively of the value for r. For $\hat{x}_2 \neq 0$ follows $\tilde{f}(u_c, \hat{x}_2) = g(\hat{x}_2)\text{sgn}(\hat{x}_2)$ and (5.8) can, therefore, be written as

$$|(b + LJ)\hat{x}_2 + rg(\hat{x}_2)\text{sgn}(\hat{x}_2)| \leq F_s,\ \hat{x}_2 \neq 0. \tag{5.10}$$

For a fixed value of r, the size of the set for $\hat{x}_2$ such that (5.10) is satisfied can only be influenced by the observer gain L. In figure 5.5, (5.10) is illustrated graphically for the under-compensated case and the average friction parameters of 2.1. From the figure it can be noted that due to the under-compensation of the actual friction a set appears where (5.10) is satisfied. In this set, system (5.7) is in equilibrium if simultaneously (5.9) also is satisfied. The width of the resulting equilibrium set for $\hat{x}_2$ (denoted as $\max(\hat{x}_2^*)$) will decrease for an increasing observer gain but zero width is not possible. It is emphasized that in the under-compensated case the resulting equilibrium set will still be smaller than in the non-compensated case ($r = 0$), but always larger than in the case of exact-compensation or over-compensation.

For an increasing observer gain $\max(\hat{x}_2^*)$ will decrease but the resulting maximum equilibrium position ($\max(x_1^*)$) following from (5.9) will increase. The relation between the observer gain (L) and the maximum steady-state position error ($\max(x_1^*)$) is, therefore, not trivial. To gain more insight in this relation, $\max(x_1^*)$ is computed for a wide range of L and n_1 ($n_2 = 0.02$)

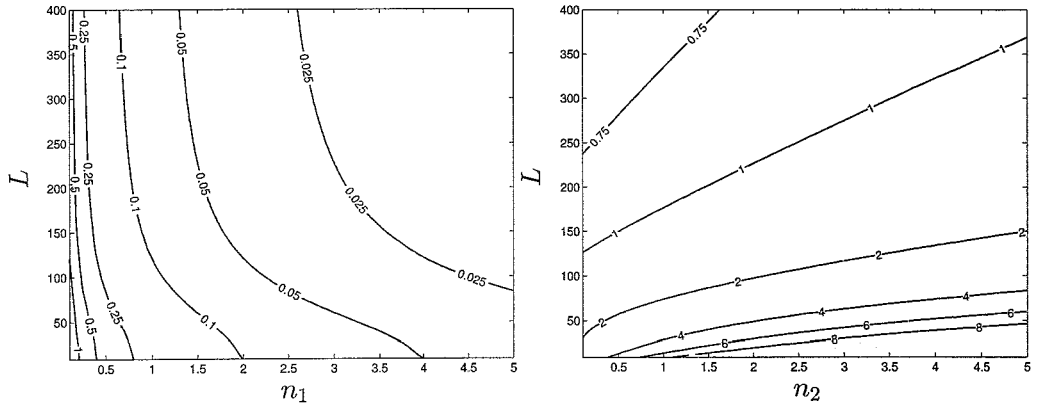

Figure 5.6: Left: Contour plot for maximum steady state position error ($\max(x_1^*)$ [rad]) for $r = 0.9$ depending on L and $\mathbf{n_1}$ with $n_2 = 0.02$. Right: Contour plot for maximum steady state position error ($\max(x_1^*)$ [rad]) for $r = 0.9$ depending on L and $\mathbf{n_2}$ with $n_1 = 0.1$.

and similar for L and n_2 ($n_1 = 0.1$), for the average friction parameters of table 2.1 and $r = 0.9$. The results are depicted in figure 5.6. For both cases the steady-state positioning error is decreasing for L increasing.

The relations $n_1 \uparrow \Rightarrow \max(x_1^*) \downarrow$ and $n_2 \uparrow \Rightarrow \max(x_1^*) \uparrow$ follow directly from (5.9). It can be noted that even for the under-compensated case ($\max(x_1^*)$) can be reduced theoretically to zero by taking $n_1 \gg (LJ + b + n_2)$.

The state equations (5.7) can not be linearized and, consequently, local stability of equilibria can not be studied by simply examining the stability of the linearized system. Stability of equilibria for (5.7) is, therefore, examined numerically. In figure 5.7 the result of this approach is depicted for $r = 0.9$, $n_1 = 0.4$, $n_2 = 0.02$, $L = 73.5$, $\eta = 1 \cdot 10^{-9}$ and the average friction parameters of table 2.1. All solutions tend to the equilibrium set and no other type of solutions, for example limit cycles, are found. For these parameter settings the resulting equilibrium set can be considered attractive. In figure 5.8 the result of this approach is depicted for three values $r > 1$ and the same parameters as in figure 5.7. For the over-compensated case the initial condition is taken just outside the thin space used for the efficient numerical integration of sliding modes (see section 4.6). It can be noted that for the used set of parameters and the origin of (5.7) is not stable for the over-compensated case. For both the under-compensated case and the over-compensated case the same results are found for other parameter settings and values for r.

As was done for the smooth case, the branch of limit cycles for a varying value for r is computed for $\eta = 1 \cdot 10^{-9}$ and an integration tolerance of TOL $= 1 \cdot 10^{-13}$ as depicted in figure 5.9 (left). Other parameters values are the same as in the smooth case, see figure 5.2. In 5.9 (right) the bifurcation diagram is zoomed in close to $r = 1$ and in this figure also the branches for the smooth case are depicted (note that the branch of stable limit cycles for the non-smooth case could only be followed until $r \approx 1 + 1 \cdot 10^{-5}$ due to the decreasing scale of the limit cycle in combination with the finite accuracy of the numerical routines).

For the non-smooth smooth system no unstable limit cycles could be found, but this is no formal proof that no other unstable limit cycles exist. However, since the friction and friction compensation for the unstable limit cycles as found for the smooth case where only described

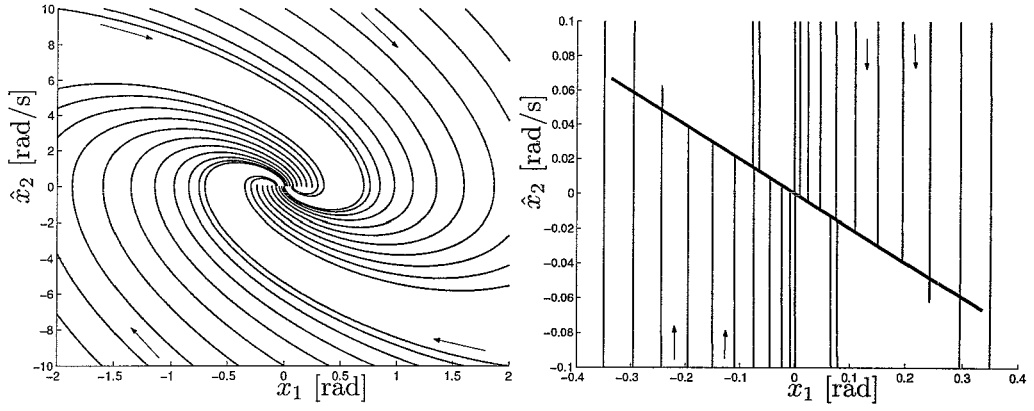

Figure 5.7: Left: Several solutions for an under-compensated system ($r = 0.9$) projected on the plane $x_2 = 0$ revealing the attractive equilibrium set for $n_1 = 0.4$, $n_2 = 0.02$, $L = 73.5$, $\eta = 1{\cdot}10^{-9}$ and the average friction parameters of table 2.1. Right: enlargement of equilibrium set.

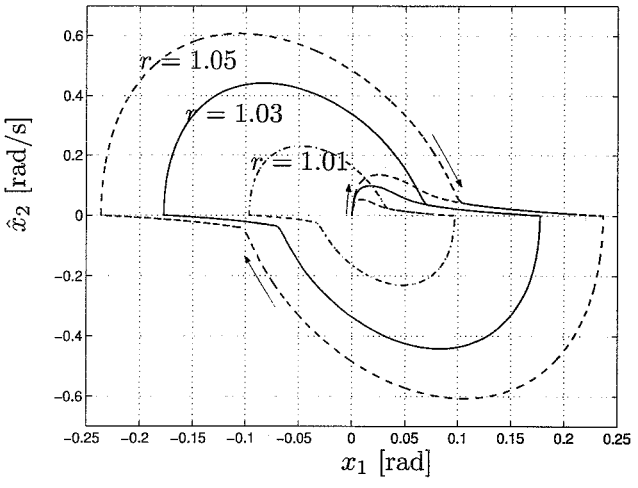

Figure 5.8: Numerical solution for (5.7) with $x_b(0) = 2\eta[0, 1, 1]$ for three values $r > 1$, $L = 73.5$, $n_1 = 0.4$, $n_2 = 0.02$, $\eta = 1 \cdot 10^{-9}$ and the average friction parameters of table 2.1, projected on the plane $x_2 = 0$.

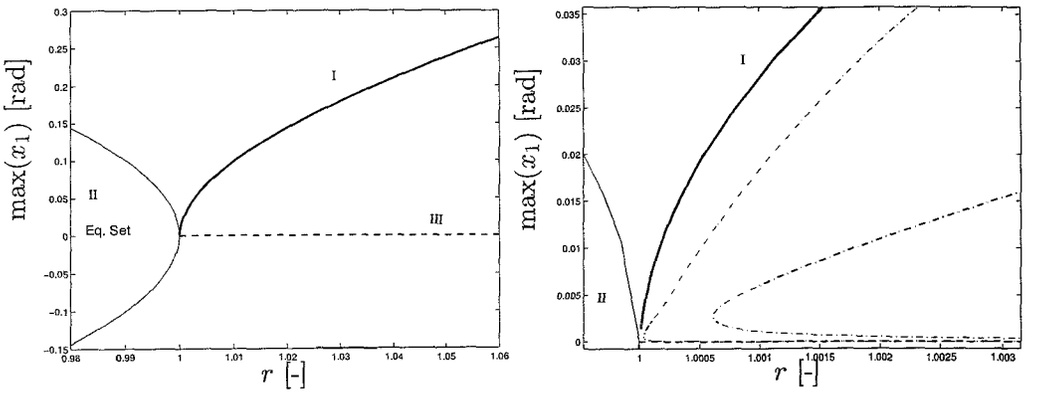

Figure 5.9: Branch of solutions for non-smooth friction model with $n_1 = 0.4$, $n_2 = 0.02$, $L = 73.5$ and the average friction parameters of table 2.1 ((I) (stable) equilibrium set (II) and (unstable) equilibrium point (III) and branches for smooth friction model (dash-dot)).

by the smoothing of the discontinuous velocity/friction mapping it is not said that unstable limit cycles must exist for the non-smooth case.

At a super-critical Hopf bifurcation, as occurring in smooth systems, stability of the equilibrium point is lost and a stable limit cycle is born. If it is assumed that the branch of limit cycles is born at exactly $r = 1$ then bifurcation diagram 5.2 shows analogues with the continuous super-critical Hopf bifurcation with the difference the decreasing equilibrium set for $r < 1$.

For the smooth case it seems that the fold bifurcation did tends to $(r, \max(x_1)) = (1, 0)$ for $\varepsilon \to \infty$. Consequently, it could be that the bifurcation diagram as shown in 5.9 is the limit case of the bifurcation diagram as shown in figure 5.3 for $\varepsilon \to \infty$. It is then said that the discontinuous super-critical Hopf bifurcation *unfolds* in a continuous fold bifurcation plus a continuous sub-critical Hopf bifurcation. Another possible cause for the movement of the Hopf bifurcation to $r = 1$ for the non-smooth case could be the discontinuous compensation rule for zero velocity ($\hat{f}(0, u_c) = F_s \text{sgn}(u_c)$). This discontinuity makes the compensation rule for zero velocity extremely sensitive which could be compared with an infinite stiff observer for a continuous compensation rule. After all, for the smooth case it has been shown analytically that the Hopf bifurcation tends to $r = 1$ for $\varepsilon, L \to \infty$. However, it is not the goal of this thesis to classify discontinuous bifurcations. The bifurcation diagram for the smooth case and for the non-smooth case are only compared to gain more insight in the non-smooth bifurcation diagram at exactly $r = 1$.

In practice, the dry friction will behave non-smooth and asymmetrical. Therefore, the bifurcation diagram for the same parameters values as in figure 5.9 is also shown for the *asymmetrical* friction parameters of table 2.1 ($L_c = 94.4$) in figure 5.10. The behaviour is, apart from the asymmetrical equilibrium set, comparable with the bifurcation diagram as depicted for the symmetrical case.

5.3 Discussion

For both the smooth case and the non-smooth case it has been shown that if the friction is slightly over-compensated, the closed-loop system exhibits stable limit cycling. Contrary to the results in the smooth case, the under-compensation of the friction for the non-smooth

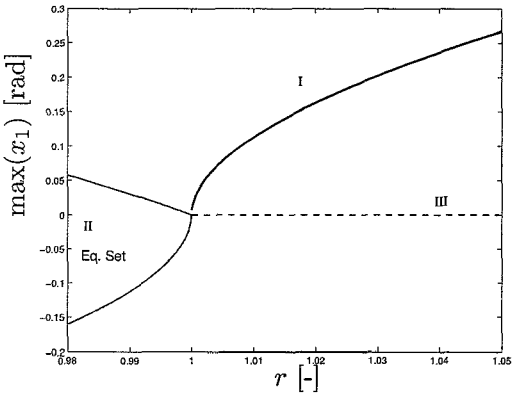

Figure 5.10: Branch of solutions for non-smooth friction model with $n_1 = 0.4$, $n_2 = 0.02$, $L = 73.5$ and the asymmetrical friction parameters of table 2.1 ((I) (stable) equilibrium set (II) and (unstable) equilibrium point (III) and branches for smooth friction model (dash-dot))

case results in the existence of an equilibrium set. A zero steady-state error is, therefore, no longer guaranteed for this case. The resulting steady-state error, due to the existence of the equilibrium set, can be minimized by increasing the observer gain and the proportional controller gain or by decreasing the derivative gain. Namely, the equilibrium set becomes smaller by taking these measures. Limit cycling is fatal for positioning tasks. Slight under-compensation of the friction is, therefore, even at the cost of a small steady state error, more advisable then over-compensation.

Chapter 6

Experimental Results

In this chapter, results of the application of the reduced-order observer based friction compensation strategy to the experimental setup of the one-link robot are presented. For the experimental implementation the friction is modelled by the non-smooth friction model (4.1) with the asymmetric friction parameters of table 2.1. This static model is able to describe dry friction phenomena, such as the Stribeck effect, pure stiction and an asymmetric friction/velocity mapping. The angular displacement of the link is measured at the experimental setup with a resolution of $2 \cdot 10^4$ increments per revolution of the motor shaft. Due to the gear ratio of the transmission of 8.192 [-], the effective resolution for the position of the link is $3.835 \cdot 10^{-5}$ rad. The induction motor is powered by Pulse Width Modulation (PWM) and the real-time control of the setup is handled by a PC with a dSPACE controller board, see figure 2.1.

For the experimental implementation the modelling and identification of dry friction will never be exact. In chapter 5 the effects of small friction modelling errors for the reduced-order observer based friction compensation is studied by simply scaling the friction compensation rule. For the experimental implementation, the error in the friction modelling is far more complicated than accounted for by simply scale the compensation model. Nevertheless, the experimental results will be compared with the numerical results for the closed-loop system (5.7) with the non-smooth asymmetric friction modelling and the scaled friction compensation rule. Since closed-loop system (5.7) will not describe the experimental implementation with small friction modelling errors exact, the result are only compared qualitatively.

At the experimental setup only position measurements x_1 and velocity estimates $\hat{x}_2$ are available. Experimental results can, therefore, only be compared with simulation results for these two states. To be able to deal with differences in phase, a proper method for the comparison is the use of the plot of $\hat{x}_2$ against x_1. This plot can be compared with the perpendicular projection of the simulation results on the plane $x_2 = 0$. Therefore, the shape of this projection for simulation results will be discussed first for the closed-loop system (5.7).

In figure 6.1 (top) two limit cycles[1] are depicted for $n_1 = 0.4$, $n_2 = 0.02$, $L = 10$, $\eta = 1 \cdot 10^{-9}$, $r = 1$ (exact compensation) and the asymmetric friction parameters of table 2.1 ($L_c = 94.4$). The perpendicular projection of these two limit cycles on the plane $x_2 = 0$ is depicted in figure 6.1 (bottom). The behaviour found is comparable with the behaviour found for the symmetrical non-smooth friction modelling as depicted in figure 4.7.

The difference with the symmetrical velocity/friction mapping is that for the asymmetrical

[1]For the sake of convenience, the two depicted steady-state solutions are said to be limit cycles. The exact nature of these two solutions, for example periodic of quasi periodic, is however not determined.

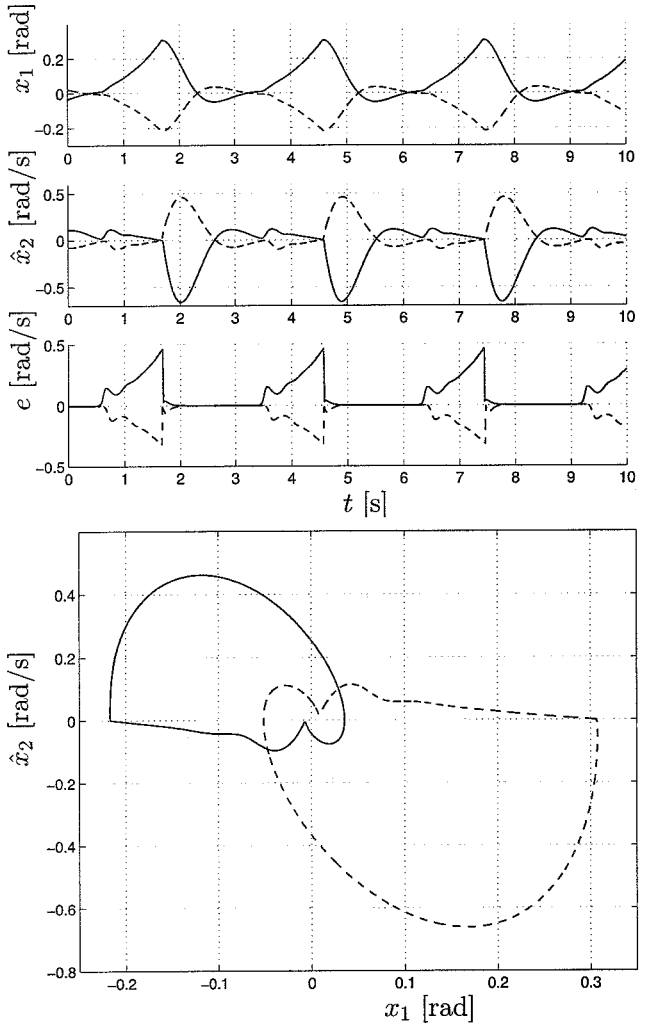

Figure 6.1: Two coexisting limit cycles found for (5.7) with $n_1 = 0.4$, $n_2 = 0.02$, $L = 10$, $\eta = 1 \cdot 10^{-9}$ and $r = 1$ (exact compensation) (top: states x_1, $\hat{x}_2$ and e against time t, bottom: projection on the plane $x_2 = 0$).

velocity/friction mapping the two limit cycles, both existing on their own side of the invariant plane $e = 0$, are no longer symmetrical.

The consequence of a small friction modelling error ($r = 1.01$) on the two limit cycles depicted in figure 6.1 is shown in figure 6.2 (top). In figure 6.2 (bottom) the perpendicular projections on the plane $x_2 = 0$ of this limit cycle and the two limit cycles found for the exact friction compensation are compared. The union of the projections of the two limit cycles found for the exact case can still clearly be distinguished in the projection of the limit cycle found for the non-exact case. Consequently, the coexisting two limit cycles for the exact case, are connected due to the small inaccuracy in the friction compensation model (note that the invariance of the plane $e = 0$ is lost due to small modelling inaccuracies).

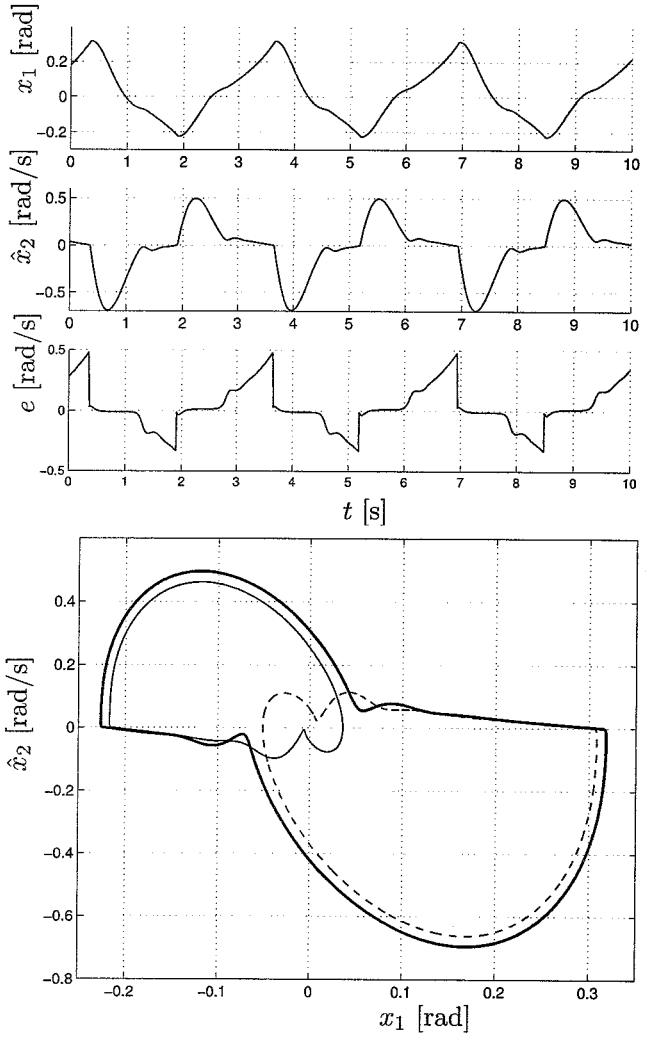

Figure 6.2: Limit cycle found for (5.7) with $n_1 = 0.4$, $n_2 = 0.02$, $L = 10$, $\eta = 1 \cdot 10^{-9}$ and $r = 1.01$ (non-exact compensation) (right from top to bottom states x_1, $\hat{x}_2$ and e against time t, left comparison of projection on the plane $x_2 = 0$ of the found limit cycle for $r = 1.01$ with the two coexisting limit cycles found for $r = 1$ also depicted in figure 6.1).

Now the numerical results are described, a comparison with experimental results can be made. In figure 6.3 (left), persistent oscillatory behaviour is depicted, found for the experimental implementation with the same parameter settings as in figure 6.2. Whether or not this behaviour is periodically in the entire state could not be checked, since measurements of x_2 are not present. The plot of $\hat{x}_2$ against x_1 is compared with the projection of the limit cycle found for similar observer and controller gains for the closed-loop system (5.7) with $r = 1.01$ (see figure 6.2) in figure 6.3 (right). From the comparison it can be noted that, although the projections do posses shape similarities, the experimental result does not exactly agree with the simulation result. However, the results do show qualitative similar behaviour.

The time history of the estimated velocity at the experimental setup (see figure 6.3 (left)) is more jagged, compared to the time history of the estimated velocity for the simulation (see figure 6.2). This difference could be due to unmodelled dynamics, such as flexible modes, backlash or dynamical friction effects, or sensor noise. However, from the plot of $\hat{x}_2$ against x_1 it seems that these disturbances exhibit a deterministic behaviour (if the disturbance would be noise the plot of $\hat{x}_2$ against x_1 would be more spread out). The exact nature and the effect of these disturbances is not further examined. However, due to amplification of noise and disturbances, the observer gain can not be increases without any limitations [8]. This is a property for observers in general but it is known that reduced-order observers are even more sensitive to noise than full-order observers [8].

In figure 6.4, measurements are depicted for the equivalent controller gains and the observer gain increased to $L = 35$. With this higher observer gain the estimated velocity becomes even more jagged as depicted in figure 6.3 (left). The measurements still show qualitative similarities with the numerical solution of (5.7), as depicted in figure 6.4 (right). However, for a better approximation the over-compensation level for (5.7) is increased to $r = 1.05$. The fact that the rate of over-compensation changes can be understood by the fact that for the experimental implementation the rate of over or under-compensation can differ for each point on the velocity/friction mapping.

In figure 6.5, the measurements are depicted for the super-critical observer gain $L = 100$ ($L_c = 94.4$). Theoretically, the origin should now be globally asymptotically stable, but from the previous experiments it is already known that the modelling of the friction is not perfect. From the projection on the plane $x_2 = 0$, it can be noted that the orbit has become more noisy. For this level of observer gain the only qualitative comparison with the numerical solutions of (5.7) which can be found is the asymmetry with respect to the line $x_1 = 0$. Further shape similarities can not be found due to the noisy character of the estimated velocity.

With the super-critical observer gain the velocity estimates become very noisy and the experimental setup still exhibits persistent oscillatory behaviour. From the study of the closed-loop system with the scaled compensation model (section 5.2) it is known that the system exhibits limit cycling behaviour if the actual friction is only slightly over-compensated. For the under-compensated case the closed-loop system does not exhibit limit cycling at the cost of (small) steady state errors. This behaviour is also found qualitatively for the experimental setup by scaling the compensation rule as was done in (5.7). In figure 6.6 (left), the equilibrium set for the experimental setup for $n_1 = 0.4$, $n_2 = 0.02$, $L = 95$ and $r = 0.8$ is illustrated by plotting multiple measurements starting from different initial conditions on the plane $x_2 = 0$.

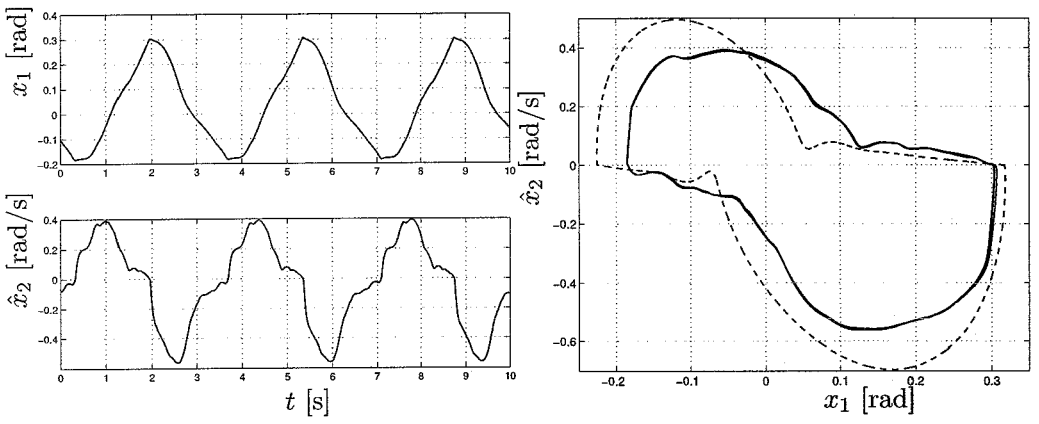

Figure 6.3: Experimental results for $n_1 = 0.4$, $n_2 = 0.02$, $L = 10$ (left: states x_1 and $\hat{x}_2$ against time t; right: projections on the plane $x_2 = 0$ of the measurements (solid) and the limit cycle found numerically for $r = 1.01$ (dashed) as depicted in figure 6.2).

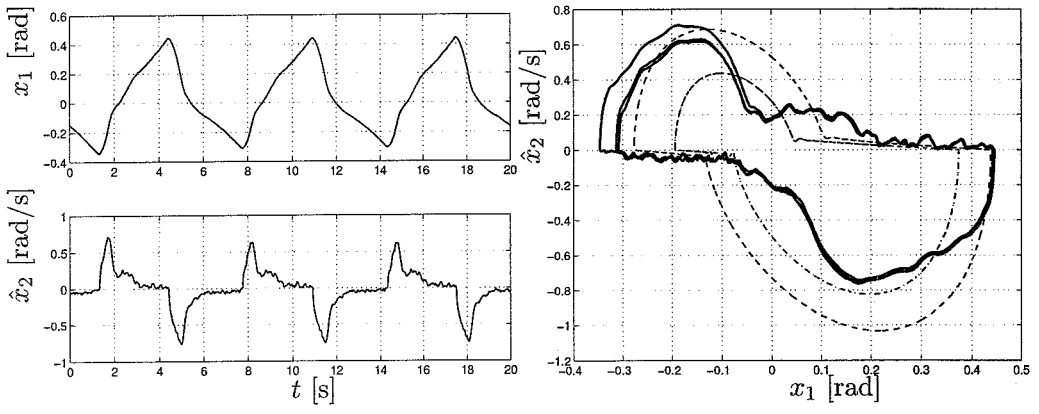

Figure 6.4: Experimental results for $n_1 = 0.4$, $n_2 = 0.02$, $L = 35$ (left: states x_1 and $\hat{x}_2$ against time t; right: projections on the plane $x_2 = 0$ of the measurements (solid) and the limit cycle found numerically for $r = 1.01$ (dash-dot) and for $r = 1.05$ (dashed)).

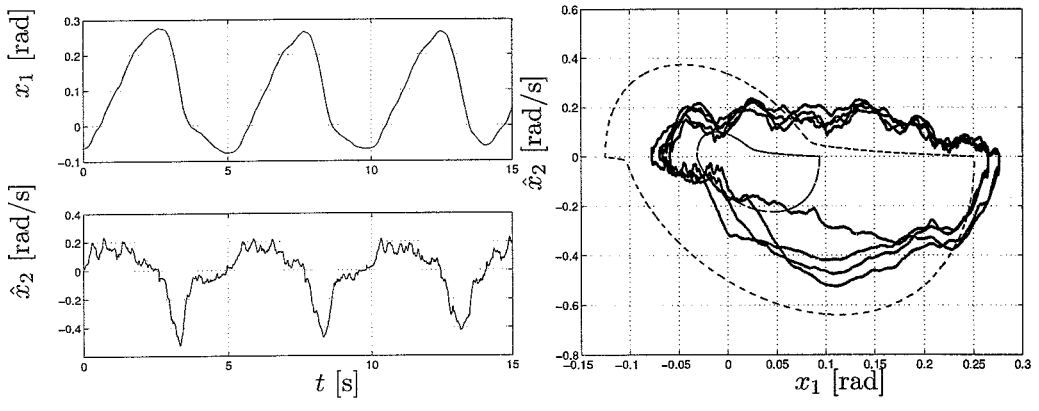

Figure 6.5: Experimental results for $n_1 = 0.4$, $n_2 = 0.02$, $L = 100$ (left: states x_1 and $\hat{x}_2$ against time t; right: projections on the plane $x_2 = 0$ of the measurements (solid) and the limit cycle found numerically for $r = 1.01$ (dash-dot) and for $r = 1.05$ (dashed)).

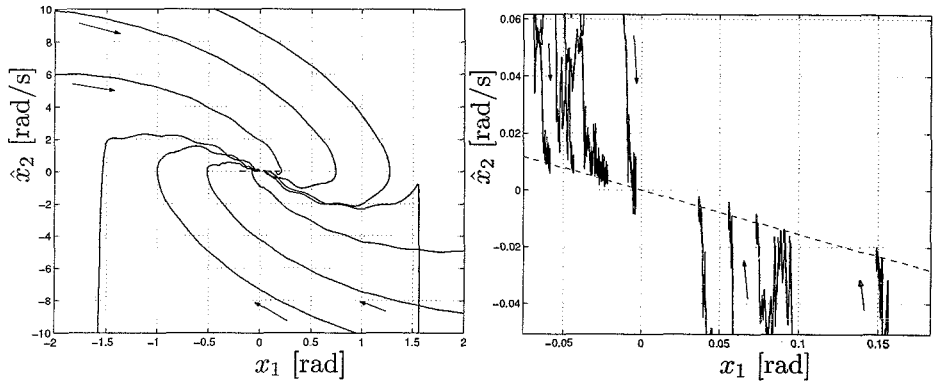

Figure 6.6: Multiple measurements for $n_1 = 0.4$, $n_2 = 0.02$, $L = 95$ and $r = 0.8$ depicted on the plane $x_2 = 0$ (right similar but zoomed in close to the equilibrium set plus the line $x_1 = -\frac{b+LJ+n_2}{n_1}\hat{x}_2$ (dashed)).

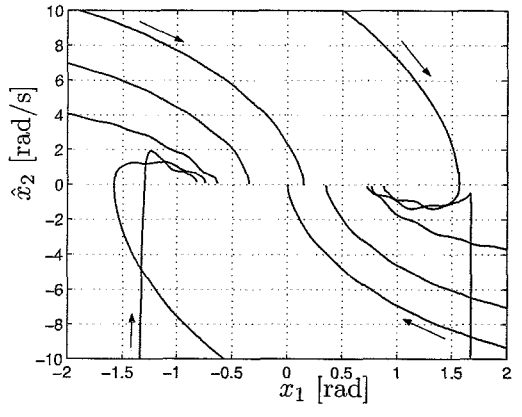

Figure 6.7: Multiple measurements for $n_1 = 0.4$, $n_2 = 0.02$, $L = 95$ and $r = 0$ (no compensation) depicted on the plane $x_2 = 0$.

In figure 6.6 (right) the similar is depicted but now zoomed in close to the equilibrium set. All measurements end close to the line (5.9) as shown in the equilibria analysis (see section 5.2). For illustration the result of a similar experiment for $r = 0$ (no compensation) is depicted in figure 6.7. It can be noted that without the friction compensation the maximum steady-state positioning error is much larger when compared to the under-compensated case as depicted in figure 6.6.

To estimate the size of the equilibrium set for varying values of r steady-state values for x_1 are measured for several initial conditions. By plotting this data, an experimental bifurcation diagram for the scaling parameter r is created. The result for $n_1 = 0.4$, $n_2 = 0.02$, $L = 95$ is depicted in figure 6.8 twice. The only difference between the two experiments is the fact that the results depicted in 6.8 (right) are gained a couple of weeks earlier. Both bifurcation diagram show qualitative the same behaviour. For increasing values of r the maximum steady-state error decreases until the point where persistent oscillatory behaviour is born. By further increasing the scaling parameter the maximum absolute value of x_1 in the limit cycle also increases.

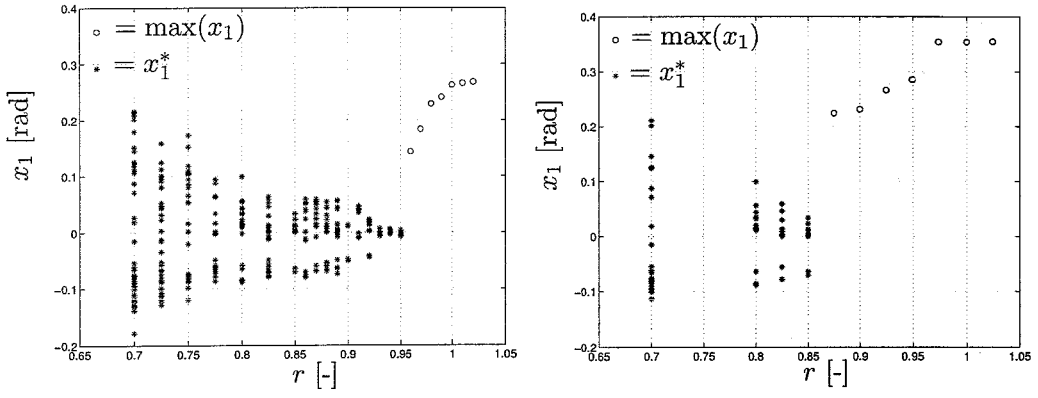

Figure 6.8: Experimentally found bifurcation diagrams for the scaling parameter r and $n_1 = 0.4$, $n_2 = 0.02$, $L = 95$ ('*' indicates equilibrium point, 'o' indicates maximum absolute value of the limit cycle).

Consequently the experimental implementation shows qualitative similar behaviour as found for the non-smooth closed-loop system with the scaled compensation rule (5.7) (see figure 5.10). The differences between the bifurcation diagram depicted in 6.8 (left) and 6.8 (right) illustrates that the friction at the experimental setup can differ daily. This fact indicates that upon designing the friction compensation rule one should realize that exact friction compensation is not possible and a deliberate choice for over-compensation or under-compensation should probably be made.

To cope with small identification errors at the practical implementation of the reduced-order observer based friction compensation, a simple strategy is, therefore, to simply scale down the compensation rule until no more persistent oscillatory behaviour is found. However, the friction can change daily, as shown in the differences in the two experimentally found bifurcation diagrams, and some extra safety on r must be taken for robustness. Consequently, application of the reduced-order observer based friction compensation can provide the positioning performance without the existence of limit cycling behaviour. This result holds even in the presence of small friction modelling errors by assuring that the not perfectly modelled dry friction is never over-compensated.

Conclusions and Further Research

In this final chapter conclusions will are drawn and recommendations for further research are be given.

6.1 Conclusions

The research as described in this thesis concerns the behaviour of a nonlinear closed-loop system, consisting of an one-link robot with friction, a proportional/derivative (PD) state feedback controller, a reduced-order observer and dry friction compensation. The reduced-order observer is used to estimate the actual velocity from the available position measurements. With this estimate for the actual velocity the required dry friction compensation force is computed using a friction model. The dynamics of this closed-loop system for is been investigated three different cases. For the first case, denoted as the smooth case, the discontinuous friction is modelled using a smooth model. For the second case, denoted as the non-smooth case, the friction is modelled by a non-smooth model. The non-smooth friction model switches between a velocity/friction mapping for non-zero velocities and an external-force/friction mapping for zero velocity. For these first two cases the friction is modelled exactly. In practice, however, the modelling of the friction will not be perfect. For the last case, denoted as the non-exact case, the friction compensation rule is simply scaled to study the effect of small friction modelling errors. Both smooth and non-smooth friction modelling are addressed for this case.

The first property of the closed-loop system, that is revealed, is the fact that solutions are bounded irrespectively on how the friction is modelled. Two facts are used to prove this property. First, the difference between the actual friction and the friction compensation is bounded. Secondly, the linear part of the closed-loop system is always globally asymptotically stable for arbitrary positive controller and observer gains.

For the smooth case, it has been shown that the zero observer error set is an invariant set. Consequently, the observer error stays equal to zero once it becomes equal to zero as desired. Next, the observer error dynamics are examined. From stability analysis of the observer error, it followed that the negative slope of the friction model, due to the Stribeck effect, could cause instability for the observer error. Fortunately, a critical value for the observer gain could be derived, such that global asymptotic stability of the observer error is guaranteed. Equilibrium analysis for the total closed-loop system showed that the origin (the set-point) is the unique equilibrium point. The origin is also locally asymptotically stable for arbitrary positive observer and controller gains. The smoothed friction model exhibits an extremely steep positive slope around zero velocity. This positive slope causes that the observer error will be locally asymptotically stable in the neighborhood of the origin for the total closed-loop system. Around the unique equilibrium point, the observer error is asymptotically stable and the equilibrium point itself is also asymptotically stable. When the observer error is globally asymptotically stable (by taking the observer gain larger than the critical value), global

asymptotically stability of the origin (the set-point) is been proven. With the origin globally asymptotically stable the system exhibits the desired dynamics: globally asymptotically stable set-point and, consequently, no other equilibrium points and no limit cycling. The critical observer gain can, therefore, be regarded as a design criteria for the total closed-loop system with smoothed friction modelling. This criterion is based on the stability of the observer error only. Since the error dynamics of the reduced-order observer are not influenced by the controller gains, the controller gains can be chosen independently of the observer gain.

For the non-smooth case, the zero observer error set is not automatically an invariant set. This is caused by the fact that the non-smooth friction for zero velocity depends on the external force and not on velocity. The actual friction is, therefore, not always cancelled by the friction compensation if the observer error is zero. Since invariance of the zero observer error set is a desired property an alternative compensation rule is designed such that the zero observer error set is again an invariant set. Similar to the smooth case the negative slope of the friction model can cause instability for the observer error. It has been shown that the similar critical value for the observer gain, as derived for the smooth case, also holds for the smooth case. For the non-smooth case, the origin is not automatically a unique equilibrium point. However, it has been shown that the derived critical value for the observer gain, such that the observer error is asymptotically stable, is also a sufficient condition for uniqueness of the equilibrium point at the origin. Due to the non-smooth friction modelling local stability of the origin could not be studied by simply linearizing the set of state equations around the origin. However, with the observer error globally asymptotically stable, global asymptotically stability for the origin is also been proven for the non-smooth case. The similar design criteria, therefore, also holds for the non-smooth case. For the case where the observer error is not asymptotically stable persistent oscillatory behaviour is found numerically. The exact nature of this behaviour, for example periodic or quasi-periodic, is not determined.

For the non-exact case, the compensation rule is simply scaled to introduce a mismatch between the actual friction and the friction compensation. For both types of friction modelling it is been shown that if the friction is slightly over-compensated, the closed-loop system exhibits stable limit cycling. Contrary to the results in the smooth case, the under-compensation of the friction for the non-smooth case results in the existence of an equilibrium set. A zero steady-state positioning error is, therefore, no longer guaranteed. The resulting steady-state error can be decreased by increasing the observer gain and the proportional controller gain or by decreasing the derivative gain, since in these cases the equilibrium set becomes smaller. Limit cycling is fatal for positioning tasks. Slight under-compensation of the friction is, therefore, even at the cost of a small steady-state error, more advisable than over-compensation.

The reduced-order observer based friction compensation is also implemented on the experimental setup of the one-link robot. Two facts are confirmed by experimental results. Firstly, the fact that under-compensation leads to the existence of an equilibrium set, which decreases for smaller level of under-compensation and, secondly, the fact that over-compensation induces persistent oscillatory behaviour, which disappears for smaller level of over-compensation. Consequently, the practical implementation shows, qualitatively, similar behaviour as the numerical model.

The two questions, as stated in the introduction, can now be answered as follows:

How will the controlled system, extended with an observer and friction compensation behave (stable or unstable, limit-cycling) depending on settings of the controller and the observer?
The resulting closed-loop system will not exhibit unbounded behaviour. If the friction is modelled exactly and the observer error is globally asymptotically stable then the set-point will be globally asymptotically stable. For the non-smooth case persistent oscillatory behaviour is found numerically for the case where the observer error is not asymptomatically stable. If the friction is not modelled exactly and if the actual friction is over-compensated then the system exhibits limit cycling. For the under-compensated case a zero steady-state error is no longer guaranteed for the non-smooth case, due to the existence of an equilibrium set.

How can one design a combination of controller, friction compensation and observer such that the resulting system is asymptotically stable (regarding to the set-point for the positioning task) and consequently does not exhibit limit-cycling?
A critical observer gain is derived such that the observer error will be globally asymptotically stable. It has been shown that if the observer error is globally asymptotically stable then the set-point for the controller is also globally asymptotically stable. The critical observer gain can, therefore, be regarded as a design criterion that ensures that the resulting closed-loop system exhibits the desired dynamics. For the practical implementation under-compensation of the actual friction is more advisable than over-compensation.

6.2 Further Research

For the controlled one-link robot with friction compensation it is shown that the stability of the observer error and the set-point are related. Perhaps this relation could be proven to be a fundamental property. With this fundamental knowledge, similar design rules for arbitrary observer based compensated system could then be derived by studying the stability of the resulting observer error dynamics only. This result would be a good starting point for the research on observer based friction compensation for controlled mechanical systems with, for example, more inputs and more degrees of freedom.

A full-state observer based friction compensation strategy applied to the similar one-link robot is already studied numerically and experimentally in [15]. The results of this thesis could also be extended to this approach. The use of a more sophisticated (dynamical) friction model could result in a more accurate description of the friction at the experimental setup. Another interesting feature would be to examine an *adaptive* reduced-order observer based friction compensation scheme. In this way the parameters for the applied friction model automatically adapt to small variations in the actual friction due to, for example, temperature changes.

Bibliography

[1] Armstrong-Hélourvy B. , Dupont P. and Canudas de Wit C., "A Survey of Models, Analysis Tools and Compensation Methods for the Control of Machines with Friction", Automatica, vol. 30, no. 7, pp. 1083-1138, 1994.

[2] Hensen, R.H.A., "Controlled Mechanical Systems with Friction". Ph.D. thesis, Eindhoven University of Technology, The Netherlands, 2002.

[3] Ipri, S.L and Asada, H., "Tunded Dither for Friction Suppression During Force-Guided Robotic Assembly", Intelligent Robots and Systems 95. 'Human Robot Interaction and Cooperative Robots', Proceedings. 1995 IEEE/RSJ International Conference on , pp. 310-315 vol.1, 1995.

[4] Canudas de Wit C., Noel P.,Aubin A. Brogliato B. Drevet P., "Adaptive Friction compensation in Robot Manipulators : Low Velocities", Robotics and Automation, 1989. Proceedings., 1989 IEEE International Conference on, pp. 1352 -1357 vol.3, 1989.

[5] Khalil H. K., "Nonlinear Systems", Macmillian Publishing Company, 1992

[6] Leine, R.I., "Bifurcations in Discontinuous Mechanical Systems of Filippov-Type", Ph.D. Thesis, Eindhoven University of Technology, The Netherlands, 2000.

[7] Sastry, S., "Nonlinear Systems, Analysis, Stability and Control", Springer-Verlag New York Inc., 1999.

[8] Franklin G.F., Powell D.A., Emami-Naeini A. "Feedback Control of Dynamic Systems" (third edition), Addison-Wesley Publishing Company, 1994.

[9] Malmborg J. and Bernhardsson B., "Control and Simulation of Hybrid Systems", Proceedings of the Second World Congress of Nonlinear Analysts, July 1996, pp. 57-64, 1997.

[10] Heath, M.T., "Scientific Computing, An Introductory Survey" (second edition), McGraw-Hill, 2002

[11] Help files of MATLAB Version 6.1.0.450 (R12.1) on PCWIN on Mathematics: Differential Equations: Questions and Answers, and Troubleshooting.

[12] Slotine J.E. and Li W., "Applied nonlinear control", Prentice Hall International, 1991

[13] Nayfey, A.H. and Balachandran, B., "Applied nonlinear dynamics; Analytical, Computational and experimental Methods", Wiley-International Chichester, 1995

[14] Parker, T.S. and Chua, L.O., "Practical Numerical Algorithems for Chaotic Systems", Springer-Verlag New York, 1989

[15] Putra D. and Nijmeijer H., "Limit cycling in observer-based controlled mechanical systems with friction", Proceedings of the European Control Conference 2003, Cambridge UK, 2003

Appendix A

Derivative of the Stribeck Curve

The shape of the Stribeck curve and first derivative for $\beta = 1$ and $\beta = 2$ are depicted in figure A.1. The first derivative of the Stribeck curve (2.2) for $v \neq 0$ is equal to

$$g'(v) = -\text{sgn}(v) \frac{\beta \left(\frac{|v|}{v_s}\right)^{\beta} \delta F e^{-\left(\frac{|v|}{v_s}\right)^{\beta}}}{|v|}. \tag{A.1}$$

Note that the derivative of the Stribeck curve times the sign of the velocity ($g(v)\text{sgn}(v)$) is strictly negative.

The second derivative of (2.2) is equal to

$$g''(v) = \left(\frac{\beta - 1 - \left(\frac{|v|}{v_s}\right)^{\beta} \beta}{|v|} \right) g'(v). \tag{A.2}$$

Extrema of the first derivative (A.1) occur where the second derivative (A.2) is equal to zero, thus

$$\left(\frac{\beta - 1 - \left(\frac{|v|}{v_s}\right)^{\beta} \beta}{|v|} \right) g'(v) = 0 \rightarrow |v| = \begin{cases} 0 & \text{if } \beta = 1 \\ \sqrt[\beta]{\frac{\beta-1}{\beta}} v_s & \text{if } \beta > 1 \end{cases}. \tag{A.3}$$

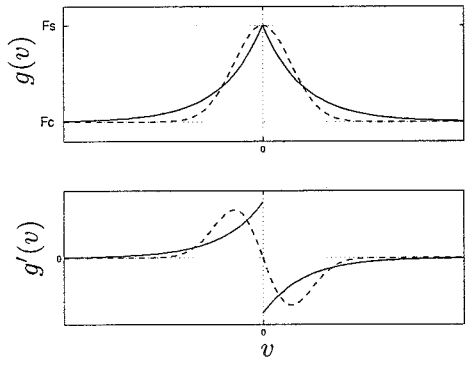

Figure A.1: Stribeck curve (top) and derivative (bottom) for $\beta = 1$ (solid) and $\beta = 2$ (dashed).

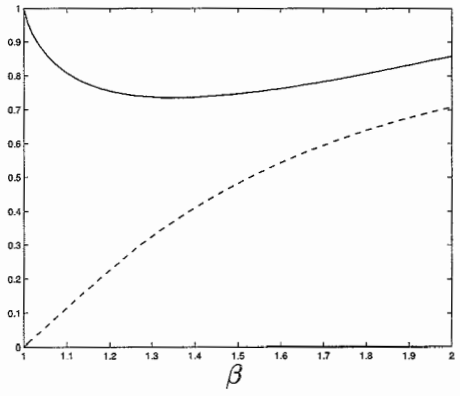

Figure A.2: Coefficients η (solid) and $\sqrt[\beta]{\frac{\beta-1}{\beta}}$ (dashed) for $1 < \beta \leq 2$.

The extrema for the first derivative (A.1) times the sign of the velocity is thus equal to

$$\left(g'(v)\mathrm{sgn}\,(v)\right)_{\min} = g'(v)_{\min} = -\eta\frac{\delta F}{v_s} \text{ with } \eta = \begin{cases} 1 & \text{if } \beta = 1 \\ \frac{(\beta-1)e^{-\frac{\beta-1}{\beta}}}{\sqrt[\beta]{\frac{\beta-1}{\beta}}} & \text{if } \beta > 1 \end{cases}. \tag{A.4}$$

The coefficients $\sqrt[\beta]{\frac{\beta-1}{\beta}}$ and η are depicted for $1 < \beta \leq 2$ in figure A.2.